Systems biology strategy to regulate the proinflammatory response and enhance the cancer cell death

Kentaro Hayashi

Graduate School of Media and Governance

Keio University

This dissertation is presented for the fulfillment of the

requirements for the degree of Doctor of Philosophy

2014

Abstract

Tumor or cancer immunology is a new and fast growing field where the interactions of the inherent immune system with malignant cancers have shown the suppression of disease progression. In this field, systems biology approach is required to understand and control the cellular response, since cellular behaviors are highly dynamic, complex and well orchestrated. This thesis describes the current understanding of the systems biology approach and addresses the connectivity between immunology and systems biology. The main aims of this research are i) to regulate the proinflammatory response in Tumor necrosis factor (TNF) signaling pathway and ii) to understand the resistance mechanisms for cancer treatment in TNF related apoptosis inducing ligand (TRAIL) signaling pathway. Therefore dynamical computational models were developed using the well-established perturbation response approach, and analyzed the dynamics of key signaling molecules and gene expressions were analyzed. Using this systems biology approach, a key molecule was identified to effectively regulate, but not abolish, the proinflammatory response in TNF signaling and we also found a target to enhance cell death in TRAIL resistant cancer cells. This work shows systems biology approach integrating computational approaches and wet bench experiments shed light on the drug development for the regulation of the immune-mediated diseases.

Keywords: TNF, TRAIL, Cell signaling, Computational model, Inflammation, Cancer, Apoptosis

Table of Contents

List of Figures

List of Tables

Chapter 1

Introduction

1.1 Background

The field of mathematical biology has very old history for understanding of biological problems such as the genetics of natural selection, nerve systems, epidemics and morphological patterns (Fisher 1930; Hodgkin *et al.* 1952; Kermack *et al.* 1933; Turing 1952). However, it is difficult to uncover crucial biological problems only by the mathematical modeling and experimental advancement is also required (Murray 2012). Over the last decades, a rapid progress was made in the development and improvement of wet bench approaches including high throughput analyses such as DNA microarrays (DeRisi *et al.* 1996), RNA-seq (Wang *et al.* 2009), CE-MS (Monton *et al.* 2007) and protein chips (Zhu *et al.* 2001), and low throughput analysis such as RT-PCR (Vandesompele *et al.* 2002) and western blotting (Burnette 1981). These experimental technologies has generated huge amount of information for gene regulatory networks, metabolic networks and protein-protein interactions. In parallel, roles of genes, metabolites and proteins have also being investigated. Although these works have allowed understanding complex cellular systems, the dynamical intracellular behaviors of their systems are still not fully understood. For example, how and when cancerous cells are mutated and change their behavior from normal cells? Nevertheless, the amount of biological information is increasing, and to analyze this information, systems biology approaches, integrating computational and theoretical methods with

experiments, are essential to understand the complexity of biological systems (Hood *et al.* 2004; Kitano 2002).

One of the main focuses of systems biology is to infer unknown components and interactions in network structures (Barabási *et al.* 2004; Kitano 2002). For this purpose, bottom-up and top-down systems biology approaches are considered for the comprehensive network analysis of gene regulatory networks and signal transduction networks (Bruggeman *et al.* 2007; Kholodenko *et al.* 2002; Selvarajoo *et al.* 2009). The bottom-up approach is used when the network topology is already known for signal transduction analysis, kinetic metabolic network analysis and gene regulatory network analysis (Guido *et al.* 2006). Since the network is developed from known components and reactions, the bottom-up approach does not consider the unknown factors, which are not fully understood (Bruggeman *et al.* 2007). And, for the bottom-up approach, it is required to investigate the details of kinetic parameters to understand the formation and depletion forms in each component (Aldridge *et al.* 2006; Karlebach *et al.* 2008). To overcome the parameter issues, flux balance analysis (FBA) is one of the major methods (Orth *et al.* 2010; Selvarajoo 2014). For FBA analysis, the reaction topologies or stoichiometry of the network need to be known (Selvarajoo 2014). Boolean network models, multi-valued logical models and Petri nets are also known (Albert *et al.* 2009; Aldridge *et al.* 2009; Chaouiya *et al.* 2007). Those approaches discretize the dynamic behaviors and it is not required for the detailed temporal and kinetic parameters. It

makes possible to understand the cellular network causality by using input-output information (Wang *et al.* 2012; Yeo *et al.* 2007).

The top-down approach, where each component has the flexibility to design the network, allows for the addition of new factors and the rewiring of the network in the system. Although the components in the systems are gradually elucidated through the progresses of technologies, their roles are not fully understood. Moreover, although common networks can be shared among species, tissues and cell types, their roles and functions can be different. Therefore, it is required to modify the networks according to the biological systems and cell types. Using the top-down approach enables to find the unknown components and processes without knowing the detailed information about the network (Helmy *et al.* 2009; Piras *et al.* 2011; Selvarajoo 2006). Therefore, systems biology top-down approaches can bring valuable insights and understandings to control and predict of the cellular behaviors and intercellular networks. In this thesis, an original top-down approach was developed to reveal novel biological features and drug targets in immune and cancer cell signaling.

1.2 Systems immunology

1.2.1 The immune system

The immune system is a well-organized and complex system to protect from the invading pathogens. This immune system is composed of two major components, innate and adoptive immunity (Akira *et al.* 2006). That provide the various proteins, called cytokines or chemokines, to protect the hosts and mediate communication between immune-related cells, such as macrophages, dendritic cells, monocytes (Janeway *et al.* 2002). These cells are called phagocytic cells and mainly work in innate immune system. Their roles are mainly, (i) recognition of the pathogens, (ii) killing these pathogens once they are recognized. Through the recognition of pathogens, macrophages and dendritic cells also initiate the adaptive immune response by presenting antigen to naïve $CD4^+$ T cells via class II MHC (Major Histocompatibility Complex) (Beutler 2004). As another important role, they also produce inflammatory cytokines, such as Interleukin-1β (IL-1β), Tumor necrosis factor-α (TNF-α), IL-6, IL-12 and IL-8. Those cytokines have pivotal roles in several diseases such as diabetes, rheumatoid arthritis, heart disease and ulcerative diseases, and also takes part in the important cellular responses, such as proliferation and differentiation (Coussens *et al.* 1997). The cytokines have a large variety of crucial functions to support the immune system, however, once they are compromised, they can cause immune diseases.

Therefore large numbers of experiments have been performed from single cell level to cell population level to control the immune response. Nevertheless, we are still far from a systematic understanding. To address this issue, systems biology approaches for immune systems are crucial.

1.2.2 Immunotherapy

Immunotherapy has the focus for the development of drugs to target malignant tumor cells, since their cellular behavior is tightly liked to inherent immune systems. For example, a particular attention has recently been paid to Natural Killer (NK) cells for the immunotherapy (Hayakawa *et al.* 2006; Wu *et al.* 2003). NK cells are recognized as the subset of the innate lymphoid cells (ILCs), distinct from T and B cells, which support the initiation of the immune response by secreting several cytokines, such as Interleukin-5 (IL-5), IL-13 and IL-17 (Spits *et al.* 2011). NK cells also produce Interferon-γ (IFN-γ), which consolidates the adaptive immune systems (Viver *et al.* 2011). NK cells can also directly attack the infected cells and tumor cells without affecting normal cells (Lanier *et al.* 2005). One of the strategies of NK cells to kill the tumor cells is to utilize the MHC class I molecule to distinguish the normal cells from tumor cells. When tumor cells are identified, NK cells release the cytotoxic components such as granzyme and perforin (Ljunggren *et al.* 2007). Furthermore, NK cells express TNF superfamily members to induce the apoptosis in tumor cells (Ljunggren *et al.*

2007). Thus, an effective treatment could be achieved by enhancing by NK cells activity.

Small molecule targeted therapy has also shown promising results for new treatment by blocking biochemical pathways that are crucial for cell survival and tumor progression. Imatinib is a small molecule inhibitor for BCR-ACL kinase and a drug for the certain types of leukemia (Druker 2011; O'Brien *et al.* 2003). This drug shows significant effect for about 76% of chronic myeloid leukemia (CML) patients, however some patients do not respond well yet (O'Brien *et al.* 2003). Likewise, the inhibitors for epidermal growth factor receptor (EGFR), BRAF, KIT and HER2 also have great potential to be drug targets (Abrams *et al.* 2003; Slamon *et al.* 2001; Su *et al.* 2012; Yaish *et al.* 1988). There are several types of BRAF inhibitors for melanoma depending on the target domain, however, several targets can enhance the tumor progression (Heidorn *et al.* 2010). Since intracellular systems are highly complex and robust, the effect of drugs can activate bypass pathways to compensate network changes and induce drug resistance. Therefore it is required to understand the resistance mechanism for drugs in dynamical signaling processes.

1.3 Objectives and summary

First, this thesis describes the current understanding of the complex immune system to protect hosts from the outside invaders. Although the immune system is well orchestrated, once it is compromised by pathogens or genetic mutations, it can lead to diseases, such as rheumatoid arthritis, bowel disease and cancers. For example, in cancer, the intensely investigated anti-cancer treatments remain suboptimal, notably there is still a large number of cancer deaths despite careful treatment. The interactions of the immune system with malignant tumors have shown the suppression of disease progression. Hence, there has recently been great interest to use the understanding of the immune process to regulate the progression of cancer. Thus we focused on the major proinflammatory cytokine, Tumor Necrosis Factor (TNF) and it's family member, Tumor Related Apoptosis Inducing Ligand (TRAIL), that have great potential to suppress the immune response and kill the cancerous cells.

In chapter 2, we analyzed TNF receptor 1 (TNFR1) signaling pathway using dynamical computational model based on the well-established perturbation response approach and experimental data from murine embryonic fibroblast cells (MEF). TNF is a widely studied cytokine (ligand) that induces proinflammatory signaling and regulates a myriad of cellular processes. In major illnesses, such as rheumatoid arthritis and certain cancers, the expression of TNF is elevated. Despite much progress in the field,

the targeted regulation of TNF response for therapeutic benefits remains suboptimal. Here, to effectively regulate the proinflammatory response induced by TNF, a systems biology approach was adopted. We developed a computational model to investigate the temporal activations of MAP kinase (p38), nuclear factor (NF)-κB, and the kinetics of 3 groups of genes, defined by early, intermediate and late phases, in murine embryonic fibroblast (MEF) and 3T3 cells. To identify a crucial target that suppresses, and not abolishes, proinflammatory genes, the model was tested in several *in silico* knock out (KO) conditions. Among the candidate molecules tested, *in silico* RIP1 KO effectively regulated all groups of proinflammatory genes (early, middle and late). To validate this result, we experimentally inhibited TNF signaling in MEF and 3T3 cells with RIP1 inhibitor, Necrostatin-1 (Nec-1), and investigated 10 genes (*Il6, Nfkbia, Jun, Tnfaip3, Ccl7, Vcam1, Cxcl10*, *Mmp3, Mmp13, Enpp2*) belonging to the 3 major groups of upregulated genes. As predicted by the model, all measured genes were significantly impaired. These results demonstrate that Nec-1 modulates TNF-induced proinflammatory response, and may potentially be used as a therapeutic target for inflammatory diseases such as rheumatoid arthritis and osteoarthritis.

In chapter 3, using our original systems biology approach, combining with computational and experimental analysis, we addressed the resistance mechanism in cancer cells. Cancer cells are highly variable and resistant to therapeutic intervention. Recently, the use of the tumor necrosis factor related apoptosis-inducing ligand

(TRAIL) induced treatment is gaining momentum, due to TRAIL's ability to specifically target cancers with limited effect on normal cells. Nevertheless, several malignant cancer types still remain non-sensitive to TRAIL. Previously, we developed a dynamic computational model, based on perturbation-response differential equations approach, and predicted protein kinase C (PKC) as the most effective target, with over 95% capacity to kill human fibrosarcoma (HT1080) in TRAIL stimulation (Piras *et al.* 2011). Here, to validate the model prediction, which has significant implications for cancer treatment, experiments on two TRAIL-resistant cancer cell lines (HT1080 and HT29) were conducted. Inhibiting PKC using Bisindolylmaleimide I showed cell viability is significantly impaired with over 95% death of both cancer types, in consistency with the predictions. Next, caspase-3, Poly (ADP-ribose) polymerase (PARP), p38 and JNK activations were measured in HT1080, confirming cell death occurs through apoptosis with significant increment in caspase-3 and PARP activations. Finally, to identify a crucial PKC isoform, the mRNA expressions from 10 known members in HT1080 cells were analyzed and shortlisted to the highest 4 for further siRNA knock-down (KD) experiments. From these KDs, PKCδ produced the most cancer cell death in conjunction with TRAIL.

Taken together with our novel findings in TNF and TRAIL signaling pathway, we demonstrate our approach combining model predictions with experimental validation holds promise for systems biology based tumor or cancer therapy. The

conventional experimental approach to understand the intercellular process is still required, however it is not sufficient to control the dynamics of the cellular behavior such as tumor progression or cancer growth. It is therefore crucial to develop approaches to elucidate the cellular behaviors and to control cellular systems. Thus, this work is anticipated to provide better understanding of system-level behaviors as well as to predict novel/original drug targets, which is difficult using conventional wet bench experiments alone.

Chapter 2

A systems biology approach to suppress TNF-induced proinflammatory gene expressions

2.1 Introduction

The tumor necrosis factor (TNF), first termed in 1962 (O'Malley *et la.* 1962), was initially known for its ability to induce programmed cell death or apoptosis. As a result, throughout the years, the TNF has been intensely investigated for its anticancer property (Balkwill 2009). Today, this cytokine is central to the regulation of myriad important cellular processes such as proliferation, differentiation, growth, and the immune response.

TNF binds to two types of outer membrane bound receptors on target cells, TNFR1 and TNFR2, and triggers the cell survival and proinflammatory NF-κB and MAP kinases activations (Locksley *et al.* 2001). In addition, the TNFR1 induces intracellular cell death pathways via caspases after internalization through endocytosis. It is, therefore, conceivable that the dysregulation of the TNF signaling process will misbalance proinflammatory and/or apoptotic responses. Notably, the chronic aberration in the baseline levels of TNF in human circulatory system has been attributed to the pathogenesis of numerous diseases, including rheumatoid arthritis, osteoporosis, sepsis and cancer (Bradley 2008; van Horssen *et al.* 2006).

The vast majority of TNF related biological processes are initiated by the death-domain (DD) containing TNFR1, which is also called TNFRSF1A. Unlike TNFR2, TNFR1 is present in almost all cell types in humans. Upon TNF binding,

TNFR1 trimerizes, and its intracellular DD recruits TRADD, which then creates a platform for RIP1 and TRAF2 to collectively form the receptor-signaling complex I. Cellular inhibitor of apoptosis proteins (cIAP)-1 and -2 bind to complex I and, consequently, together with K63-linked ubiquitin chains, modify RIP1 and TRAF2 (Falschlehner *et al.* 2012). This creates docking sites for an E3 ligase or linear ubiquitin chain assembly complex (LUBAC) consisting of heme-oxidized IRP2 ubiquitin ligase-1 (HOIL-1), HOIL-1-interacting protein (HOIP), and SHANK-associated RH domain interacting protein (SHARPIN). Subsequently, the activation of TAK1 and the ubiquitination of NEMO (or IKKγ), a subunit of IKK complex, lead to cell survival or proinflammatory response through NF-κB and MAP kinases activations. Other TRAF superfamily members (TRAF5 and 6) are also known to play a role in the NF-κB and MAP kinases activations (Funakoshi-Tago *et al.* 2009; Tada *et al.* 2001).

On the other hand, for the apoptotic pathways, clathrin, AP-2 and Dyn first mediate receptor internalization. Receptor-signaling complex I becomes modified, and dissociates from TNFR1, allowing FADD and caspase-8 to form complex II. Within complex II, caspase-8 becomes activated to induce extrinsic apoptosis through caspase-3 activation. Alternatively, caspase-8 activates caspase-7, and eventually, the cleavage of Bid to tBid in the mitochondria activates caspase-9 via cathepsin D. This induces the intrinsic apoptosis through caspase-3 activation.

Due to its ability to signal numerous cellular processes via the survival and death pathways, the TNFR1 signaling research has received immense attention over the years, especially on understanding the downstream signaling cascades to regulate and control proinflammatory diseases and cancer. Despite numerous studies, the control of proinflammatory diseases through therapeutic treatments, where TNF is over-expressed, remains suboptimal. For example, biologic response modifiers or biologics, such as Etanercept and Infliximab, are TNF decoy receptors or antibodies that suppress TNFR1 signaling through competition for TNF. Although these drugs have shown successful downregulation of inflammation in many cases, they can immuno-compromise patients to secondary infections such as tuberculosis (Fallahi-Sichani *et al.* 2012), or have been ineffective in a substantial number of administered patients (Wien *et al.* 2010).

To find alternatives, there have been major efforts on selectively suppressing the intracellular signaling of TNFR1. For example, genetic knockouts (KOs) of TRAFs and TRADD acting on the proinflammatory pathways have been investigated (Ermolaeva *et al.* 2008; Funakoshi-Tago *et al.* 2009; Tada *et al.* 2001). However, the experimental outcomes, so far, have not been optimistic. In TRAF2 KO, there is compensatory activation of NF-κB through TRAF5 (Tada *et al.* 2001) or TRAF6 (Funakoshi-Tago *et al.* 2009), and vice-versa. On the other hand, TRADD KO almost completely abolishes NF-κB activation (Ermolaeva *et al.* 2008), which is not desirable for the general survivability of cells. Thus, a systemic approach where the propagation

of signal transduction to all known branching pathways during target intervention should be monitored. This will allow the elucidation of effective target candidate(s) that overcomes and balances the deficiencies of current investigations.

In this chapter, we adopted a systems biology approach to study TNFR1 signaling dynamics. Firstly, we developed a computational model of TNF-induced proinflammatory response leading to NF-κB, MAP kinase activations, and three groups of gene expressions (classified according to their temporal profiles (Hao *et al.* 2009)). The model is based on the perturbation-response approach (Moran *et al.* 2007; Ross *et al.* 2008; Selvarajoo *et al.* 2009; Vance *et al.* 2002), which has been successfully used to elucidate novel signaling features and behaviors in Toll-like receptor-4 (Selvarajoo *et al.* 2006; Selvarajoo *et al.* 2008), -3 (Helmy *et al.* 2009), and TNF-related apoptosis-inducing ligand (TRAIL) signaling (Piras *et al.* 2011). Secondly, the TNFR1 model parameters were selected to fit the temporal activation profiles of NF-κB and MAP kinase p38 for fibroblast cell type in several available conditions (wildtype (Tada *et al.* 2001), TRAF2 KO (Tada *et al.* 2001), TRAF5 KO (Tada *et al.* 2001), TRAF2/TRAF5 double KO (DKO) (Tada *et al.* 2001), TRAF6 KO (Funakoshi-Tago *et al.* 2009), TRADD KO (Ermolaeva *et al.* 2008) and RIP1KO (Devin *et al.* 2000)). Using the resultant TNFR1 model with robust parameters, we performed simulations of multiple *in silico* KOs to determine an optimal target that suppresses, but not abolishes, proinflammatory genes. Finally, to validate the modeling results, we performed

experiments measuring various key proinflammatory gene expressions in MEF and 3T3 cells for TNF stimulation. Overall, our study presents evidence that systems biology research can be useful to elucidate important target(s) to suppress proinflammatory diseases such as rheumatoid arthritis and osteoarthritis.

2.2 Materials and methods

2.2.1 Computational model

The model is based on perturbation-response approach (Helmy *et al.* 2009; Piras *et al.* 2011; Selvarajoo 2006; Selvarajoo *et al.* 2008; Selvarajoo *et al.* 2009). The basic principle behind the approach is to induce a controlled perturbation of input reaction species of a system (TNFR1), and monitor the response of the activation/concentration levels of other output species (e.g. TAK1, p38, NF-κB, *Il6*, etc.) from steady-state. To briefly explain the principle, let a stable network consisting of *n* species be perturbed from the reference steady-state. In general, the resultant changes in the concentration of species are governed by the kinetic evolution equation (Ross *et al.* 2008; Moran *et al.* 2007):

$$\frac{\partial X_i}{\partial t} = F_i\left(X_1, X_2, .., X_n\right), i = 1, .., n \qquad (1)$$

where the corresponding vector form of equation 1 is $\frac{\partial \boldsymbol{X}}{\partial t} = \boldsymbol{F}(\boldsymbol{X})$. $\boldsymbol{F}$ is a vector of any non-linear function including diffusion and reaction of the species vector $\boldsymbol{X} = (X_1, X_2, .., X_n)$, which represents activated concentration levels of reaction species. The response to perturbation can be written by $\boldsymbol{X} = \boldsymbol{X}_0 + \delta\boldsymbol{X}$, where $\boldsymbol{X}_0$ is the reference steady-state vector and $\delta\boldsymbol{X}$ is the relative response from steady-states ($\delta\boldsymbol{X}_{t=0} = \mathbf{0}$).

The generally non-linear kinetic evolution equation 1 can be approximated or linearized by using Taylor series:

$$\frac{\partial \delta \boldsymbol{X}}{\partial t} = \frac{\partial \boldsymbol{F}(\boldsymbol{X})}{\partial \boldsymbol{X}} \delta \boldsymbol{X} + \frac{\partial^2 \boldsymbol{F}(\boldsymbol{X})}{\partial \boldsymbol{X}^2} \delta \boldsymbol{X}^2 + \ldots \qquad (2)$$

As the general volume of perturbing substance is usually very small (order of 1%) compared to the total volume of cells that are perturbed (Theobald *et al.* 1997), now consider a small perturbation around the steady-state in equation 2, in which higher-order terms become negligible and result in the approximation of the first-order term. In vector form $\frac{\partial \delta \boldsymbol{X}}{\partial t} = \left.\frac{\partial \boldsymbol{F}(\boldsymbol{X})}{\partial \boldsymbol{X}}\right|_{X=X_0} \delta \boldsymbol{X}$ (note the change from partial derivative to total derivative of time), where the zeroth order term $\boldsymbol{F}(\boldsymbol{X}_0) = 0$ at the steady-state $\boldsymbol{X}_0$ and the *Jacobian* matrix, or linear stability matrix, is $\boldsymbol{J} = \left.\frac{\partial \boldsymbol{F}(\boldsymbol{X})}{\partial \boldsymbol{X}}\right|_{X=X_0}$. The elements of $\boldsymbol{J}$, based on the initial activation topology, are chosen by fitting $\delta\boldsymbol{X}$ with

corresponding experimental profiles. Hence, the amount of response (flux propagated) along a biological pathway can be approximated using *first order mass-action response*, i.e. $\frac{d\delta \boldsymbol{X}}{dt} = J\delta \boldsymbol{X}$. That is, the basic principle so far suggests that the response rate of species in a mass-conserved system at an initial steady-state can be approximated by first order mass-action response equations, given a small perturbation to one or more species.

Note that *Jacobian* matrix elements (or response coefficients) can include not only reaction information, but also spatial information such as diffusion and transport mechanisms. Thus, each species in the perturbation-response model can represent a molecule, a different modified state of a molecule (e.g. ubiquitinated state) or a molecular process such as diffusion, endocytosis, etc. That is, each species in the biological network does not necessarily represent a specific molecular species. For illustration, in a pathway $X_1 \rightarrow X_2 \rightarrow X_3 \rightarrow X_4 \rightarrow X_5$, X_1 to X_5 can each be a different species or the same species at different stages in signaling, for example, X_1 being internalized (becoming X_2), transported to a different organelle (X_3), ubiquitinated (X_4) and become part of a protein complex (X_5).

2.2.2 Sensitivity analysis

We performed a sensitivity analysis to test the robustness of the optimized model parameters using the COPASI sensitivities module with default values. The variation in

the response of signaling molecules/steps, $x_i(t)$, was analyzed when a small variation of each model parameter k_j was applied. The response sensitivity coefficient (Zi 2011) of the i^{th} molecule with regard to the j^{th} parameter is defined by

$$R_{i,j} = \frac{\partial x_i(t)}{\partial k_j} \frac{k_j}{x_i(t)} \tag{3}$$

The obtained values, $R_{i,j}$ are then scaled, to reflect the relative changes in response, such as a change of p% in the value of parameter k_j, results in a $R_{i,j} \cdot p$% change in the value of the peak activation of the i^{th} molecule. The response sensitivity coefficients of p38, IκBα, and Group I, Group II and Group III genes were obtained at peak time (t = 15 min for p38 and IκB, 30 min, 2 h and 12 h for Group I, II and III respectively, see Table 2.2).

2.2.3 Experiments

Reagents and cell culture

Recombinant mouse TNF was purchased from R&D systems. Necrostatin-1 was purchased from Merck Millipore. 3T3 cells were obtained from JCRB cell bank. 3T3 and MEF were grown in DMEM (Nissui Seiyaku Co.) containing 10% calf serum, 100 U/mL of penicillin at 37 °C in a 5% CO_2 humidified atmosphere.

Evaluation of cell survival by 3-(4,5-dimethylthiazol-2-yl)-2,5-diphenyltetrazolium bromide (MTT) assay

The sensitivity of cells to hyperosmotic stress was measured with the MTT colorimetric assay in 96-well plates. Cells (2×10^4) were inoculated in each well and incubated for 24 h. Thereafter, 50 μL of MTT (2 mg/mL in PBS) was added to each well and the plates were incubated for a further 2 h. The resultant formazan was dissolved with 100 μL of dimethyl sulfoxide after aspiration of culture medium. Plates were placed on a plate shaker for 1 min and then read immediately at 570 nm using TECAN microplate reader with Magellan software (Männedorf, Switzerland).

Real-time PCR analysis

Total cellular RNA was extracted from cells using the TRIzol reagent according to the manufacturer's instructions (Invitrogen). One microgram of RNA was reverse-transcribed using a first-strand cDNA synthesis kit (ReverTra Aceα; Toyobo). Quantitative real-time PCR was performed using SYBR premix Ex Taq (Takara) on the Applied Biosystems StepOnePlus™ according to the technical brochure of the company. RT-PCR primers designed in this study are listed in Table 2.1 Quantitative measurements were determined using the ΔΔCt method and expression of GAPDH was used as the internal control. Melt curve analyses of all real-time PCR products were performed and shown to produce the sole DNA duplex.

Table 2.1 List of primer sequences for RT-PCR

Name	Species	Primer name	Sequence
Tnfaip3[1]	mouse	A20_F	GAACAGCGATCAGGCCAGG
		A20_R	GGACAGTTGGGTGTCTCACATT
Il6[1]	mouse	IL6_F	TAGTCCTTCCTACCCCAATTTCC
		IL6_R	TTGGTCCTTAGCCACTCCTTC
Nfkbia[1]	mouse	I*k*Ba_F	CTGCAGGCCACCAACTACAA
		I*k*Ba_R	CAGCACCCAAAGTCACCAAGT
Jun[1]	mouse	Jun_F	ACTCGGACCTTCTCACGTC
		Jun_R	CGGTGTAGTGGTGATGTGCC
Ccl7[1]	mouse	CCL7_F	GCTGCTTTCAGCATCCAAGTG
		CCL7_R	CCAGGGACACCGACTACTG
Vcam1[1]	mouse	Vcam1_F	AGTTGGGGATTCGGTTGTTCT
		Vcam_R	CCCCTCATTCCTTACCACCC
Cxcl10[1]	mouse	Cxcl10_F	AGGACGGTCCGCTGCAA
		Cxcl10_R	CATTCTCACTGGCCCGTCAT
Mmp3	mouse	mmp3_F	CTCGTGGTACCCACCAAGTC
		mmp3_R	AGTCCTGAGAGATTTGCGCC
Mmp13	mouse	mmp13_F	CTTCTGGCACACGCTTTTCC
		mmp13_R	ATCCAGACCTAGGGAGTGGC
Enpp2	mouse	Enpp2_F	ACTCCGAGCAGCCTGATTTT
		Enpp2_R	CCGGAGTAAGAGGTGAGCCA

(1) Sequences obtained from Hao & Baltimore (2009).

2.3 Results

2.3.1 TNFR1 signaling topology and model

To develop a computational model of proinflammatory TNFR1 signaling dynamics, we first require the known signal transduction pathways. We curated the KEGG database, and performed literature survey of the latest TNF research. After carefully considering several sources, we were able to propose a signaling topology mainly by combining the knowledge from KEGG, Falschlehner *et al.* (2012) and Wertz *et al.* (2010) (Figure 2.1).

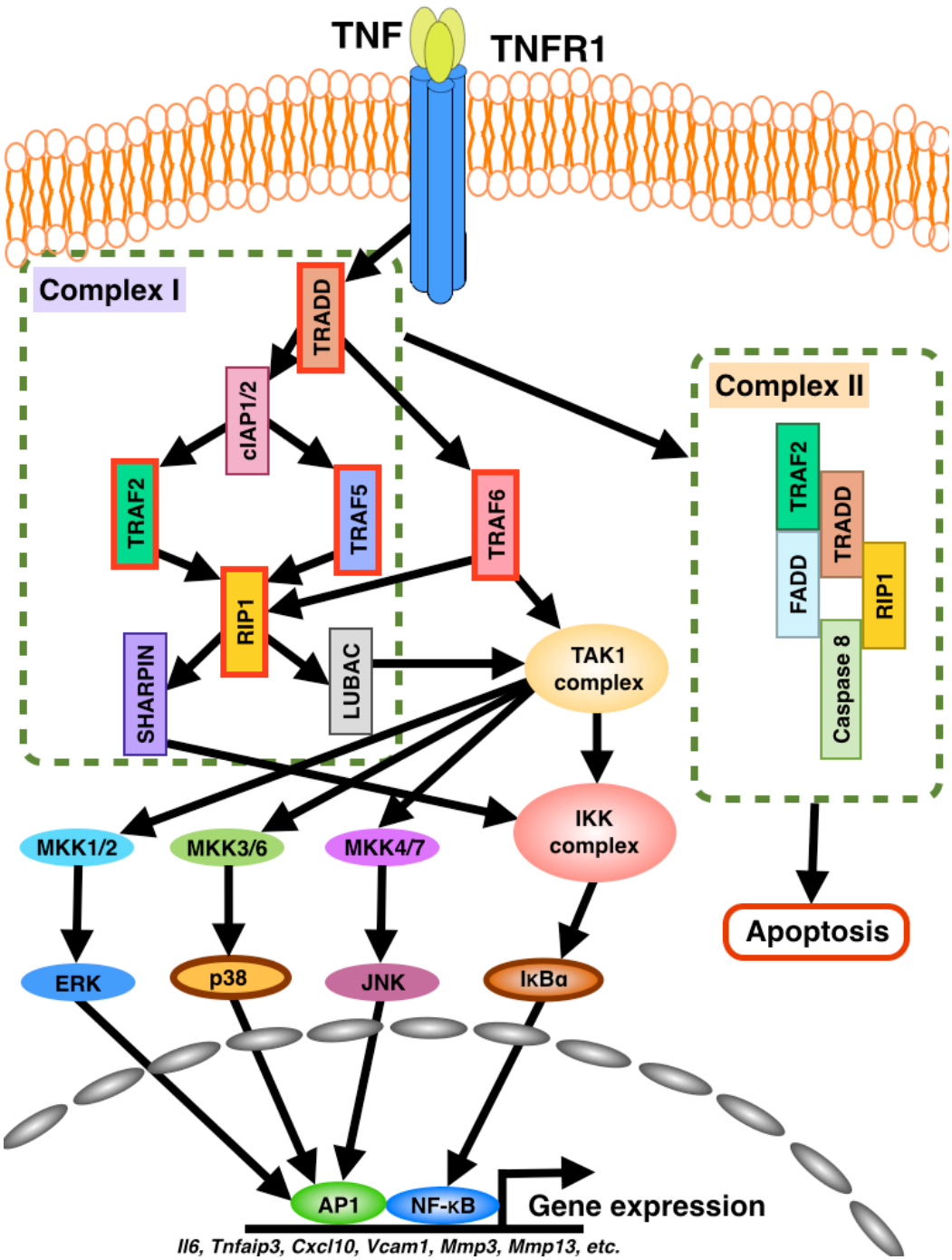

Figure 2.1 Schematic of TNFR1 signaling of cell survival/proinflammatory and apoptosis pathways. Upon TNF receptor activation, complexes I (survival pathway) and II (apoptosis) are formed. Complex I subsequently activates transcription factors, such as activator protein (AP)-1 and NF-κB through MAP kinases and IKK complex, respectively, which subsequently bind to promoter regions of genes to induce numerous proinflammatory genes.

Next, to simulate TNF-induced dynamics of NF-κB and MAPK activations using the topology, we developed a dynamic model based on perturbation-response approach (Materials and Methods), using COPASI simulation platform (Hoops *et al.* 2006). Unlike common biochemical reaction models (Tasseff *et al.* 2010; Werner *et al.* 2005), the perturbation-response approach does not require detailed knowledge of all signaling species and their reaction kinetics. This is because it analyses the response waves of signal transduction instead of individual reaction kinetics (Helmy *et al.* 2009; Moran *et al.* 2007; Piras *et al.* 2011; Ross *et al.* 2008; Selvarajoo 2006; Selvarajoo *et al.* 2008; Selvarajoo *et al.* 2009). The response waves can be approximated using linear response rules (*Response Rules*, Figure 2.2) combined with the law of mass conservation, and this approach has been previously used to successfully model the TLRs and TRAIL signaling pathways (Helmy *et al.* 2009; Piras *et al.* 2011; Selvarajoo 2006; Selvarajoo *et al.* 2008).

Briefly, each reaction in model is represented by a first-order response equation with activation or deactivation term. The activation term generally refers to protein binding, transformation, complex formation, phosphorylation and transcription. The deactivation term refers to protein unbinding, dephosphorylation and negative regulation such as mRNA decay through microRNA regulation.

Figure 2.2 Response rules.

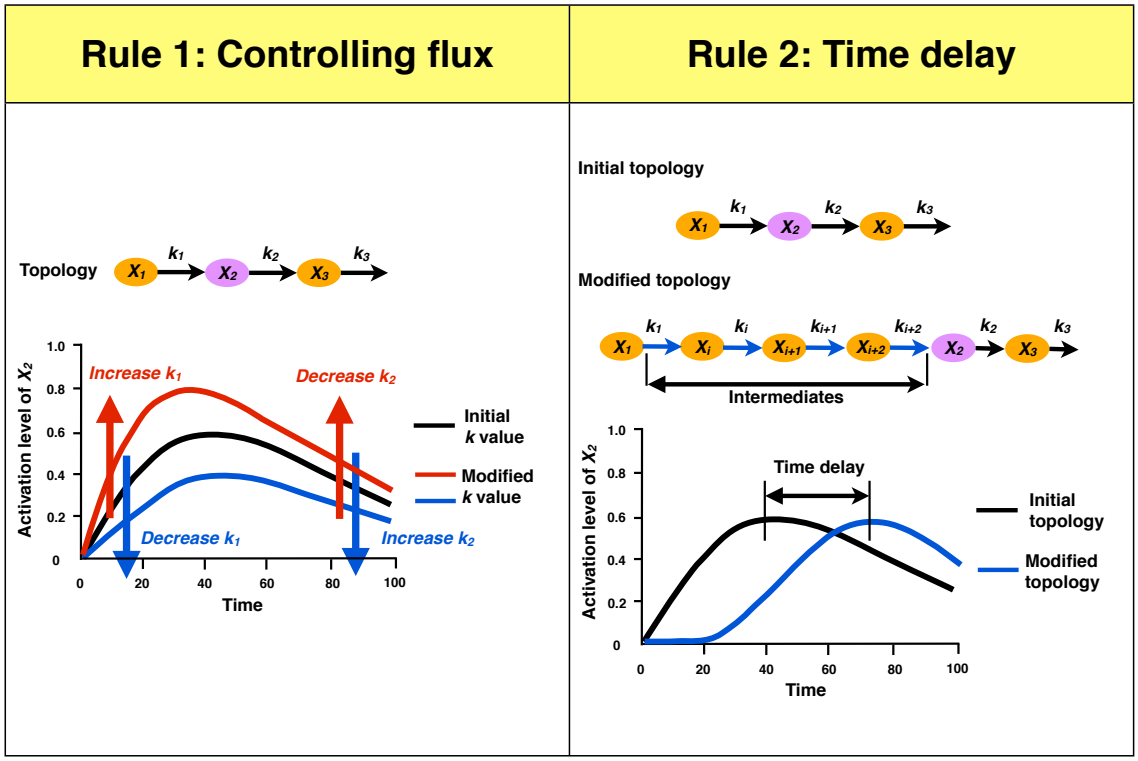

Figure 2.2 Response rules (continued)

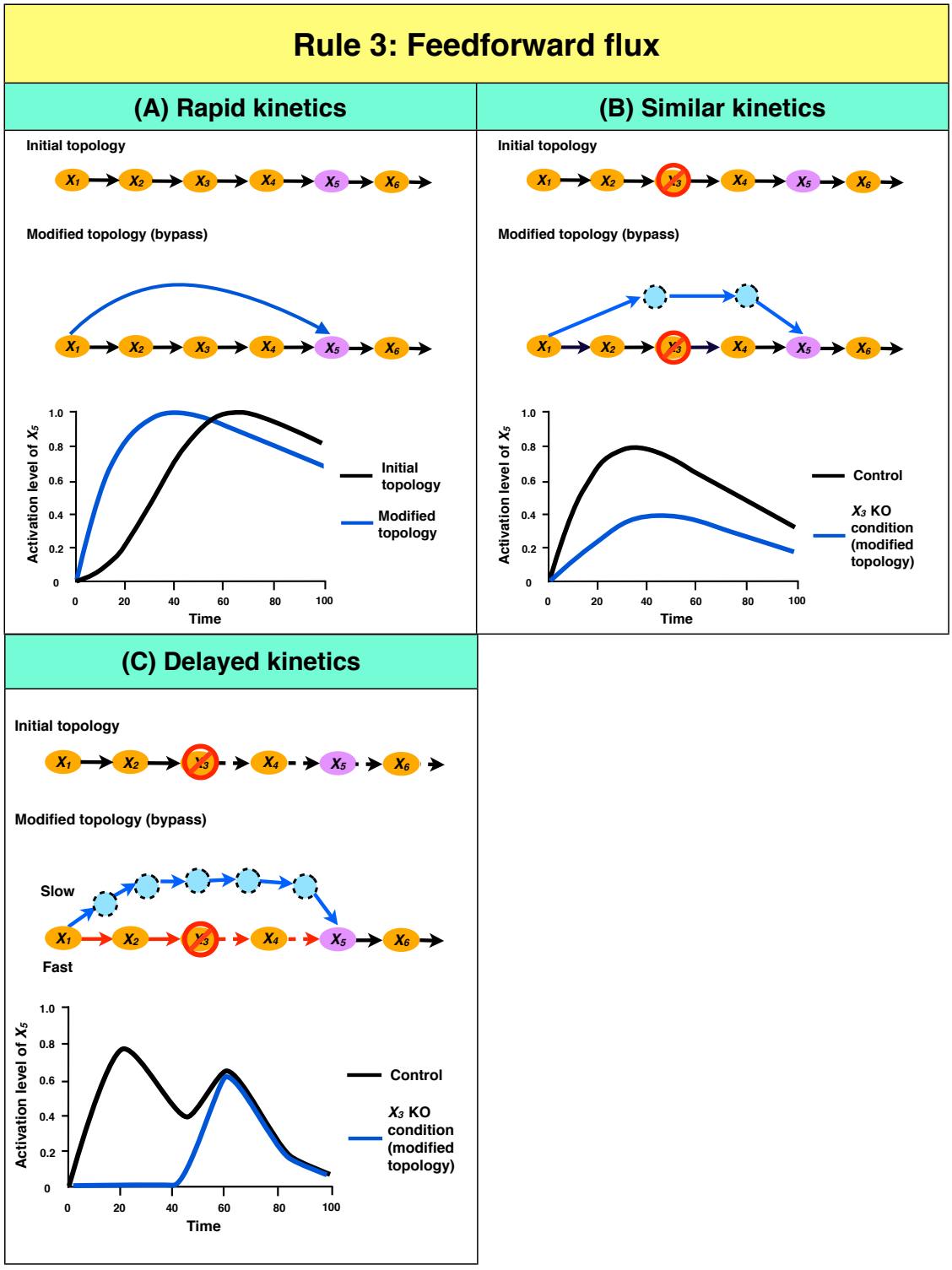

Figure 2.2 Response rules (continued)

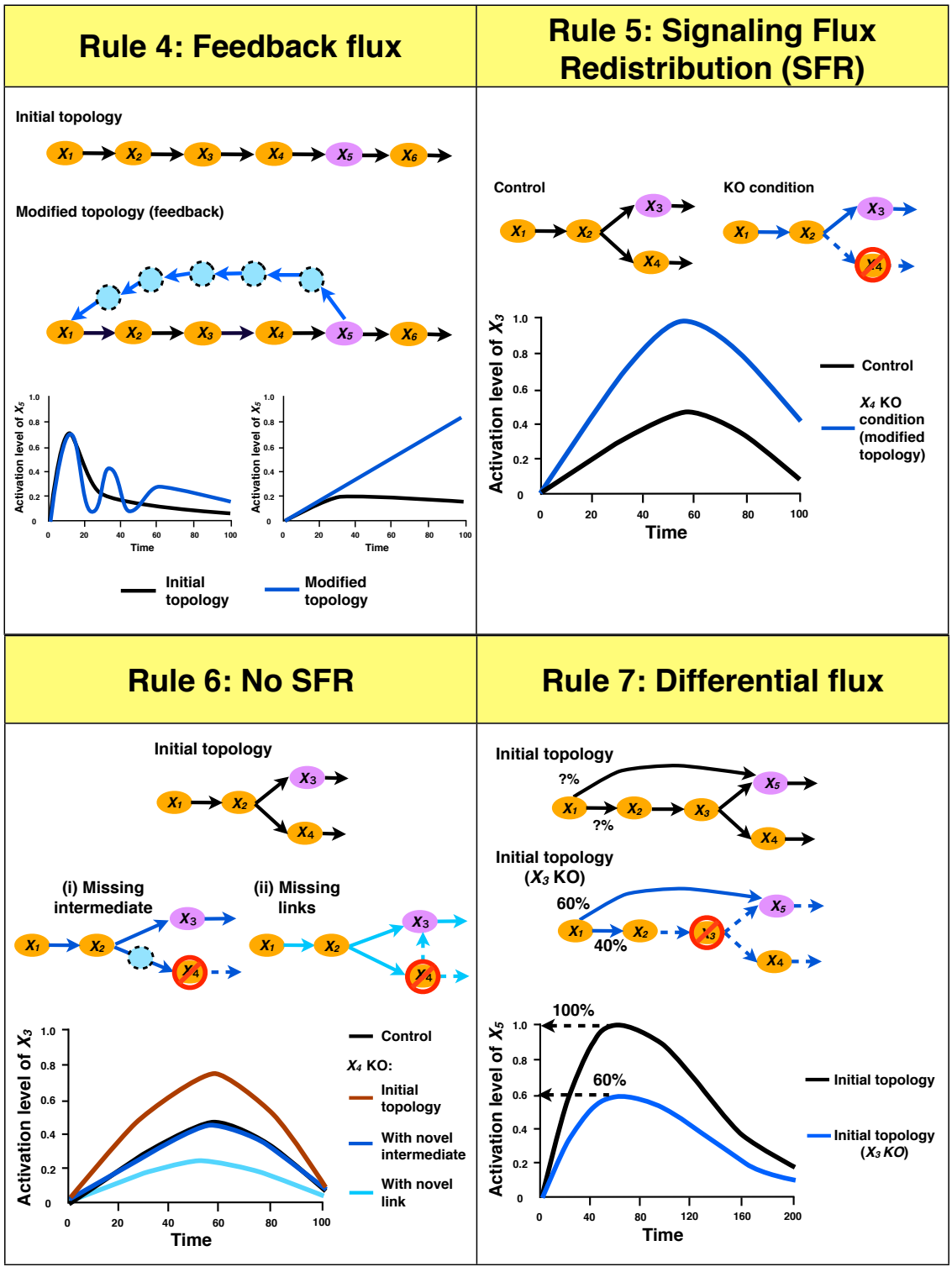

Figure 2.2 Response rules (continued)

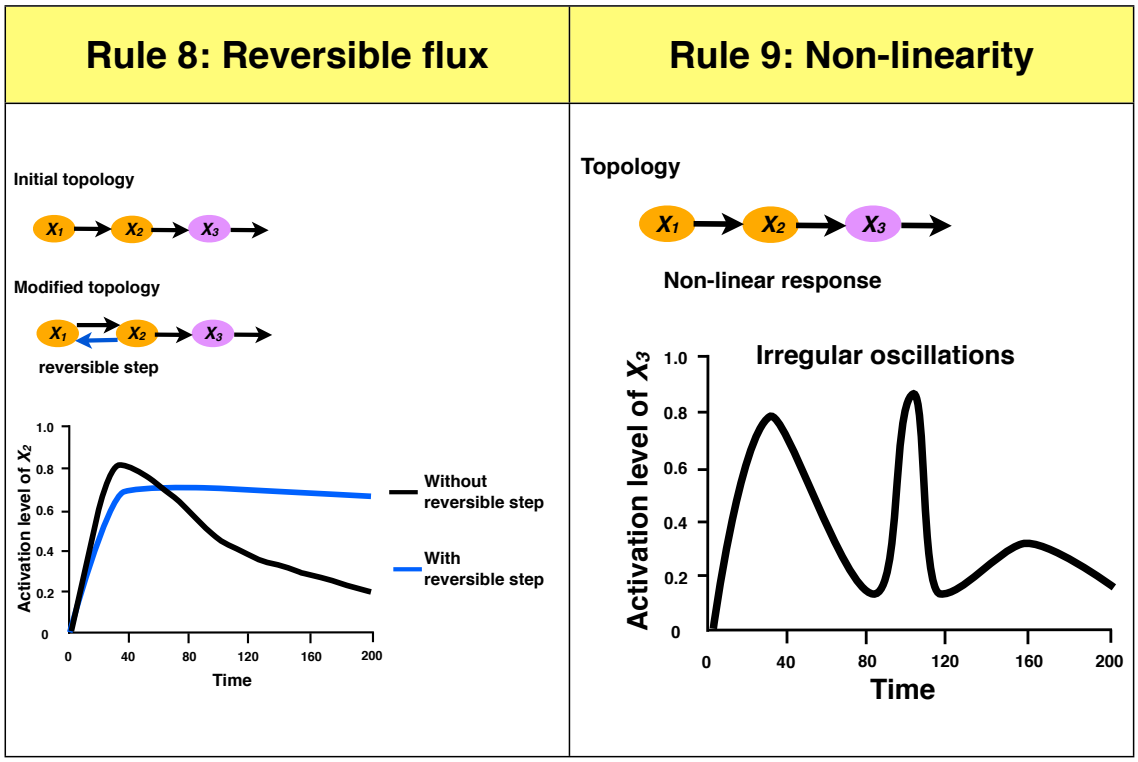

Figure 2.2 Response rules (continued)

Response rules. ***Rule 1, Controlling flux***: Controlling the upstream parameter (k_1) of a hypothetical molecule X_2 mostly affects the slope of the formation part of the expression profile. Alternatively, controlling the downstream parameter (k_2) mainly modifies the expression profile's depletion part. ***Rule 2, Time delay***: by comparing the time to reach peak activation, any time delay in target signaling molecule's activation represents 'missing' cellular features such as directed transport machinery, protein complex formation, and novel molecular interactions. ***Rule 3, Feedforward flux***: **(A)** *Rapid kinetics*: when simulation of a downstream molecule is noticeably quicker than experimental dynamics, **(B)** *Similar kinetics*: when removing a molecule along a pathway does not completely abolish its downstream intermediates, **(C)** *Delayed kinetics*: when removing a molecule along a pathway show significant delay. In all these cases, the superposition principle suggests a novel feedforward pathway with different number of intermediates. ***Rule 4, Feedback flux***: when a response profile shows multiple peaks or continuous increase of activation not following pulse perturbation response, this indicates feedback pathways such as posttranslational effect or secondary (autocrine/paracrine) signaling. ***Rule 5, Signaling Flux Redistribution (SFR)***: At pathway junctions, removing a molecule enhances the entire alternative pathways. ***Rule 6, No SFR***: At pathway junctions, removing a molecule does not enhance the alternative pathway, suggesting novel i) intermediate(s) between the removed molecule and the pathway junction or ii) pathway link between the removed molecule and the alternative pathway. ***Rule 7, Differential flux***: quantifies each pathway branch by comparing activation levels between wildtype and mutants data. ***Rule 8, Reversible flux***: when a response profile show limiting decay that cannot be modeled by first-order decay, the presence of reversible step is expected to produce limiting decay. ***Rule 9, Non-linearity***: When complex dynamics is observed, the linear response approach breaks down, and non-linear approaches are needed.

2.3.2 Simulating TNF-induced NF-κB and MAP kinase dynamics

The parameters of the initial model (rate constants, or the elements of Jacobian matrix ***J***, Materials and Methods) were estimated by fitting the simulation profiles with experimental profiles of signaling molecules where data is available. We obtained published semi-quantitative experimental profiles of IκBα phosphorylation (NF-κB activation) and p38 (MAP kinase) activation in wildtype and various genetically mutant MEFs generally treated with 10 ng/mL of TNF (Figure 2.3A, Figure 2.4 and Table 2.2) (Devin *et al.* 2000; Ermolaeva *et al.* 2008; Funakoshi-Tago *et al.* 2009; Tada *et al.* 2001). (Note that the kinetics of other MAP kinases, JNK and ERK, were also similar to p38 (Devin *et al.* 2000; Ermolaeva *et al.* 2008; Funakoshi-Tago *et al.* 2009; Tada *et al.* 2001). Thus, we used p38 as a representative MAP kinase for our investigation).

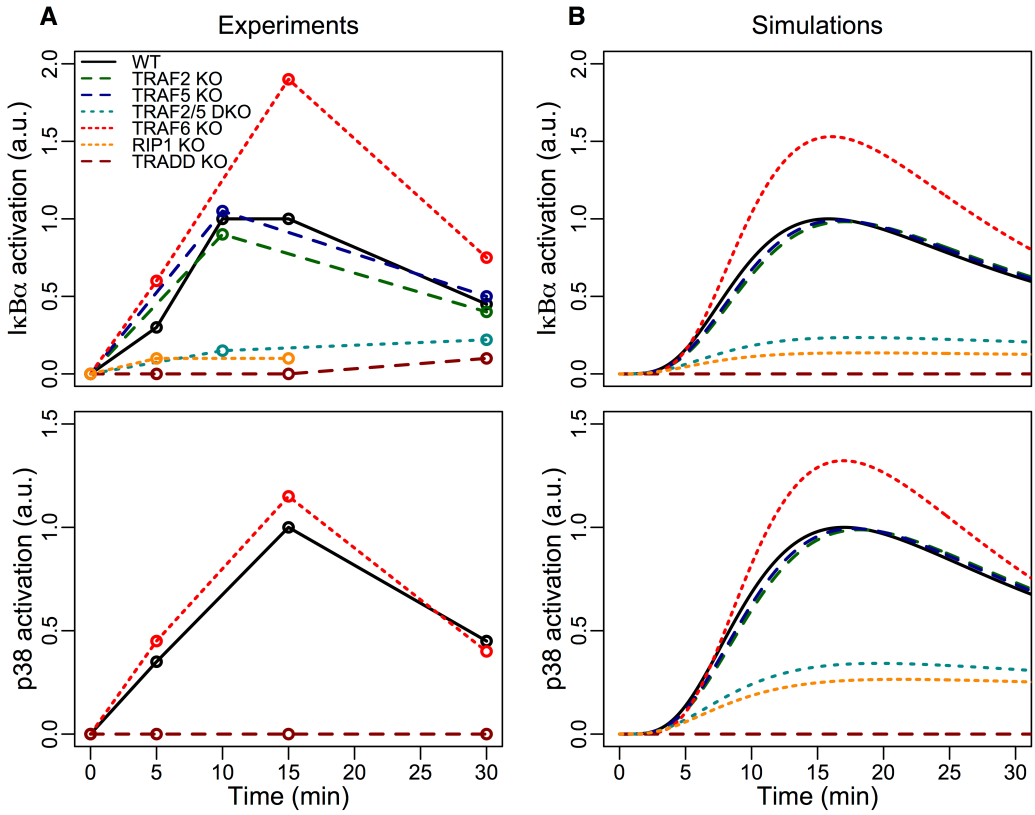

Figure 2.3 Experimental and simulated profiles of IκBα and p38 activations in wildtype and mutant conditions. (A) Experimental profiles, MEFs were generally treated with 10 ng/mL of TNF, and **(B)** simulated profiles of IκBα (top panels) and p38 (bottom panels) activations up to 30 min in wildtype (WT), TRAF2 KO, TRAF5 KO, TRAF2/TRAF5 double KO (TRAF2/5 DKO), TRAF6 KO, TRADD KO and up to 15 min in RIP1 KO. Note: p38 experimental profiles are available only for WT, TRAF6 KO and TRADD KO. Experimental details and data are found in references (Devin *et al.* 2000; Ermolaeva *et al.* 2008; Funakoshi-Tago *et al.* 2009; Tada *et al.* 2001). ImageJ was used to estimate the intensities of the activation dynamics (Table 2.1) for each molecule in each condition relative to wildtype peak activation values found in Figure 2.4. IκBα phosphorylation refers to NF-κB activation throughout the text.

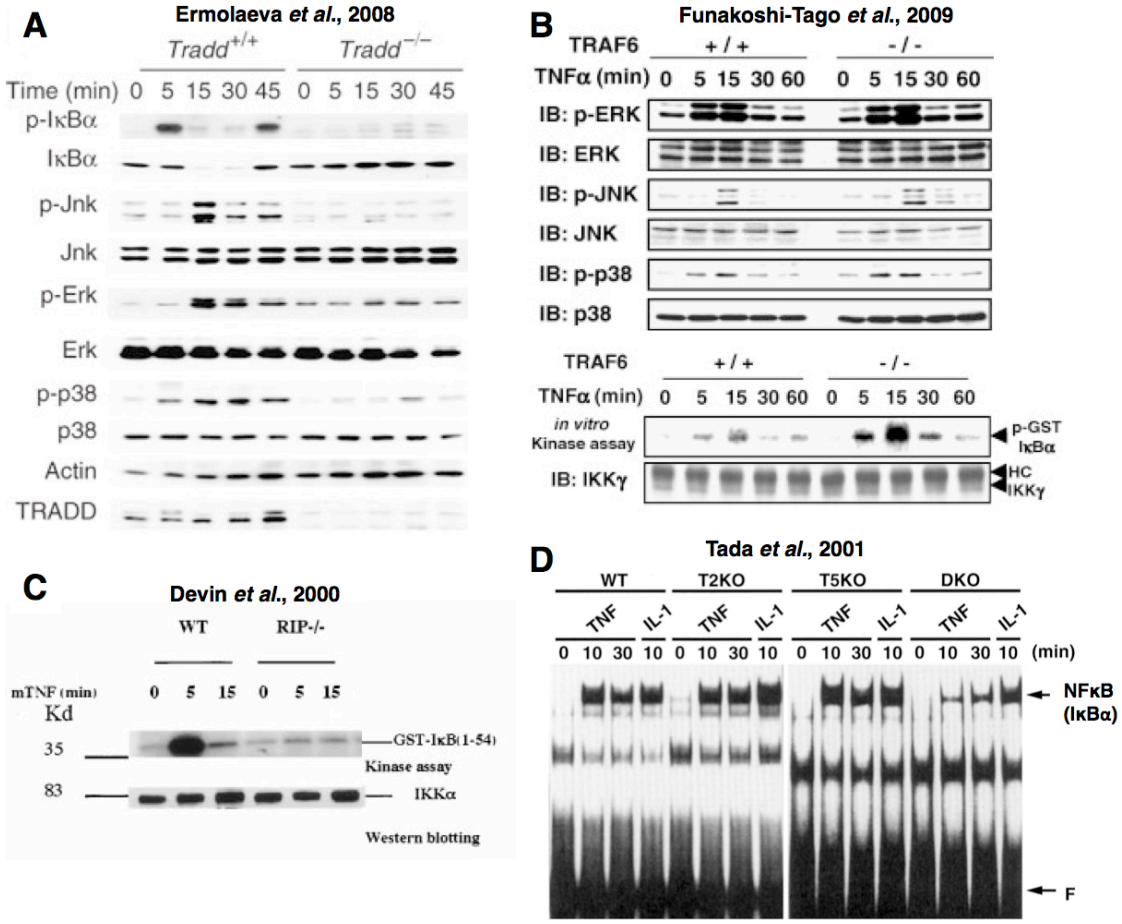

Figure 2.4 Experimental data used for model fitting.

ImageJ was used to estimate the intensities of the activation dynamics for each molecule in each condition relative to wildtype peak activation values. We obtained the temporal activation profiles of signaling molecules after TNF stimulation (10 ng/mL) in (**A**) wildtype and TRADD KO from Ermolaeva *et al.* (2008) (Fig. 1A, adapted) for p38 and IκBα, (**B**) wildtype and TRAF6 KO murine fibroblasts from Funakoshi-Tago *et al.* (2009) (Fig. 2B and 3B, adapted) for p38 and IκBα, (**C**) wildtype and RIP1 KO from Devin *et al.* (2000) (Fig. 1A, adapted) for IκBα, and (**D**) wildtype, TRAF2 KO, TRAF5 KO and TRAF2/5 double KO from Tada *et al.* (2001) (Fig. 1A, adapted) for IκBα. Figures adapted from their respective publications.

Table 2.2 Estimation of the relative intensities of IκBα and p38 activation dynamics

IκBα

Time (min)	WT[1]	TRADD KO[1]	TRAF6 KO[2]	TRAF2 KO[3]	TRAF5 KO[3]	TRAF2/5 DKO[3]	RIP1 KO[4]
0	0	0	0	0	0	0	0
5	0.3	0	0.6				0.1
10				0.9	1.05	0.15	
15	1	0	1.9				0.1
30	0.45	0.1	0.75	0.4	0.5	0.22	

p38

Time (min)	WT[1]	TRADD KO[1]	TRAF6 KO[2]
0	0	0	0
5	0.35	0	0.45
15	1	0	1.15
30	0.45	0	0.4

ImageJ was used to estimate the intensities of the activation dynamics for each molecule in each KO condition relative to wildtype peak activation values. Data was obtained from **(1)** Ermolaeva *et al.* (2008), **(2)** Funakoshi-Tago *et al.* (2009), **(3)** Tada *et al.* (2001), **(4)** Devin *et al.* (2000).

The parameter values were selected by using Genetic Algorithm (Carroll 1996) module in COPASI software (Hoops *et al.* 2006) to fit the experimental profiles (Figure 2.3A, WT). Following, we performed sensitivity analysis (Materials and Methods) of the model parameters and found them to be robust to a small degree of uncertainty to their values (Table 2.3). As a further validity of the parameter values, we tested the wildtype model in other conditions, namely TRAF2 KO, TRAF5 KO, TRAF2/5 double KO, TRAF6 KO, RIP1 KO and TRADD KO (Figure 2.3B). (Note that *in silico* KOs were generated from the wildtype model by setting the activation parameter value of the KO molecule to null).

Remarkably, we were able to obtain a single set of model parameters (Table 2.4, reactions 1–29), which could be used to simulate the semi-quantitative profiles of IκBα phosphorylation and p38 kinase activation in multiple experimental conditions. In wildtype, TRAF2 KO, TRAF5 KO and TRAF6 KO, the IκBα phosphorylation and p38 kinase activation reach peak values around 15 min and gradually decay at 30 min. Notably, TRAF6 KO shows enhanced IκBα phosphorylation and p38 kinase activation due to *Signaling Flux Redistribution* (*Response Rule 5*, Figure 2.2) (Selvarajoo *et al.* 2008). In the remaining conditions, the activation levels of both molecules are very weak (RIP1 KO and TRAF2/5 DKO) or absent (TRADD KO).

It is noteworthy that although there have been previous models on TNF signaling (Cho *et al.* 2003; Werner *et al.* 2005; Werner *et al.* 2008), to our knowledge,

this is the first time a single model of TNF signaling with fixed parameter values recapitulates the proinflammatory signaling dynamics in multiple experimental conditions.

To compare our linear response model (TNFR1 model A) simulations with other models that contain more detailed descriptions of IKK (Cho *et al.* 2003) and MAPK (Kholodenko 2000) signaling, using higher order terms and Michaelis-Menten type kinetics, we developed an alternative TNFR1 model B incorporating the relevant reaction details (Table 2.5). Notably, the simulations of TNFR1 models A and B show very similar dynamics for a fixed amount of TNF perturbation (Figure 2.5). Thus, we concur that our linear response model can be appropriately used for further investigations.

Table 2.3 Sensitivity analysis

k	Reaction			R				
				IκBα	p38	GI	GII	GIII
1	TNFR1	→	TRADD	0.18	0.13	0.04	0.00	0.00
2	TRADD	→	cIAP1/2	0.27	0.17	0.14	-0.01	0.01
3	cIAP1/2	→	TRAF2	0.01	0.00	0.00	0.00	0.00
4	cIAP1/2	→	TRAF5	0.01	0.00	0.00	0.00	0.00
5	TRAF2	→	RIP1	0.29	0.23	0.15	-0.01	0.01
6	TRAF5	→	RIP1	0.23	0.19	0.12	-0.01	0.00
7	TRADD	→	TRAF6	-0.26	-0.16	-0.14	0.01	-0.01
8	TRAF6	→	RIP1	0.09	0.08	0.08	0.04	0.01
9	TRAF6	→	TAK1 complex	0.11	0.22	0.22	0.16	0.03
10	RIP1	→	LUBAC	-0.02	0.38	0.32	0.15	0.02
11	RIP1	→	SHARPIN	0.05	-0.37	-0.33	-0.15	-0.02
12	LUBAC	→	TAK1 complex	0.00	0.00	0.00	0.00	0.00
13	SHARPIN	→	IKKγ	0.04	0.00	0.00	0.00	0.00
14	TAK1 complex	→	IKKγ	0.09	-0.82	-0.73	-0.41	-0.05
15	IKKγ	→	IκBα	0.06	0.00	0.00	0.00	0.00
16	IκBα	→	NF-κBc	-0.90	0.00	0.00	0.01	0.01
17	NF-κBc	→	NF-κBn	0.00	0.00	0.00	0.01	0.01
18	TAK1 complex	→	MKK1/2	-0.01	-0.01	0.05	0.03	0.00
19	TAK1 complex	→	MKK3/6	-0.04	0.92	0.34	0.19	0.03
20	TAK1 complex	→	MKK4/7	-0.04	-0.08	0.34	0.19	0.03
21	MKK1/2	→	ERK	0.00	0.00	0.01	0.00	0.00
22	MKK3/6	→	p38	0.00	0.13	0.01	0.00	0.00
24	MKK4/7	→	JNK	0.00	0.00	0.01	0.00	0.00
24	p38	→	p38n	0.00	-0.99	0.00	0.00	0.00
25	JNK	→	JNKn	0.00	0.00	0.00	0.00	0.00
26	ERK	→	ERKn	0.00	0.00	0.01	0.00	0.00
27	p38n	→	AP1	0.00	0.00	0.00	0.00	0.00
28	ERKn	→	AP1	0.00	0.00	0.00	0.00	0.00
29	JNKn	→	AP1	0.00	0.00	0.00	0.00	0.00
30	AP1	→	GI promoter	0.00	0.00	0.12	-0.48	-0.15
31	NF-κBn	→	GI promoter	0.00	0.00	0.09	0.00	-0.02
32	G1 promoter	→	GI pre-mRNA	0.00	0.00	0.00	0.00	0.00

k	Reaction			R				
				IκBα	p38	GI	GII	GIII
33	GI pre-mRNA	→	GI mRNA	0.00	0.00	0.00	0.00	0.00
34	GI mRNA	→	GI mRNA decay	0.00	0.00	-0.78	0.00	0.00
35	AP1	→	GII promoter	0.00	0.00	-0.09	0.51	-0.02
36	NF-κBn	→	GII promoter	0.00	0.00	0.00	0.43	-0.02
37	GII promoter	→	GII pre-mRNA/1	0.00	0.00	0.00	0.00	0.00
38	GII pre-mRNA/1	→	GII pre-mRNA/2	0.00	0.00	0.00	0.00	0.00
39	GII pre-mRNA/2	→	GII mRNA	0.00	0.00	0.00	0.00	0.00
40	GII mRNA	→	GII mRNA decay	0.00	0.00	0.00	-0.46	0.00
41	AP1	→	GIII promoter	0.00	0.00	-0.04	-0.02	0.16
42	NF-κBn	→	GIII promoter	0.00	0.00	0.00	0.00	0.04
43	GIII promoter	→	GIII pre-mRNA/1	0.00	0.00	0.00	0.00	0.00
44	GIII pre-mRNA/1	→	GIII pre-mRNA/2	0.00	0.00	0.00	0.00	0.05
45	GIII pre-mRNA/2	→	GIII pre-mRNA/3	0.00	0.00	0.00	0.00	0.02
46	GIII pre-mRNA/3	→	GIII mRNA	0.00	0.00	0.00	0.00	0.10
47	GIII mRNA	→	GIII mRNA decay	0.00	0.00	0.00	0.00	-0.32
48	GI mRNA	→	X1	0.00	0.00	0.00	0.00	0.00
49	NF-κBn	→	X1	0.00	0.00	-0.09	-0.42	0.00
50	X1	→	X2	0.00	0.00	0.00	0.02	0.06
51	X2	→	X3	0.00	0.00	0.00	0.02	0.06
52	X3	→	X4	0.00	0.00	0.00	0.02	0.06
53	X4	→	X5	0.00	0.00	0.00	0.02	0.06
54	X5	→	X6	0.00	0.00	0.00	0.02	0.06
55	X6	→	X7	0.00	0.00	0.00	0.02	0.06
56	X7	→	X8	0.00	0.00	0.00	0.02	0.06
57	X8	→	X9	0.00	0.00	0.00	0.02	0.06
58	X9	→	X10	0.00	0.00	0.00	0.02	0.06
59	X10	→	X11	0.00	0.00	0.00	0.02	0.06
60	X11	→	X12	0.00	0.00	0.00	0.02	0.06
61	X12	→	X13	0.00	0.00	0.00	0.02	0.06
62	X13	→	X14	0.00	0.00	0.00	0.02	0.06
63	X14	→	IkBa	0.00	0.00	0.00	0.02	-0.71
64	X14	→	Y	0.00	0.00	0.00	0.00	0.78
65	Y	→	GIII promoter	0.00	0.00	0.00	0.00	0.01

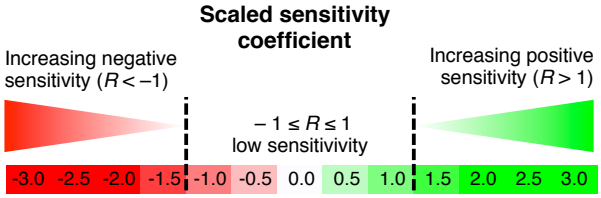

The scaled response sensitivity coefficients, R, of each molecule/gene response at peak activation time (p38: 15 min, IκBα: 15 min, Group I: 30 min, II: 2 h, and III: 12 h) indicate the relative changes in response when individual parameters (rows) are varied, such as a change of p% in the value of parameter k, results in a $R{\cdot}p$% change in the value of the peak activation of each molecule of interest. Absolute values of R higher than 1 indicate increasingly sensitive parameters.

Table 2.4 TNFR1 model A

	Reaction			Formula and parameters (s^{-1})						Remarks
1[1]	TNFR1	→	TRADD	k_1	*	TNFR1	k_1	=	5e-3	Activation of TRADD by TNFR1
2[2]	TRADD	→	cIAP1/2	k_2	*	TRADD	k_2	=	2e-2	Formation of Complex 1 containing TRADD, cIAP1/2, TRAF2, TRAF5, RIP1 and the TAB/TAK complex
3[3]	cIAP1/2	→	TRAF2	k_3	*	cIAP1/2	k_3	=	1e-2	
4[4]	cIAP1/2	→	TRAF5	k_4	*	cIAP1/2	k_4	=	8e-3	
5[5]	TRAF2	→	RIP1	k_5	*	TRAF2	k_5	=	1e-3	
6[5]	TRAF5	→	RIP1	k_6	*	TRAF5	k_6	=	1e-3	
7[6]	TRADD	→	TRAF6	k_7	*	TRADD	k_7	=	2e-2	Activation of TRAF6 by TRADD
8[5]	TRAF6	→	RIP1	k_8	*	TRAF6	k_8	=	1e-4	Activation of RIP1 and TAK1 complex by TRAF6
9[7]	TRAF6	→	TAK1 complex	k_9	*	TRAF6	k_9	=	1.3e-4	
10[8]	RIP1	→	LUBAC	k_{10}	*	RIP1	k_{10}	=	7e-3	Complex 1 ubiquitination by LUBAC and SHARPIN
11[9]	RIP1	→	SHARPIN	k_{11}	*	RIP1	k_{11}	=	7e-3	
12[7]	LUBAC	→	TAK1 complex	k_{12}	*	LUBAC	k_{12}	=	1e-1	
13	SHARPIN	→	IKK complex	k_{13}	*	SHARPIN	k_{13}	=	1e-2	Activation of IKK complex by Complex 1
14	TAK1 complex	→	IKK complex	k_{14}	*	TAK1 complex	k_{14}	=	1e-1	
15[10]	IKK complex	→	IκBα	k_{15}	*	IKK complex	k_{15}	=	1e-2	Phosphorylation of IκBα by IKK
16	IκBα	→	NF-κBc	k_{16}	*	IκBα	k_{16}	=	8e-3	Degradation of IκBα forms NF-κB
17	NF-κBc	→	NF-κBn	k_{17}	*	NF-κBc	k_{17}	=	1.7e-2	Translocation of NF-κB to nucleus
18	TAK1 complex	→	MKK1/2	k_{18}	*	TAK1 complex	k_{18}	=	1.5e-3	Activation of MAP kinases kinases by TAK1 complex
19[11]	TAK1 complex	→	MKK3/6	k_{19}	*	TAK1 complex	k_{19}	=	1e-2	
20	TAK1 complex	→	MKK4/7	k_{20}	*	TAK1 complex	k_{20}	=	1e-2	
21	MKK1/2	→	ERK	k_{21}	*	MKK1/2	k_{21}	=	5e-3	Activation of MAP kinases
22[12]	MKK3/6	→	p38	k_{22}	*	MKK3/6	k_{22}	=	5e-3	
24	MKK4/7	→	JNK	k_{23}	*	MKK4/7	k_{23}	=	5e-3	
24	p38	→	p38n	k_{24}	*	p38	k_{24}	=	5e-2	Translocation of MAP kinases into nucleus
25	JNK	→	JNKn	k_{25}	*	JNK	k_{25}	=	5e-2	
26	ERK	→	ERKn	k_{26}	*	ERK	k_{26}	=	5e-3	
27	p38n	→	AP1	k_{27}	*	p38n	k_{27}	=	1e-2	Activation of AP1 by MAP kinases
28	ERKn	→	AP1	k_{28}	*	ERKn	k_{28}	=	1e-2	
29	JNKn	→	AP1	k_{29}	*	JNKn	k_{29}	=	1e-2	
30	AP1	→	GI promoter	k_{30}	*	AP1	k_{30}	=	1e-1	Promoter binding of AP1 and NF-κB for group I genes
31	NF-κBn	→	GI promoter	k_{31}	*	NF-κBn	k_{31}	=	5e-3	
32	G1 promoter	→	GI pre-mRNA	k_{32}	*	GI promoter	k_{32}	=	1e-2	Group I genes transcription, splicing (1 step) and decay
33	GI pre-mRNA	→	GI mRNA	k_{33}	*	GI pre-mRNA	k_{33}	=	5e-2	
34	GI mRNA	→	GI mRNA decay	k_{34}	*	GI mRNA	k_{34}	=	2e-3	
35[13]	AP1	→	GII promoter	k_{35}	*	AP1	k_{35}	=	1.1e-2	Promoter binding of AP1 and NF-κB for group II genes
36	NF-κBn	→	GII promoter	k_{36}	*	NF-κBn	k_{36}	=	4e-3	
37	GII promoter	→	GII pre-mRNA/1	k_{37}	*	GII promoter	k_{37}	=	2e-3	Group II genes transcription, splicing (2 steps) and decay
38	GII pre-mRNA/1	→	GII pre-mRNA/2	k_{38}	*	GII pre-mRNA/1	k_{38}	=	5e-2	
39	GII pre-mRNA/2	→	GII mRNA	k_{39}	*	GII pre-mRNA/2	k_{39}	=	5e-2	
40[13]	GII mRNA	→	GII mRNA decay	k_{40}	*	GII mRNA	k_{40}	=	1.2e-4	

Table 2.4 TNFR1 model A (continued)

41	AP1	→	GIII promoter	k_{41}	*	AP1	k_{41}	=	5e-3	Promoter binding of AP1 and NF-κB for group III genes
42	NF-κBn	→	GIII promoter	k_{42}	*	NF-κBn	k_{42}	=	1e-4	
43	GIII promoter	→	GIII pre-mRNA/1	k_{43}	*	GIII promoter	k_{43}	=	1e-1	Group III genes transcription, splicing (3 steps) and decay
44	GIII pre-mRNA/1	→	GIII pre-mRNA/2	k_{44}	*	GIII pre-mRNA/1	k_{44}	=	4e-4	
45	GIII pre-mRNA/2	→	GIII pre-mRNA/3	k_{45}	*	GIII pre-mRNA/2	k_{45}	=	1e-3	
46	GIII pre-mRNA/3	→	GIII mRNA	k_{46}	*	GIII pre-mRNA/3	k_{46}	=	2e-4	
47	GIII mRNA	→	GIII mRNA decay	k_{47}	*	GIII mRNA	k_{47}	=	2e-5	
48	***GI mRNA***	→	***X1***	k_{48}	*	GI mRNA	k_{48}	=	1e-5	Feedback processes via group I genes or NF-κB
49	***NF-κBn***	→	***X1***	k_{49}	*	NF-κBn	k_{49}	=	5e-1	
50	***X1***	→	***X2***	k_{50}	*	X1	k_{50}	=	2e-3	
51	***X2***	→	***X3***	k_{51}	*	X2	k_{51}	=	2e-3	
52	***X3***	→	***X4***	k_{52}	*	X3	k_{52}	=	2e-3	
53	***X4***	→	***X5***	k_{53}	*	X4	k_{53}	=	2e-3	Steps of the secondary feedback processes (cytosolic or autocrine signaling): • expression (e.g. translation) • transport (e.g. secretion) • signaling (e.g. receptor binding, activation of transcription factors)
54	***X5***	→	***X6***	k_{54}	*	X5	k_{54}	=	2e-3	
55	***X6***	→	***X7***	k_{55}	*	X6	k_{55}	=	2e-3	
56	***X7***	→	***X8***	k_{56}	*	X7	k_{56}	=	2e-3	
57	***X8***	→	***X9***	k_{57}	*	X8	k_{57}	=	2e-3	
58	***X9***	→	***X10***	k_{58}	*	X9	k_{58}	=	2e-3	
59	***X10***	→	***X11***	k_{59}	*	X10	k_{59}	=	2e-3	
60	***X11***	→	***X12***	k_{60}	*	X11	k_{60}	=	2e-3	
61	***X12***	→	***X13***	k_{61}	*	X12	k_{61}	=	2e-3	
62	***X13***	→	***X14***	k_{62}	*	X13	k_{62}	=	2e-3	
63	***X14***	→	***IκBα***	k_{63}	*	X14	k_{63}	=	2e-3	IκBα feedback activation
64	***X14***	→	***Y***	k_{64}	*	X14	k_{64}	=	1e-5	Group III feedback activation via transcription factor Y
65	***Y***	→	***GIII promoter***	k_{65}	*	Y	k_{65}	=	2e-3	

Table 2.4 TNFR1 model A

(1–12): *in-silico* knock-out conditions are performed by setting parameter values (k_i) to 0 for targeted reactions in TRADD KO **(1)**, cIAP1/2 KO **(2)**, TRAF2 KO **(3)**, TRAF5 KO **(4)** TRAF2/5 DKO **(3,4)**, RIP KO **(5)**, TRAF6 KO **(6)**, TAK1 complex KO **(7)**, LUBAC KO **(8)**, SHARPIN KO **(9)**, IκBα KO **(10)**, MKK3/6 KO **(11)** and p38 KO **(12).** **(13)** Kinetics of Group II mRNA transcription and decay processes were refitted after adding feedback (without feedback: k_{35} = 7e-3, k_{40} = 1.2e-5). Bold italic fonts (reactions 48–65) indicate additional feedback activation pathways required for group III continuous activation. * indicates the multiplication sign.

Table 2.5 TNFR1 model B

	Reaction	Formula and parameters		Remarks
1	TNFR1 → TRADD	k_1 * TNFR1	k_1 = 5e-3	Activation of TRADD by TNFR1
2	TRADD → cIAP1/2	k_2 * TRADD	k_2 = 2e-2	Formation of Complex 1 containing TRADD, cIAP1/2, TRAF2, TRAF5, RIP1 and the TAB/TAK complex
3	cIAP1/2 → TRAF2	k_3 * cIAP1/2	k_3 = 1e-2	
4	cIAP1/2 → TRAF5	k_4 * cIAP1/2	k_4 = 8e-3	
5	TRAF2 → RIP1	k_5 * TRAF2	k_5 = 1e-3	
6	TRAF5 → RIP1	k_6 * TRAF5	k_6 = 1e-3	
7	TRADD → TRAF6	k_7 * TRADD	k_7 = 2e-2	Activation of TRAF6 by TRADD
8	TRAF6 → RIP1	k_8 * TRAF6	k_8 = 1e-4	Activation of RIP1 and TAB/TAK by TRAF6
9	TRAF6 → TAK1	k_9 * TRAF6	k_9 = 1.3e-4	
10	RIP1 → LUBAC	k_{10} * RIP1	k_{10} = 7e-3	Complex 1 ubiquitination by LUBAC and SHARPIN
11	RIP1 → SHARPIN	k_{11} * RIP1	k_{11} = 7e-3	
12	LUBAC → TAK1	k_{12} * LUBAC	k_{12} = 1e-1	
13	SHARPIN → IKKγ	k_{13} * SHARPIN	k_{13} = 1e-2	Activation of IKK complex by Complex 1
14	TAK1 → IKKγ	k_{14} * TAK1	k_{14} = 1e-1	
15	IKKγ + IκBα/NF-κB → IκB complex	k_{15} * IKKγ * IκBα/NF-κB	k_{15} = 2.1e-3	Formation of the IκB complex (IKKγ/IκBα/NF-κB) (and reverse step)
16	IκB complex → IKKγ + IκBα/NF-κB	k_{16} * IκB complex	k_{16} = 8.9e-7	
17	IκB complex → IKKγ + IκBα + NF-κB	k_{17} * IκB complex	k_{17} = 2e0	Dissociation of the IκB complex into IKKγ, phosphorylated IκBα and NF-κB
18	IκBα → IκBα degradation	k_{18} * IκBα	k_{18} = 1.7e-2	Degradation of IκBα
19	IKKγ → IKKγ degradation	k_{19} * IKKγ	k_{19} = 4.6e-3	Degradation of IKKγ
20	NF-κB → NF-κBn	k_{20} * NF-κB	k_{20} = 1.5e-2	Translocation of NF-κB to nucleus
21	TAK1 + TAB → TAK1/TAB	k_{21} * TAK1 * TAB	k_{21} = 1e-2	Formation and degradation terms for the TAK1/TAB complex
22	TAK1/TAB → TAK1/TAB degradation	k_{22} * TAK1/TAB	k_{22} = 7.1e-2	
23	MKK → MKKp	$\frac{k_{23} * (MKK * TAK1/TAB)}{(K_{23} + MKK)}$	k_{23} = 2.7e-2 K_{23} = 5.9e-2	Activation (double phosphorylation) of MAP kinase kinases (MKKs, e.g. MKK3/6) by the TAK1/TAB complex
24	MKKp → MKK	$\frac{V_{24} * (MKKp)}{(K_{24} + MKKp)}$	V_{24} = 5.7e-4 K_{24} = 2.9e-2	
25	MKKp → MKKpp	$\frac{k_{25} * (MKKp * TAK1/TAB)}{(K_{25} + MKKp)}$	k_{25} = 2.6e-2 K_{25} = 1.9e-7	
26	MKKpp → MKKp	$\frac{V_{26} * (MKKpp)}{(K_{26} + MKKpp)}$	V_{26} = 3.8e-4 K_{26} = 9e-2	
27	MAPK → MAPKp	$\frac{k_{27} * (MAPK * MKKpp)}{(K_{27} + MAPK)}$	k_{27} = 6.1e-2 K_{27} = 3.9e-1	Activation (double phosphorylation) of MAP kinases (MAPKs, e.g. p38) by MKKs
28	MAPKp → MAPK	$\frac{V_{28} * (MAPKp)}{(K_{28} + MAPKp)}$	V_{28} = 9.7e-5 K_{28} = 5.2e-4	
29	MAPKp → MAPKpp	$\frac{k_{29} * (MAPKp * MKKpp)}{(K_{29} + MAPKp)}$	k_{29} = 2.5e-1 K_{29} = 9.9e-7	
30	MAPKpp → MAPKp	$\frac{V_{30} * (MAPKp}{(K_{30} + MAPKp)}$	V_{30} = 2.6e-6 K_{30} = 4.4e-1	
31	MAPKpp → MAPKn	k_{31} * MAPKpp	k_{31} = 8.2e-2	Translocation of MAPKs into nucleus
32	MAPKn → AP1	k_{32} * MAPKn	k_{32} = 1e-2	Activation of AP1 by MAPKs

Table 2.5 TNFR1 model B (continued)

Initial concentrations (nmol.mL^{-1}): $[TNFR1]_{t=0}$ = 1, $[TAB]_{t=0}$ = 1, $[MAPK]_{t=0}$ = 46, $[MKK]_{t=0}$ = 52, $[I\kappa B/NF\text{-}\kappa B]_{t=0}$ = 5. Units: K_i in nmol.mL^{-1}, V_i in nmol.mL^{-1}.s^{-1}, k_i in s^{-1} except k_{15} and k_{21} in mL.nmol^{-1}.s^{-1} Colored rows indicate IKK (orange) and MAPK (light purple) modules adapted from Cho *et al.* (2003) and Kholodenko (2000) respectively. Parameters and initial concentrations were determined through automated fitting of wildtype model using Genetic Algorithm optimization module in COPASI software.

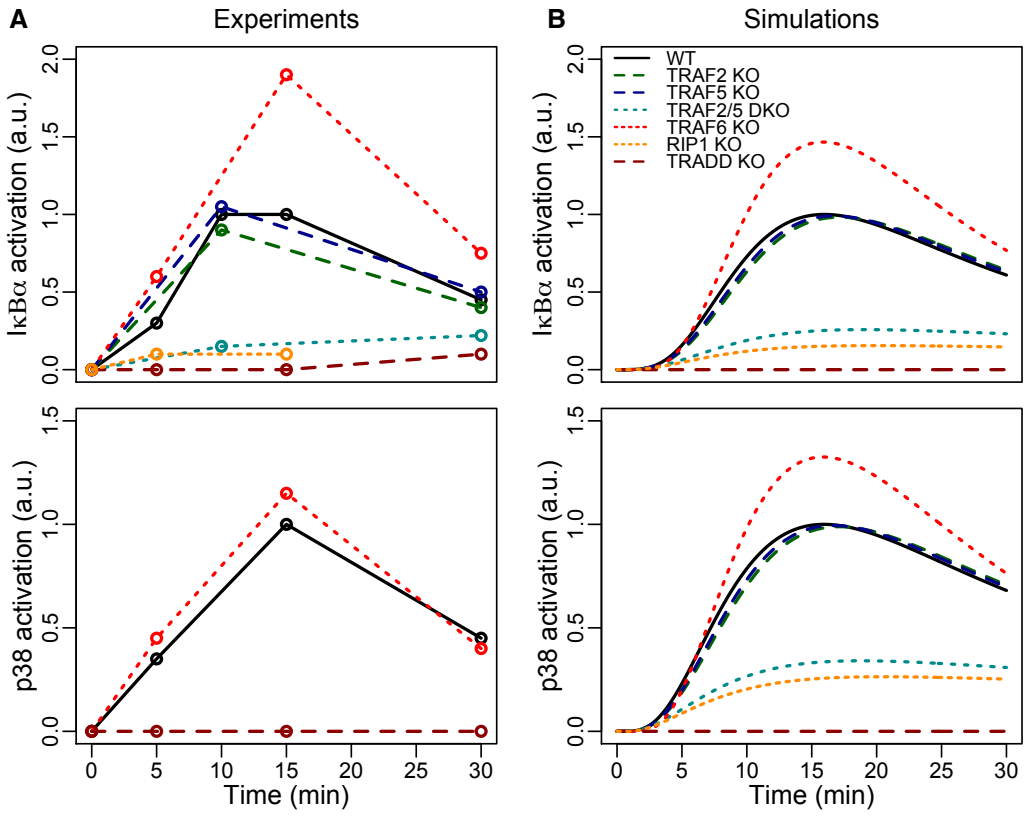

Figure 2.5 Experimental vs. simulated profiles of IκBα and p38 activations in wildtype and mutant conditions using model B. (A) Experimental profiles and **(B)** simulated profiles of TNFR1 model B (see Table 2.5) for IκBα (top panels) and p38 (bottom panels) activations.

2.3.3 Simulating distinct TNF-induced gene expression patterns

Next, we extended the TNFR1 model (we will now simply call TNFR1 model A as TNFR1 model) to simulate downstream proinflammatory gene expression dynamics. Recently, time-series high throughput microarray and quantitative real time PCR experiments on TNF simulated mouse 3T3 fibroblasts cells have revealed 3 distinct groups of upregulated gene expression patterns, with possibly corresponding distinct biological roles (Hao *et al.* 2009; Hao *et al.* 2013). The groups were labeled into "early I", "intermediate or middle II" and "late III" response, according to their time to reach peak expressions between 0.5-1, 2-3, and 6-12 h, respectively, after TNF stimulation (Figure 2.6A) (Hao *et al.* 2009; Hao *et al.* 2013; Tian *et al.* 2005). Here, we extended the TNFR1 model to simulate the temporal profiles of the 3 groups of gene expressions.

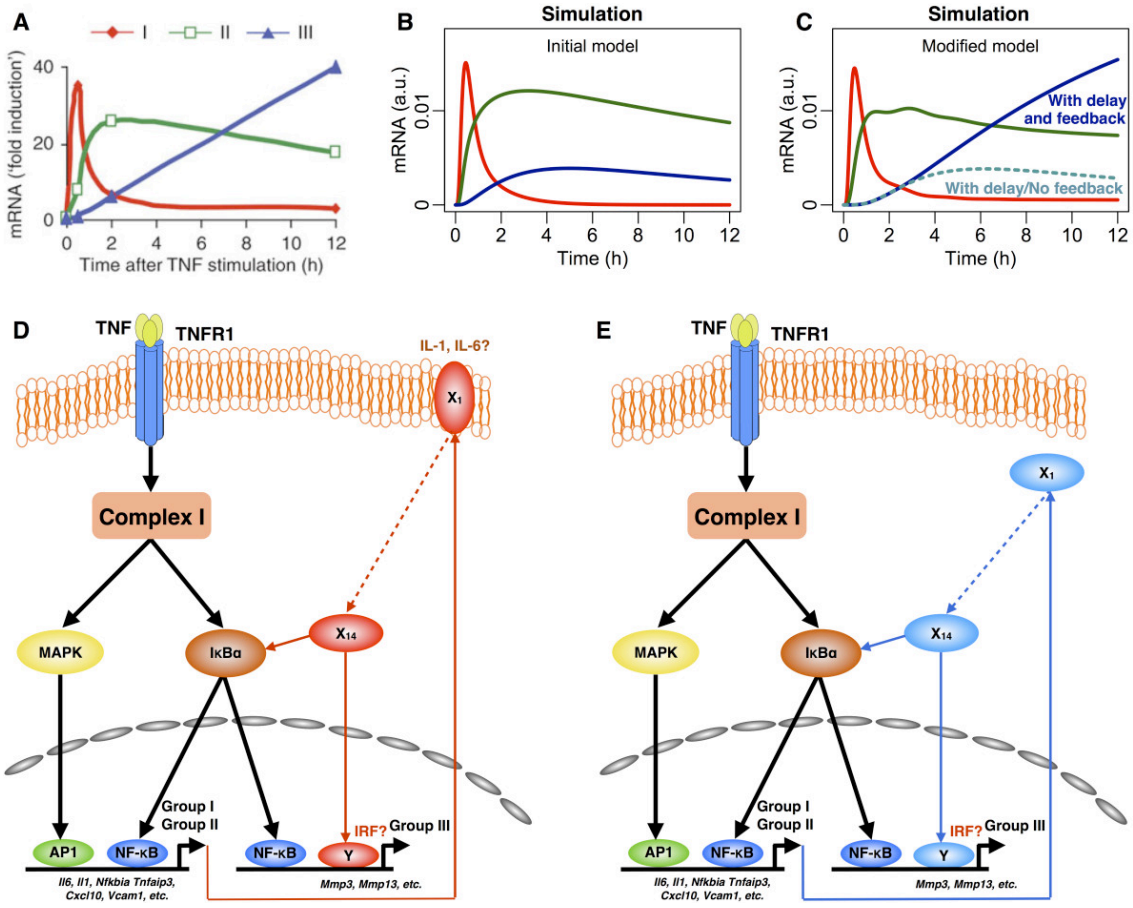

Figure 2.6 Three distinct groups of TNF-activated genes. (A) Average expression profiles of genes in groups I (red), II (green) and III (blue) in 3T3 fibroblasts stimulated for 0.5, 2 or 12 h with recombinant mouse TNF. Figure was reproduced from Hao *et al.* (2009). **(B)** Simulation profiles of the 3 groups of genes using TNFR1 model. **(C)** Simulation of the modified TNFR1 model with transcriptional delay and novel feedback mechanisms (solid lines) or with transcriptional delay and without feedback mechanisms (dotted lines) or with transcriptional delay and novel feedback mechanisms (solid lines). **(D, E)** Proposed novel feedback pathway to provide additional signaling flux through translation of group I genes into proteins for autocrine signaling (red lines; **D)** or cytosolic positive feedback (blue lines; **E)**. Red and blue dotted lines indicate several intermediary molecular reactions (refer to Table 2.4). X_1 to X_{14} refer to the novel intermediates included in the updated TNFR1 model (refer to Table 2.4, reactions 48–65), and Y refers to a novel transcription factor.

According to our modeling approach, the time to peak activation can be controlled by reaction parameter values and/or the number of signaling intermediates (Helmy *et al.* 2009; Piras *et al.* 2011; Selvarajoo 2006; Selvarajoo *et al.* 2008; Selvarajoo *et al.* 2009). Briefly, decreasing (increasing) the activation or transcription parameter value will show lower (sharper) gradients of formation part of the expression profiles. Alternatively, decreasing (increasing) the deactivation or decay parameter value will show lower (sharper) gradients of depletion part of expression profiles (*Response Rule 1*, Figure 2.2). In addition, inserting intermediary reactions between transcription process and gene induction will increase delay for gene expression dynamics (*Response rule 2*, Figure 2.2). The intermediates can represent the complexities of transcription process involving the pre-initiation, initiation, promoter clearance, elongation and termination (Solomon *et al.* 2011), or post-transcriptional processes such as messenger RNA editing and splicing. Using this approach, the TNFR1 model was extended to simulate the temporal dynamics of group I, II and III genes. Note that the *response rules* (Figure 2.2) are used to modify an initial signaling topology only after all parameter space has been exhaustively searched, and a reasonable model fit is unable to be achieved (Piras *et al.* 2011).

Previous investigations on the 3 groups of genes have indicated distinct mechanisms for the differential dynamical response (Hao *et al.* 2009; Hao *et al.* 2013). Hao and Baltimore have found lesser presence of AU Rich Element (ARE) region on

the 3'UTR of group III genes, targeted by microRNAs and ARE-binding proteins (such as tristetraprolin) that enhance RNA decay processes. Hence, it was postulated as one possible reason for the lower decay response of group III genes compared with genes from groups I and II (Hao *et al.* 2009). More recently, by studying the kinetics of pre-mRNA and mRNA, Hao and Baltimore observed delays in splicing of groups II and III genes compared to group I genes. The differential delays were suggested as another biological mechanism for the distinct gene profiles (Hao *et al.* 2013).

In our extended model, we, therefore, considered both mechanisms to reproduce the temporal profiles of the 3 groups of genes. Notably, our simulations of pre-mRNA and mRNA for all groups of genes matched the data of Hao and Baltimore for the first 60 min (Figure 2.7). However, subsequently for 12 h, although the simulations of group I and II genes were recapitulated, group III simulation was poor (Figure 2.6B, blue line). Specifically, reducing the parameter value for the decay term representing lower miRNA and ARE-binding proteins regulating decay processes (*Response rule 1*, Figure 2.2), and adding intermediates (*Response rule 2*, Figure 2.2) to provide delays in RNA splicing in our model were not sufficient to produce the continuous activation of group III genes (Figure 2.6C, cyan dotted line).

To overcome the shortfall in the model simulations, we hypothesized that novel activation or transcription term(s) (positive feedback) may be present to provide additional flux for the continuous increase in group III expressions (*Response rule 4*,

Figure 2.2). This could result from secondary post-transcriptional/translational mechanisms through i) autocrine signaling such as IL-1 (Chaudhry *et al.* 2013), IL-6 (Grivennikov *et al.* 2008) or TGF-β (Ihn 2008) signaling (Figure 2.6D), or ii) cytosolic feedback mechanisms specifically for group III genes (Hoffmann *et al.* 2002) (Figure 2.6E). Thus, a novel feedback mechanism predominantly affecting the transcription of group III genes was added to the TNFR1 model (Table 2.4, equations 30–65).

The modified TNFR1 model with feedback mechanisms to group III genes produced simulations that matched all 3 groups of gene expression profiles (Figure 2.6A and 2.6C, solid lines). To scrutinize the feedback mechanism, we re-monitored the simulation profile of NF-κB for 10 hours (Figure 2.8). The resultant profile mimics the damped oscillatory dynamics of NF-κB previously observed in murine fibroblasts (Hoffmann *et al.* 2002). Overall, these data suggest that low miRNA regulation and additional delay in RNA splicing are not sufficient to produce the continuous activation of group III genes, and that a novel transcription process, possibly through secondary post-transcriptional/translational autocrine signaling, such as IL-1 signaling or other novel feedback mechanisms that activate NF-κB, and not MAPK (Figure 2.8), are required.

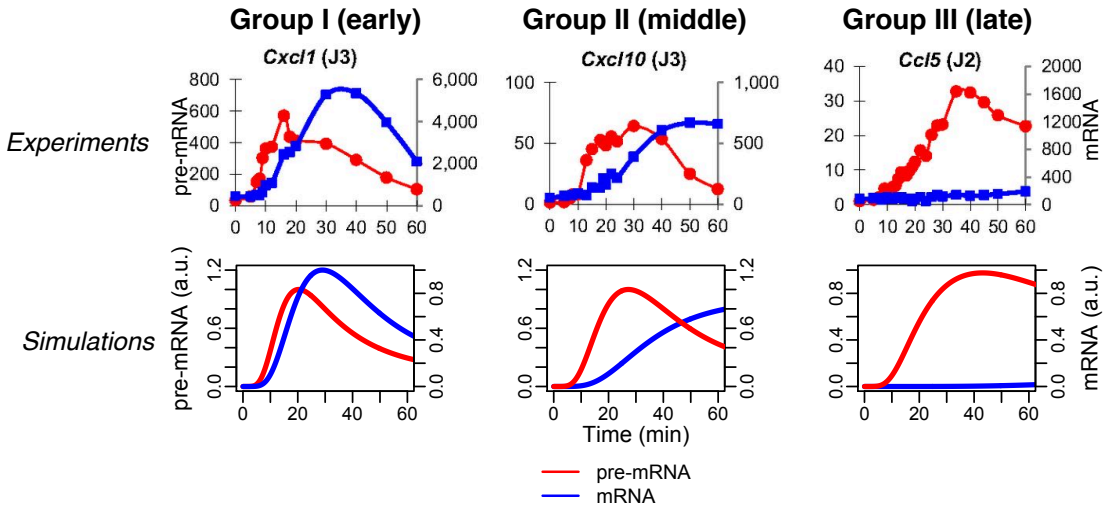

Figure 2.7 Simulation of pre-mRNA and mRNA expression profiles of the 3 groups of genes. Upper panels: experimental pre-mRNA (red lines) and mRNA (blue lines) expression profiles in 3T3 cells of 3 representative genes from groups I, II and III, respectively, up to 60 minutes after TNF stimulation (10 ng/mL). **Lower panels:** simulations of pre-mRNA (red lines) and mRNA (blue lines) expressions using updated TNFR1 model. Upper panels are obtained from Hao & Baltimore (2013).

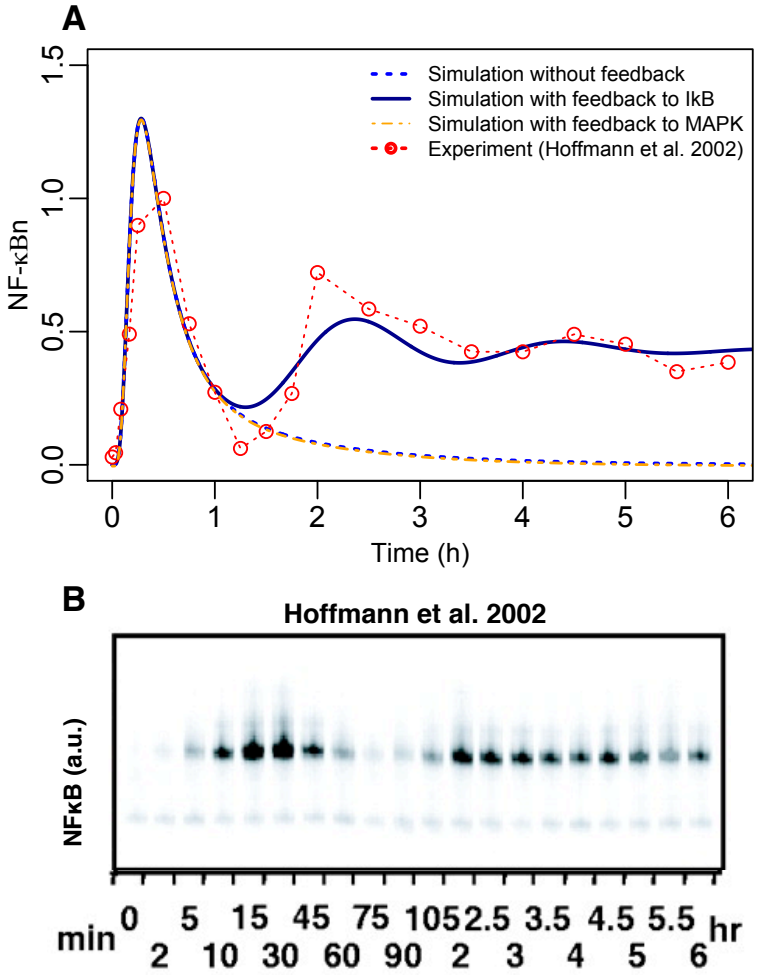

Figure 2.8 Simulation of NF-κB activation profiles with and without feedback mechanisms. (**A**) Simulations of nuclear NF-κB activation profiles up to 6 hours after TNF stimulation in wildtype condition without (dotted blue lines) feedback mechanisms and with feedback mechanism branched to IκBα (solid blue lines) or MAP kinases pathway (dotted orange lines) activation, are compared with experimental profiles obtained in TNF stimulated (10 ng/mL) 3T3 cells (red dots). (**B**) ImageJ was used to estimate the intensities of the activation dynamics relative to peak activation values from the data presented in Hoffmann *et al.* (2002) (Fig. 2E, adapted).

2.3.4 Predicting key target for regulating proinflammatory response

Now that the TNFR1 model is able to successfully simulate the three groups of upregulated genes in wildtype, we investigated the significance and effect of removing or suppressing key intracellular signaling molecules for controlling proinflammatory response, *in silico*.

It is well known that TNFR1 signaling is enhanced in proinflammatory diseases and cancer (Balkwill 2009; Bradley 2008; Locksley *et al.* 2001; O'Malley *et al.* 1962). To investigate which known molecules would be potential target to regulate the cell survival or proinflammatory activity, we performed *in silico* KOs of all possible signaling molecules within the TNFR1 model. In total, we simulated groups I, II and III dynamic gene expressions in 12 (TRADD, cIAP1/2, TRAF2, TRAF5, TRAF6, RIP1, SHARPIN, LUBAC, TAK1 complex (TAK1/TAB1/2), IκBα, MKK3/6 and p38) KO conditions and compared with wildtype profiles (Figure 2.9).

Among the candidates, the removal of TAK1 complex or RIP1 produced the most noticeable downregulation of all 3 gene groups, which chiefly consist of well-known proinflammatory mediators (Figure 2.10). However, in TAK1 complex KO, our simulations show almost no induction for group 1 genes. The substantial impairment in gene expressions (> 90%) is usually detrimental to the general survivability of living cells, and this has been particularly demonstrated in

TAK1-deficient mice (Lamothe *et al.* 2013; Tang *et al.* 2008). RIP1, on the other hand, showed about 50-70% impairment compared to wildtype peak expressions. Our simulations, therefore, suggest that RIP1 is possibly a crucial single molecule target for controlling enhanced proinflammatory response due to TNFR1 signaling in proinflammatory disease conditions, such as in rheumatoid arthritis, without compromising the normal functioning of other cellular activities.

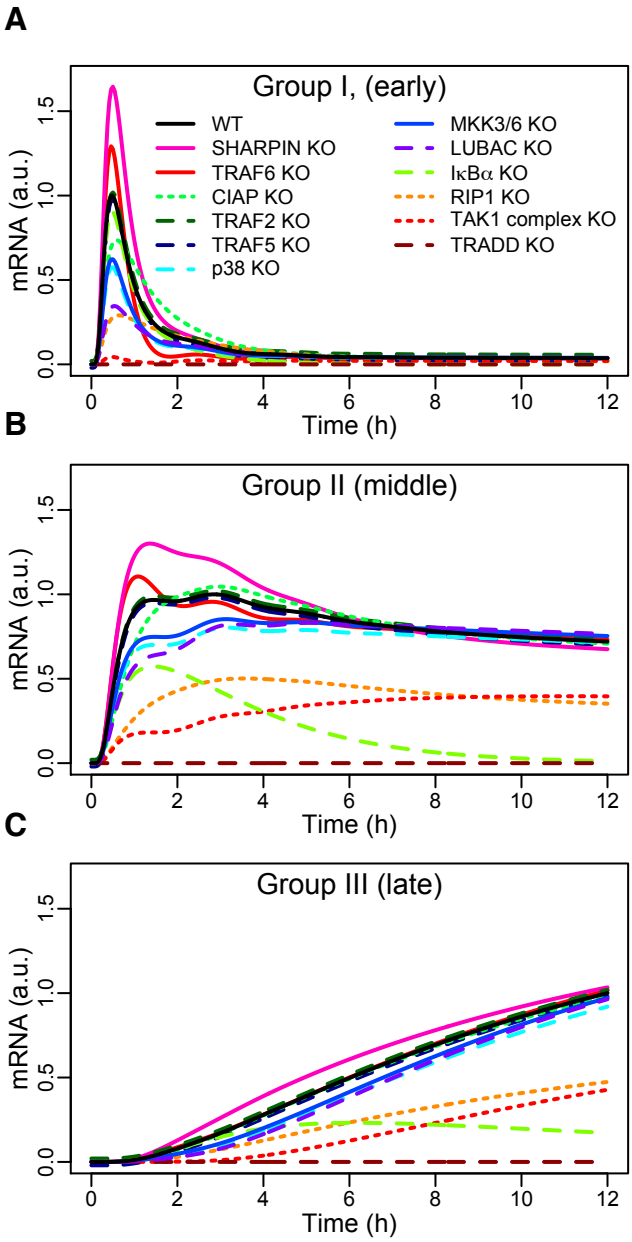

Figure 2.9 The effects of *in silico* KOs on the expression profiles of the 3 groups of genes. Simulated expression profiles of groups I **(A)**, II **(B)**, and III **(C)** genes in wildtype and 12 *in silico* KOs conditions for 12 hours using the modified TNFR1 model A (with feedback).

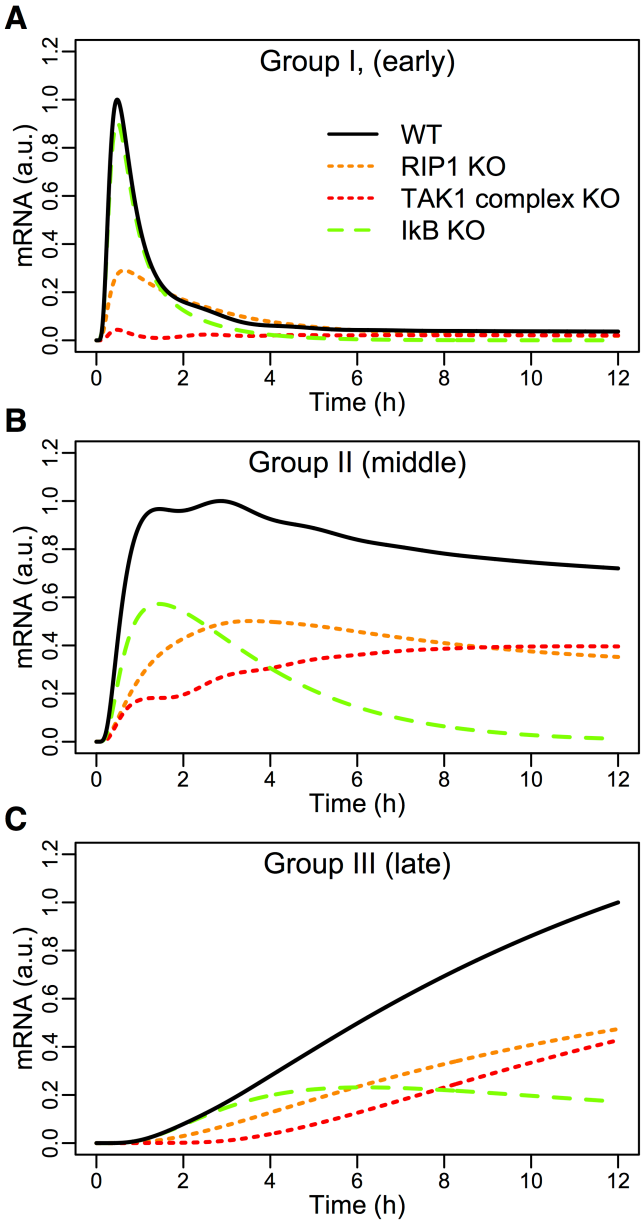

Figure 2.10 The effects of *in silico* KOs on the expression profiles of the 3 groups of genes (best candidates). Simulated expression profiles of group I **(A)**, group II **(B)**, and group III **(C)** genes in 4 experimental conditions: wildtype (WT), IκBα KO, RIP1 KO and TAK1 complex KO for 12 hours using the modified TNFR1 model (with feedback). Predictions of RIP1 KO (orange curves) indicate suppression, but not abolishment, of all groups of gene expressions compared to wildtype (black curve).

2.3.5 Experimental inhibition of RIP1 downregulates proinflammatory genes in TNF stimulation

To verify the predictions of TNFR1 model simulations, we prepared corresponding MEF and BALB/3T3 cells treated with TNF in wildtype and in RIP1 suppression. Necrostatin-1 (Nec-1) was originally identified as a potent small molecule inhibitor of necroptosis or non-apoptotic cell death (Degterev *et al.* 2005). Further interests in Nec-1 led to its specificity towards the inhibition of RIP1 (Degterev *et al.* 2008). Although Nec-1 has recently been extensively studied, its effect on the expressions of groups I, II and III genes in TNF stimulation remains largely unknown. Therefore, here, we used Nec-1 to suppress RIP1 *in vivo*.

To check the effect of cell death by Nec-1, we compared MEF and BALB/3T3 cells treated with different doses of Nec-1 in the presence or absence of TNF (Figure 2.11). The data revealed that Nec-1 has no substantial effect on cell death after 24 h incubation, and hence, could be tested for its efficacy on the 3 groups of genes. We next performed quantitative RT-PCR for a total of 10 genes: *Il6*, *Tnfaip3*, *Jun*, *Nfkbia* (group I), *Ccl7*, *Vcam1*, *Cxcl10* (group II), and *Mmp3*, *Mmp13*, *Enpp2* (group III). We intentionally included key proinflammatory mediators, genes of matrix metalloproteinase (*Mmp3*, *Mmp13*), which are known to degrade collagen in cartilage and thereby enhance rheumatoid arthritis and osteoarthritis progression (Liacini *et al.* 2002; Liacini *et al.* 2003; Roman-Blas *et al.* 2006; Sellam *et al.* 2010).

A previous study has shown that 30 μM of Nec-1 effectively inhibited RIP1 kinase activity (Liacini *et al.* 2002). Therefore, we investigated gene expressions for cells stimulated with 10 ng/mL TNF, in the presence or absence of 30 μM Nec-1 for a period of 10 hours with measurements made at least every hour (Figure 2.12). Remarkably, as predicted by the TNFR1 model, RIP1 inhibition by Nec-1 resulted in the suppression of all 3 groups of genes. The effect of suppressing RIP1 is significant for groups I and II genes in both MEF and BALB/3T3 cells, especially during the first 2–3 hours after stimulation. For group III genes, Nec-1 had more pronounced effect in MEF compared with BALB/3T3 cells. Overall, these results are consistent with the TNFR1 model predictions that suppressing RIP1 in TNF stimulation significantly impairs the activation of all 3 groups of genes.

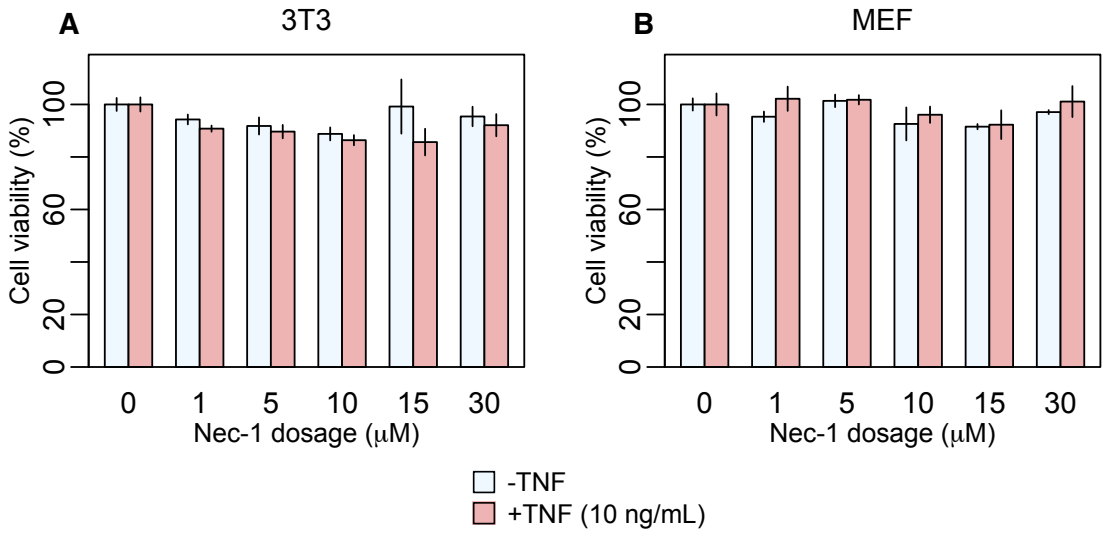

Figure 2.11 Cell viability using Nec-1. Cell sensitivity (MTT) assay for **(A)** 3T3 and **(B)** MEF cells treated in absence (light blue bars) or presence (brown bars) of 10 ng/mL of TNF, with indicated doses (0, 1, 5, 10, 15, 30 mM) of Nec-1 for 24 h. Average cell viability percentage for n = 3 independent experiments is shown. Error bars indicate mean values ± SD.

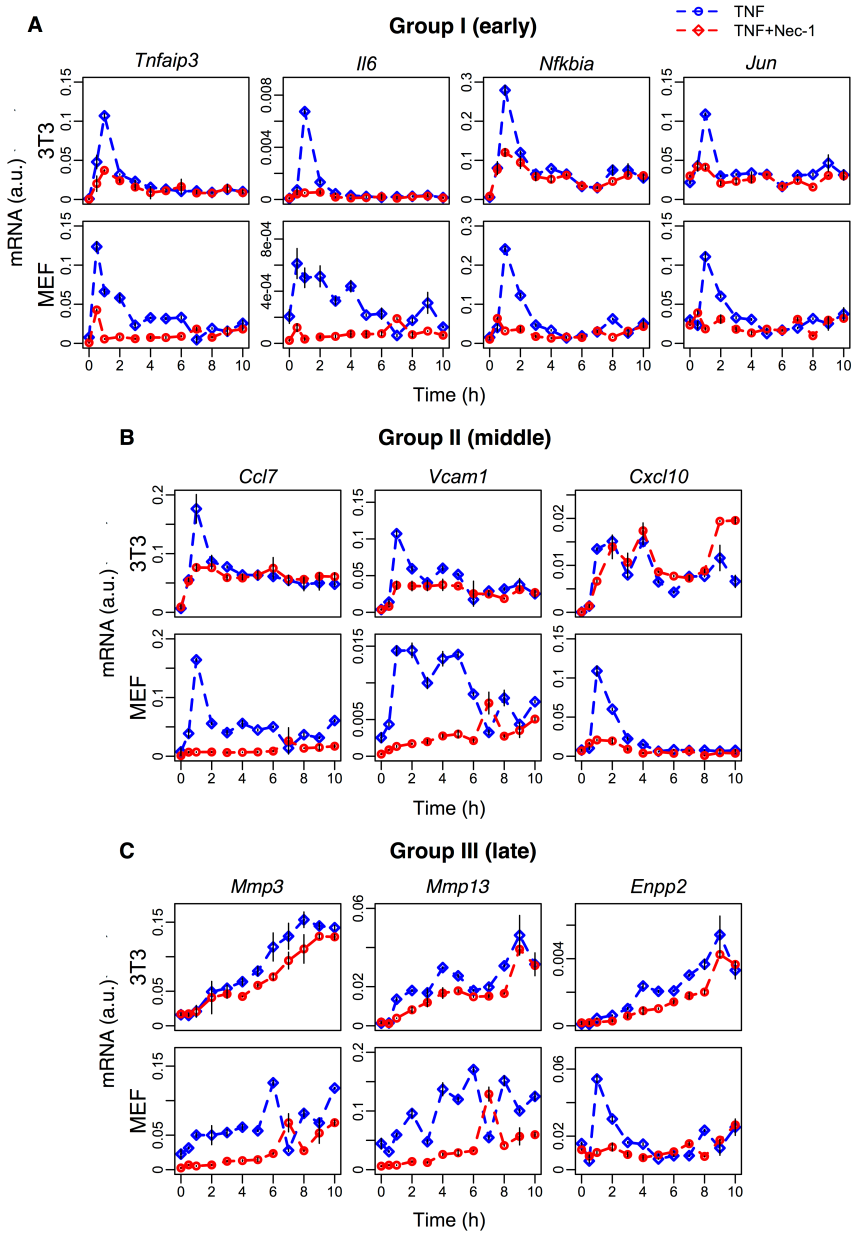

Figure 2.12 Experimental verification of RIP1 inhibition through Nec-1. Temporal gene expressions of groups I (*Tnfai3p, Il6*, *Jun*, *Nfkbia*) **(A)**, II (*Ccl7*, *Vcam1*, *Cxcl10*) **(B)**, and III (*Mmp3*, *Mmp13*, *Enpp2*) **(C)** genes in 10 ng/mL of TNF-stimulated BALB/3T3 (top panels) and MEF (bottom) cells, treated without (blue curves) and with (red curves) Nec-1. Nec-1 treatment was applied for 30 min before TNF stimulation. Curves indicate average profiles relative to *GAPDH* gene expression for $n = 3$ independent experiments, and error bars show mean values ± SD.

2.4 Discussion

TNF is a crucial cytokine that regulates myriad vital cellular processes. However, its levels are enhanced in major proinflammatory diseases. Here, to understand the TNF-induced proinflammatory signaling process, and to carefully regulate its dynamic response, a systems biology approach was adopted. We first developed a dynamic computational model using well-established publicly available experimental data of NF-κB, MAP kinase p38, and the average profiles of 3 groups of 180 upregulated genes in mouse fibroblast cells.

Despite the simplicity of using first-order response equations to simulate the profiles of the intracellular molecules, the computational model of TNFR1 recapitulated the experimental response in wildtype and several mutant conditions for NF-κB and p38 activations. This result is surprising, as we know that the innate immune response of TNF is highly complex. It is important to note here that there have been previous other computational efforts on NF-κB and MAPK signaling that had utilized detailed biochemical reactions modeling, to elucidate local properties of signal transduction, such as the ability of common molecules to produce distinct feedback mechanisms to different stimuli (Bruggeman *et al.* 2002; Santos *et al.* 2007; Werner *et al.* 2005). In our work, however, we have shown that even a simpler representation of the signal transduction pathways, through first order response equations and the law of mass

conservation can reproduce experimental dynamics. This strongly indicates the presence of simple organizing rules governing the deterministic population average signaling response (Selvarajoo 2011; Selvarajoo 2012; Selvarajoo 2013a; Selvarajoo 2013b; Selvarajoo *et al.* 2012; Selvarajoo *et al.* 2013).

Next, through the analyses of downstream temporal gene expression profiles, the model suggests the presence of additional novel post-transcriptional/translational processes that is required for the continuous activation of group III genes. This result is additional to previous postulations, which had indicated that the continuous activation is due to lesser ARE region for group III genes leading to a very low decay process (Hao *et al.* 2009), and due to the presence of differential delays in the RNA splicing process (Hao *et al.* 2013). Our model suggests that, on top of these effects, a novel time-delayed secondary transcriptional mechanism is required.

Literature survey indicates that the novel positive feedback processes could be a result of autocrine signaling, example through IL-1 or IL-6, or derive from a still unknown intracellular feedback mechanisms regulating mainly the promoter regions of group III genes. For example, the role of interferon regulatory transcription factor (IRF) family in inducing *Ccl5* or RANTES expression, which belongs to one of the group III genes, is reported in a previous study (Yarilina *et al.* 2008), however, was not considered in the initial TNFR1 model. It is, therefore, necessary to perform further

experimental work to confirm and elucidate the exact mechanisms for the continuous activations of group III genes.

On the other hand, for down-regulating TNF signaling, which is enhanced in several proinflammatory diseases and cancer, we performed the simulations for 12 *in silico* KOs of signaling molecules. The resultant simulations indicated that RIP1 is a major regulator of the 3 groups of upregulated gene expressions. To verify the result, we performed experiments on MEF and BALB/3T3 cells using Nec-1 as an inhibitor of RIP1. The measurement of 10 genes belonging to groups I (*Il6*, *Tnfaip3*, *Jun*, *Nfkbia*), II (*Ccl7*, *Vcam1*, *Cxcl10*) and III (*Mmp3*, *Mmp13*, *Enpp2*) all showed significant impairment with Nec-1 compared to wildtype.

Most importantly, the expressions of key proinflammatory genes such as *Il6, Vcam1, Ccl7, Mmp3*, *Mmp13*, enhanced in rheumatoid arthritis and osteoarthritis (Liacini *et al.* 2002; Roman-Blas *et al.* 2006), were reduced. In particular are the levels of matrix metalloproteinase genes *Mmp3*, *Mmp13*, which are known to directly affect type II collagen in bone cartilages and degrade the extracellular matrix. Although recent therapeutics have been focusing on the specific regulations of MMPs (Kaneva *et al.* 2012; Liacini *et al.* 2003; Roman-Blas *et al.* 2006; Sellam *et al.* 2010), it remains to be seen what effect such treatments will have on other proinflammatory or vital genes.

In summary, our approach provides a systemic analysis of TNFR1 signaling, and suggests Nec-1 is potentially an important therapeutic target for effectively

regulating major proinflammatory mediators in chronic diseases where TNF is overexpressed.

Chapter 3

Systems biology strategy reveals PKCδ is key for sensitizing TRAIL-resistant human fibrosarcoma

3.1 Introduction

Numerous recent studies have revealed the close link between inflammation and cancer. Firstly, various types of immune cells, which support tumor growth progression, are found within the tumor microenvironment (Grivennikov *et al.* 2010; Swann *et al.* 2008). Secondly, the vicinity of cancer cells displays increased proinflammatory activity, through the detection of elevated levels of major cytokines such as the tumor necrosis factor (TNF) (Balkwill 2006; Mantovani *et al.* 2002). One notable cytokine found within the tumor microenvironment is the TNF related apoptosis-inducing ligand or TRAIL, which has been shown to induce apoptosis in certain types of malignant cancers with no significant effect on normal cells (Pitti *et al.* 1996; Wiley *et al.* 1995). The findings have led to a major stride in the ongoing research aimed at optimizing TRAIL-induced cancer therapy (Jo *et al.* 2000; Zhang *et al.* 2000;). Despite some success, TRAIL-based therapies still show dismal results for several types of cancers such as the breast cancer, neuroblastoma, adenocarcinoma, glioma, etc. (Eggert *et al.* 2001; Hao *et al.* 2001; Keane *et al.* 1999; Trauzold *et al.* 2006).

Computational modeling approaches are becoming increasing useful for interpreting complex dynamical cellular responses (Birtwistle *et al.* 2007; Hoffmann *et al.* 2002; Piras *et al.* 2014; Selvarajoo 2012; Selvarajoo *et al.* 2013; Selvarajoo *et al.* 2014; Vance *et al.* 2002; Yeo *et al.* 2007). Previously, to understand the mechanism for

TRAIL-resistance in cancer, we developed a dynamic computational model of TRAIL signaling, from extracellular receptor activation to downstream intracellular activation of cell survival (MAP kinases and IκB) and apoptosis (caspases -8 and -3) pathways (Piras *et al.* 2011, appendix A). Our model was based on perturbation-response approach utilizing first-order response equations (Hayashi *et al.* 2013; Helmy *et al.* 2009; Piras *et al.* 2011; Selvarajoo 2006; Selvarajoo 2011; Selvarajoo *et al.* 2008; Selvarajoo *et al.* 2009; Selvarajoo *et al.* 2007; Tan *et al.* 2003), that was shown to successfully simulate the temporal experimental profiles IκB, JNK, p38, caspase-8 and -3 in wildtype and four (FADD, RIP1, TRAF2 and caspase-8) knock-down conditions for human fibrosarcoma (Varfolomeev *et al.* 2005). We, subsequently, predicted targeting a novel molecule interacting with p62 in the model would significantly increase caspase-3 activation and enhance cancer apoptosis to TRAIL stimulation. Further protein-protein interaction (PPI) database analysis suggested that the novel molecule is most probably a protein kinase C (PKC) family member.

Here, we tested the model prediction by experimentally verifying whether targeting PKC will enhance apoptosis in TRAIL-resistant cancer cell lines. Experiments were performed on TRAIL-induced human fibrosarcoma (HT1080) and human colon adenocarcinoma (HT29) cells, and the cell viability was compared with control normal fibroblasts (TIG-1 and MRC-5). Moreover, to investigate the intracellular mechanisms for resultant cell viability, we measured time-course activation levels of caspase-3,

PARP, p38 and JNK. Subsequently, we analyzed the expressions of each PKC isoform member in HT1080 cells. To identify a crucial target member for enhanced cancer apoptosis, we prepared relevant siRNA knock-down experiments. In summary, our study investigates i) whether the model prediction of PKC suppression will enhance cancer cell death is true, and ii) whether computational modeling using perturbation-response approach are valuable for biological research focusing on cancer treatment.

3.2 Materials and methods

3.2.1 Reagents and cell culture

Recombinant human TRAIL was purchased from Peprotech. Bisindolylmaleimide I (BIM-I) was purchased from Merck Millipore. Human fibrosarcoma cell lines (HT1080), human embryo fibroblasts (TIG-1), human colorectal adenocarcinoma cells (HT29) were obtained from Japanese Collection of Research Bioresources (JCRB) cell bank. Human fetal lung fibroblasts (MRC-5) were obtained from American Type Culture Collection (ATCC). HT1080, TIG-1, HT29 and MRC-5 were grown in DMEM (Nissui Seiyaku Co.) containing 10% calf serum, 100 U/mL of penicillin at 37°C in a 5% CO_2 humidified atmosphere.

3.2.2 Cell viability assay

The cell viability was measured by 3-(4,5-dimethylthiazol-2-yl)-2,5-diphenyltetrazolium bromide (MTT) assay and trypan blue exclusion. MTT assay: Cells (10×10^4) were inoculated in each well and incubated for 24 h. Thereafter, 50 μL of MTT (2 mg/mL in PBS) was added to each well and the plates were incubated for a further 2 h. The resultant formazan was dissolved with 100 μL of dimethyl sulfoxide (DMSO) after aspiration of culture medium. Plates were placed on a plate shaker for 1 min and then read immediately at 570 nm using TECAN microplate reader with Magellan software (Männedorf, Switzerland). Trypan blue exclusion: Cells were detached with 1 mL of trypsin and suspended in DMEM. After staining with trypan blue, viable cells were counted using a microscopy (n = 3). The percentage of trypan blue exclusive viable cells was determined as a percentage of the total number of cells.

3.2.3 Western blot analysis

Anti-PARP, anti-phospho-p38 and anti-β-actin antibody were purchased from Cell Signaling Technology. Proteins were extracted from the cell lines using radioimmunoprecipitation assay (RIPA) buffer according to the manufacturer's instructions. Next, their concentrations were measured by Bradford protein assay. Equal amounts of protein were loaded in each well and separated by 10% sodium dodecyl sulfate-polyacrylamide gel electrophoresis (SDS-PAGE), which was subsequently

transferred onto a polyvinylidene difluoride (PVDF) membrane. The membrane was blocked for 1 h with 5% BSA in TBST on the shaker at room temperature. The membrane was placed on PARP and p-p38 antibody diluted at a 1:1000 proportion in diluent buffer (5% (w/v) BSA and 0.1% Tween 20 in TBS) and incubated overnight at 4°C on the shaker. The membrane was washed three times in TBS as above and incubated with secondary antibody diluted at a 1:10000 proportion for 1 h on the shaker at room temperature. The membrane was again washed three times for 5 min each time as above and finally the results were generated by using an enhanced chemiluminescence (ECL) Western blotting kit.

3.2.4 Enzyme linked immunosorbent assays (ELISA) of cleaved caspase-3 and phosphorylated JNK

Cleaved caspase-3 and phosphorylated JNK concentrations were measured by ELISA Duo Sets IC Kit (R&D Systems) following the instructions of the manufacturer.

3.2.5 Transfection

siRNA duplexes were purchased from Sigma. The transfection of classic PKCs (PKCα, PKCβ, PKCγ), the novel PKCs (PKCδ, PKCε, PKCη, PKCμ, PKCθ) and the atypical PKCs (PKC ζ, PKCι) and scrambled siRNA were carried out using Lipofectamine 2000 according to the manufacturer's instructions (Invitrogen).

3.2.6 Quantitative real-time PCR analysis

Total cellular RNA was extracted from cells using the TRIzol reagent according to the manufacturer's instructions (Invitrogen). One microgram of RNA was reverse-transcribed using a first-strand cDNA synthesis kit (ReverTra Aceα; Toyobo). Quantitative real-time PCR (qRT-PCR) was performed using SYBR premix Ex Taq (Takara) on the Applied Biosystems StepOnePlus^{TM} according to the technical brochure of the company. qRT-PCR primers in this study are listed in Table 3.1. Quantitative measurements were determined using the ΔΔCt method and expressions of GAPDH gene for *pkc* and RPL27 gene for *rela*, *mtor*, *bcl2*, *bax, cytoc* and *jun* were used as the internal control. Melt curve analyses of all qRT-PCR products were performed and shown to produce the sole DNA duplex.

3.3 Results

3.3.1 Effect of PKC inhibitor in TRAIL-resistant HT1080 cells

Based on our previous computational TRAIL model, the removal of PKC family members would enhance HT1080 cell death by 95% (Piras *et al.* 2011). Here we investigated the actual experimental effect of PKC inhibition to HT1080 cells in TRAIL stimulation. HT1080 cells were stimulated with 1000 ng/mL of TRAIL in the presence or absence of 10 μM of PKC inhibitor (Davis *et al.* 1989; Toullec *et al.* 1991; Wilkinson *et al.* 1993), BIM-I, pre-treatment and compared with unstimulated control

with and without BIM-I pre-treatment (Figure 3.1). We observed, phenotypically, that HT1080 cell death was significantly increased in combinatorial treatment of TRAIL and BIM-I (Figure 3.1A, forth column), while control pre-treated with BIM-I did not induce any noticeable cell death (Figure 3.1A, second column).

Next, we investigated cell survival ratio using MTT assays for HT1080 cells pre-treated with BIM-I with increasing dosage (0, 3, 10 μM) for 30 min prior to increasing TRAIL stimulation (0, 100, 200, 400 and 1000 ng/mL) for 24 h (Figure 3.1B). Notably, from these experiments, it is clear that HT1080 cell death is almost unaffected with any dosage of BIM-I without TRAIL stimulation. However, when BIM-I was treated in the presence of TRAIL, the effect synergistically produced significant cell death, compared with TRAIL alone (Figure 3.1B). Remarkably, as predicted by our previous computational TRAIL model (Piras *et al.* 2011), the inhibition of PKC (with 10 μM of BIM-I) resulted in about 99% cell death for TRAIL stimulation (with 100 ng/mL or more) in HT1080 cells. We further investigated the cell viability of HT1080 with respect to stimulation time, and noticed that significant cell death occurs at 3 hours and onwards (Figure 3.1C).

Next, in addition to HT1080, we also investigated another TRAIL-resistant cancer cell type (HT29) and compared with normal fibroblasts (TIG-1 and MRC-5). Experiment-matched MTT assays revealed that both HT1080 and HT29 cell cultures treated with BIM-I were sensitized to TRAIL-induced cell death (approximately 99%

and 95% cell death, respectively), while normal TIG-1 and MRC-5 largely survived (Figure 3.1D and E). These results indicate that PKC inhibitor, BIM-I, has specific ability to enhance cell death in TRAIL-resistant cancer cells while having little effect on normal cells.

Figure 3.1 The effect of TRAIL and PKC inhibitor (BIM-I) on cancer (HT1080 and HT29) and normal (TIG-1 and MRC-5) cells.

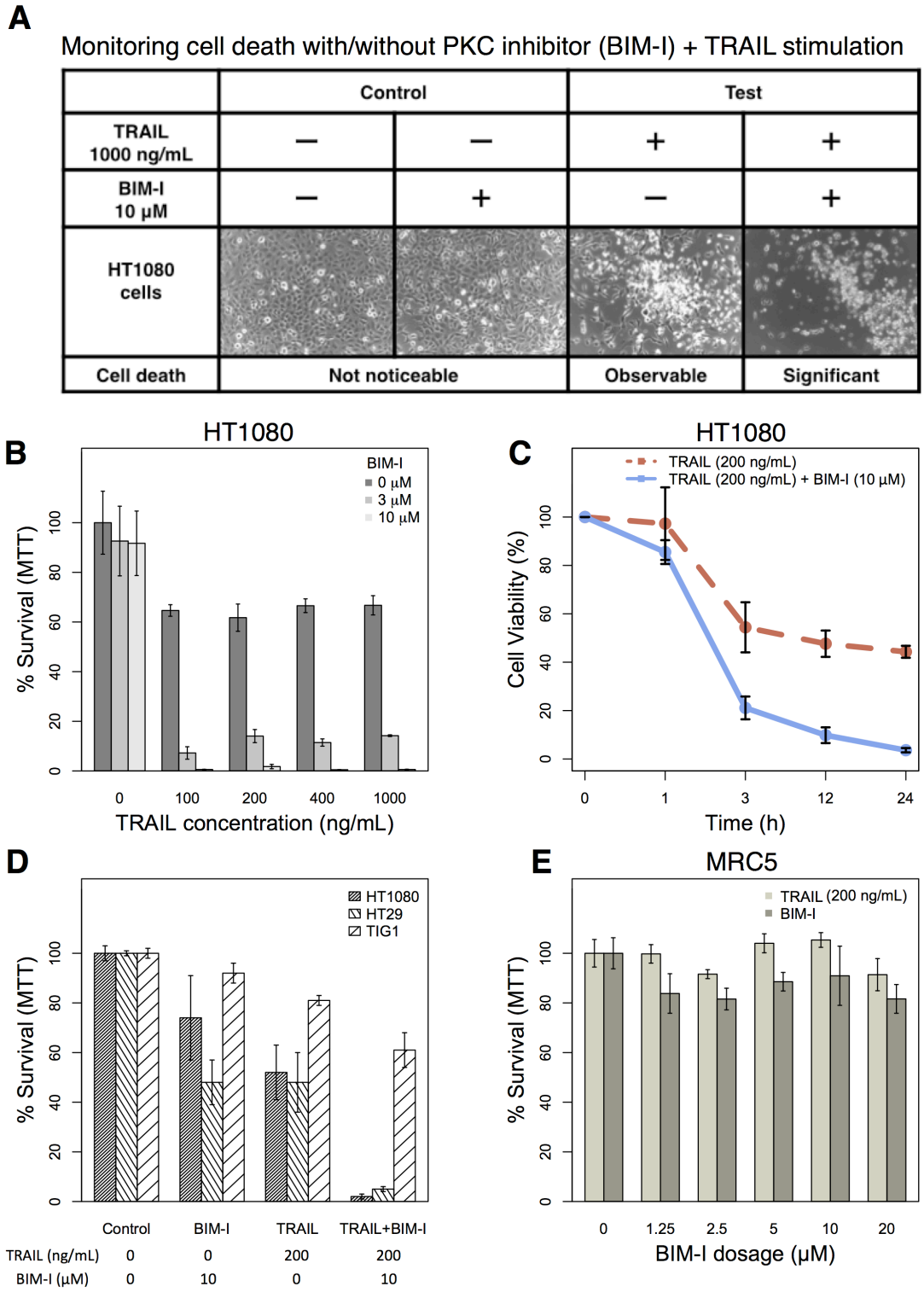

Figure 3.1 The effect of TRAIL and PKC inhibitor (BIM-I) on cancer (HT1080 and HT29) and normal (TIG-1 and MRC-5) cells (continued) (**A**) Phase contrast microscopic images of HT1080 cells in the presence or absence of TRAIL (1000 ng/mL) and/or BIM (10 μM). Living cells appear as adherent cells, while dead cells float in the dish and are highlighted in white. (**B**) TRAIL and BIM-I dosage-dependent cell survival (MTT assay) rate of HT1080 cells (1×10^5), 24 h after treatment (TRAIL: 0, 100, 200, 400, 1000 ng/mL, BIM-I: 0, 3, 10 μM). (**C**) Cell viability (trypan blue assay) of HT1080 over time cells (3×10^5) at 1, 3, 12, 24 h after treatment (TRAIL: 200 ng/mL, BIM-I: 10 μM). (**D**) Cell survival (MTT assay) rate of HT1080 (1×10^5), HT29 (1.5×10^5) cancer cells and TIG-1 (2×10^5) normal cells was observed 24 h after treatment in presence of TRAIL (200 ng/mL) or BIM-I (10 μM), or both, compared to unstimulated cells (control). (**E**) BIM-I dosage-dependent (0, 1.25, 2.5, 5, 10, 20 μM) cell survival rate of MRC-5 (0.5×10^5) normal cells after TRAIL stimulation (200 ng/mL) obtained through MTT assay after 24 h. Average cell viability is shown in percentage for *n*=3 independent experiments. Error bars indicate mean values±SD.

3.3.2 Treatment of PKC inhibitor with TRAIL enhances cell death through apoptosis

The experimental results, so far, are consistent with our previous model simulations. To further scrutinize the result, that is, to explore the origins of cell death, we performed analysis to observe intracellular markers prior to cell death. According to our model, PKC inhibition causes enhancement of apoptotic pathways through *signaling flux redistribution* (SFR) (Piras *et al.* 2011; Selvarajoo *et al.* 2008). To check whether apoptosis is increased in TRAIL stimulated and BIM-I treated HT1080 cells, we measured PARP cleavage and p38 phosphorylation using western blotting assays and, caspase-3 activation and JNK phosphorylation using ELISAs (Figure 3.2).

Consistent with the prediction of computational model, we observed substantial induction of PARP and caspase-3 cleavage, indicating increased apoptosis in HT1080 cells treated with BIM-I when compared with untreated cells in TRAIL stimulation (Figure 3.2A, top panel and 3.2B, right panel). We further noticed enhanced p38 activations and low activity of JNK in TRAIL-stimulated cells treated with BIM-I (Figure 3.2A, middle panel and 3.2B, left panel), in agreement with our model predictions for SFR at p62 pathway junction (Piras *et al.* 2011) (Figure 3.2C). Note that the housekeeping protein β-actin remained almost unaffected in the western blots. These results clearly demonstrate that BIM-I is a potential therapeutic target for HT1080 treatment.

Figure 3.2 Enhancement of apoptotic signaling molecules in the presence of BIM-I in TRAIL-stimulated HT1080 cells.

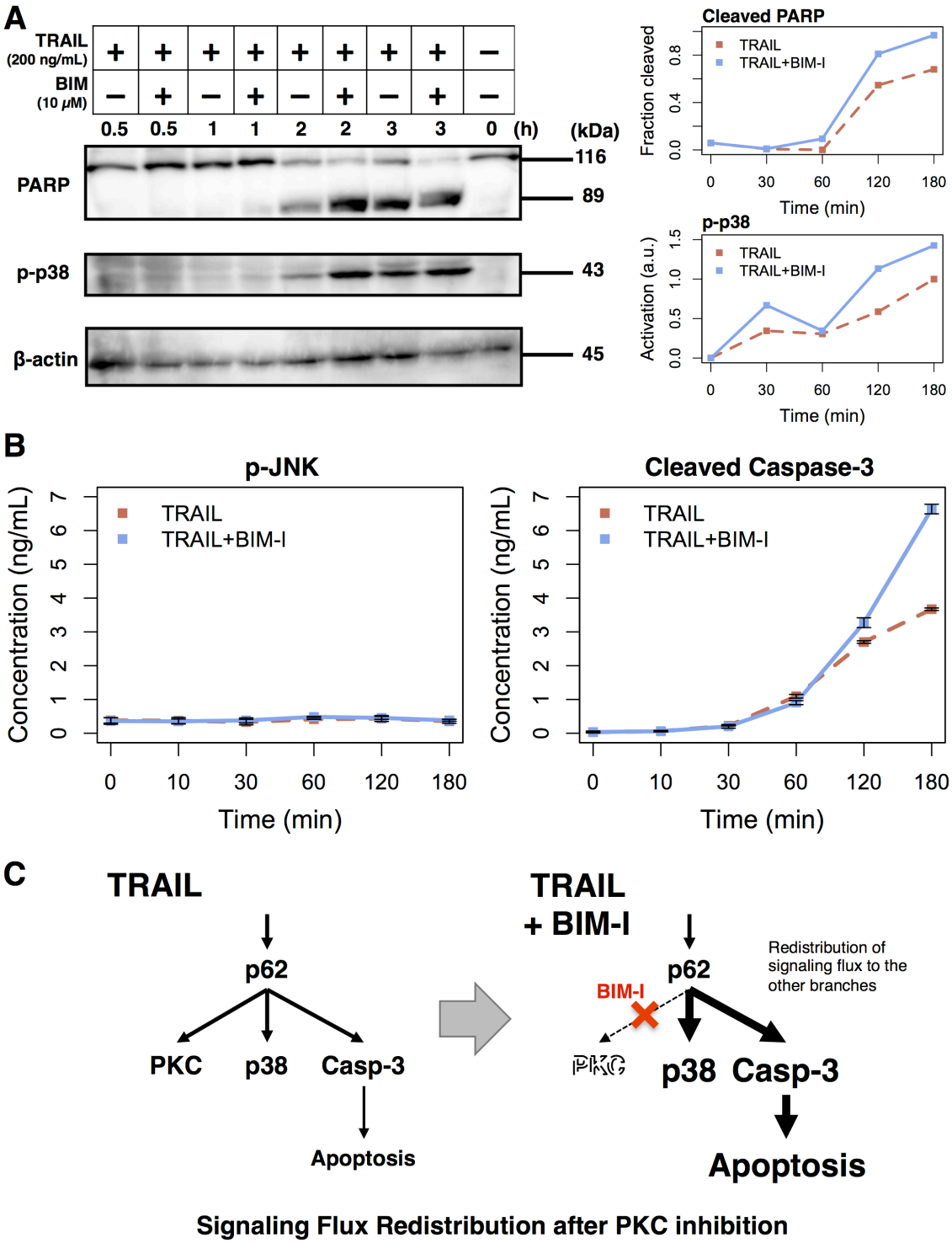

Figure 3.2 Enhancement of apoptotic signaling molecules in the presence of BIM-I in TRAIL-stimulated HT1080 cells (continued) (**A**) Cleavage of PARP, phosphorylation of p38 and concentration β-actin were determined by western blotting at 0, 30, 60, 120 and 180 min after TRAIL stimulation (200 ng/mL) of HT1080 cells in absence or presence of BIM-I (10 μM). Right panels represent the quantification of fraction of cleaved PARP (top, cleaved PARP/total PARP for each time point) and p38 activation (bottom, relative to maximum value of TRAIL stimulation without BIM-I) using ImageJ (http://imagej.net). (**B**) Phosphorylation of JNK and levels of cleaved caspase-3 protein were measured by ELISA at 0, 10, 30, 60, 120 and 180 min after TRAIL stimulation (200 ng/mL) of HT1080 cells in absence or presence of BIM-I (10 μM). Error bars indicate mean values±SD for n = 3 independent experiments. (**C**) Schematic representing the mechanism of signaling flux redistribution at p62 pathway junction towards p38 and caspase-3 signaling branches when PKC is inhibited.

To examine the expression levels of appropriate genes in TRAIL stimulated HT1080, with and without BIM-I, we performed qRT-PCR experiments for several survival and apoptotic genes (*rela*, *mtor*, *bcl2*, *bax, cytoc* and *jun*) at 0, 20, 40, 60, 120 and 180 min (Figure 3.3). Except for *jun*, the levels of genes were stable for up to 60 min, after which their expressions were significantly reduced, especially for BIM-I treated HT1080 cells, in correlation with the cell death dynamics (Figure 3.1C). This data indicates that, except for *jun*, transcription of the genes does not occur, perhaps due to the increased signaling flux through the apoptosis process depriving transcriptional signaling and, or due to the repression of pre- and post-transcriptional mechanisms found during apoptosis (Bushell *et al.* 2006; Bushell *et al.* 2004; Del Prete *et al.* 2002; Elmore *et al.* 2008; Tomas *et al.* 2013). Our observations are also consistent with other TRAIL-induced apoptosis studies investigating gene expressions in HeLa (Bushell *et al.* 2004) and MCF7 (Bushell *et al.* 2006) cells.

Interestingly, *jun* levels showed an initial decrease during the first 20 min and then increased and stabilized after 120 min. This pattern indicates *jun* may evade the global transcriptional repression and play a role during apoptosis. Such behavior has been previously observed for other genes, in particular, genes translated through Internal Ribosome Entry Site (IRES)-mediated translation, which is known to occur during apoptosis after TRAIL stimulation of MCF7 cells (Bushell *et al.* 2006; Spriggs *et al.* 2005). Notably, the presence of IRESs in *jun* transcriptional machinery has also been

previously shown (Blau *et al.* 2012). Nevertheless, further investigation is required to define the exact role of *jun* during TRAIL and BIM-I mediated apoptosis.

Overall, the experiments demonstrate that the enhancement of cell death of BIM-I pre-treated TRAIL-stimulated cancer occurs through apoptosis.

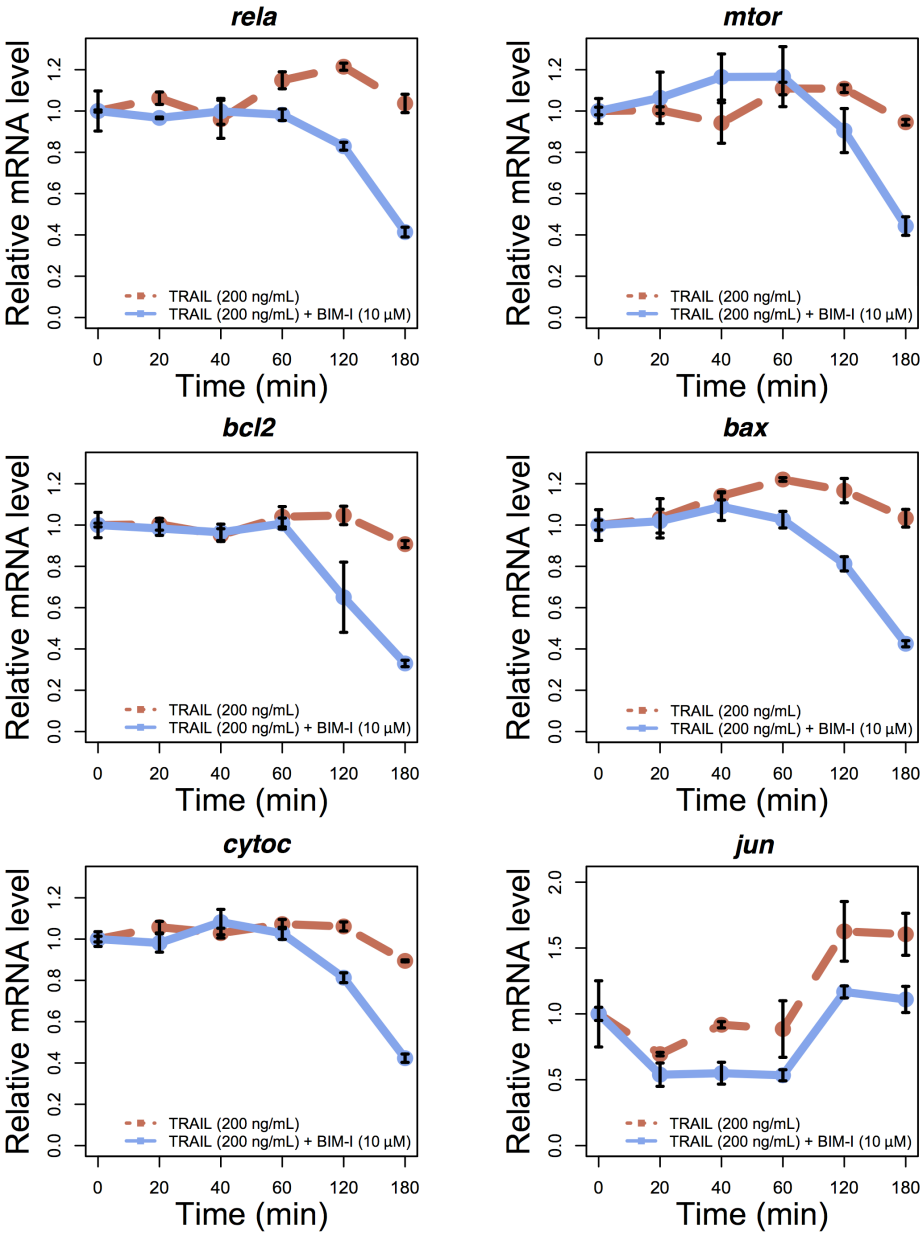

Figure 3.3 Temporal relative mRNA expression in TRAIL and BIM-I treated HT1080 cells. Temporal expression profiles of anti-apoptotic (*rela*, *mtor*, *bcl2* and *jun*) and pro-apoptotic (*bax* and *cytoc*) genes in HT1080 cells at 0, 20, 40, 60, 120, and 180 min after TRAIL stimulation (200 ng/mL) without (red line) or with (blue line) pre-treatment of BIM-I (10 μM) 30 min prior to TRAIL stimulation. Note that *jun* can also be considered as a pro-apoptotic gene (Blau *et al.* 2012). Reported values are the mean expression values (n = 3 independent experiments) relative to time 0 of each condition. Error bars indicate mean values±SD.

3.3.3 Identification of specific PKC isoform target for enhanced cell death

Although we have demonstrated that PKC is a key target to enhance apoptosis in TRAIL-resistant cancer cells, it is unknown which PKC family isoform, among the 10 major members (α, β, γ, δ, ε, ι, θ, η, ζ, μ), is a crucial single target. To investigate this, we first measured the mRNA expressions of all 10 isoforms (the sequence of primers are available in Table 3.1) in unstimulated HT1080 cells using qRT-PCR.

We observed the gene expressions of four PKC isoforms (α, δ, ε and ι) were noticeably elevated, indicating that these isoforms may be crucial targets (Figure 3.4A). To investigate the effect of suppressing each of the four isoforms in TRAIL-stimulated HT1080 cells, we next performed siRNA-mediated PKC (α, δ, ε and ι) knockdowns. The effect of each PKC knockdown was first confirmed after 24h (Figure 3.4B). Consequently, we investigated cell viability by trypan blue for each of the 4 PKC knockdown conditions with and without TRAIL stimulation (200 ng/mL). Notably, PKCδ knockdown produced the most significant cell death of approximately 83% after 3 h (Figure 3.4C). Note that this result is almost identical to TRAIL-stimulated HT1080 pretreated with BIM-I at 3 h (Figure 3.1C). Thus, our experiments reveal that PKCδ is the optimal single target for enhancing cancer apoptosis in TRAIL-based therapy.

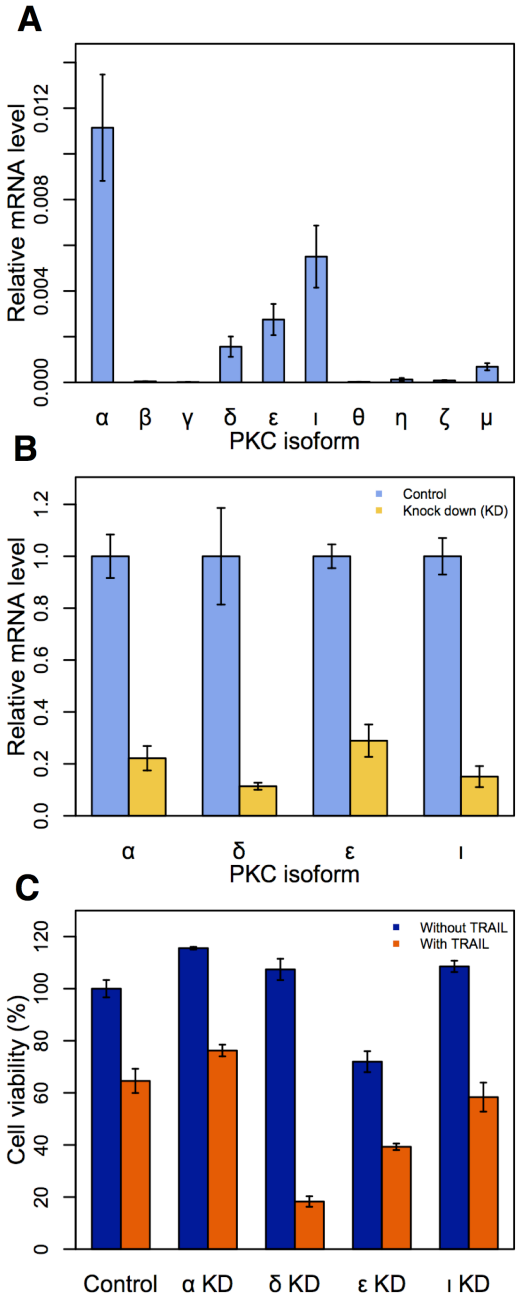

Figure 3.4 Identification of specific PKC isoform target to enhance apoptosis in HT1080 cells. (A) Relative mRNA expressions of 10 PKC isoform in HT1080 unstimulated cells. **(B)** Effect of siRNA knock-down (KD) for *PKCα*, *PKCι*, *PKCε*, and *PKCδ* . HT1080 cells were incubated in the presence of each isoform of PKC siRNA (50 μM) for 24 h. Relative mRNA expressions of 4 PKC isoforms are measured by qPCR. **(C)** Cell viability assay (trypan blue) of HT1080 cells incubated in the presence of PKC isoforms siRNA (50 μM) for 3 h. *** indicate $p < 0.05$ in student *t*-test. Error bars indicate mean values±SD for $n = 3$ independent experiments.

Table 3.1 List of primer sequences for RT-PCR (2)

Name	Species	Primer name	Sequence(5'-3')
PKCα	human	PKCα_F	CCACACTAAATCCGCAGTGG
	human	PKCα_R	CAGCTCCGAAACTCCAAAGGA
PKCβ	human	PKCβ_F	TTGTGGACCTGAAGGCGAAC
	human	PKCβ_R	CGGGTGAAAAATCGGTCGAAG
PKCγ	human	PKCγ_F	GCTTGTAACTACCCCCTGGAAT
	human	PKCγ_R	GAAGCTGAAGTCGGAGATGTG
PKCδ	human	PKCδ_F	TGGTGGTTGGTGCGTTGTAG
	human	PKCδ_R	ATAGGAGTTGAAGGCGATGCG
PKCε	human	PKCε_F	CAAGCCACCCTTCAAACCAC
	human	PKCε_R	CGTCCACAAGGGTGAGTACC
PKCη	human	PKCη_F	GTGTCGTCCATAAACGCTGC
	human	PKCη_R	ATCCCGAACCTCTGTTCTGC
PKCμ	human	PKCμ_F	GAGGACGCCAACAGAACCAT
	human	PKCμ_R	CCTTGCTGGTGTAGTGGACC
PKCθ	human	PKCθ_F	GCTGATTGGTCAGTCGCCTT
	human	PKCθ_R	TCTTCTCAGGTTCTCGCACG
PKCζ	human	PKCζ_F	CACATGCAGAGGCAGAGGAA
	human	PKCζ_R	GAGGACGTTGTCCAGCTTCA
PKCι	human	PKCι_F	GCCATCTGCACAGACCGAAT
	human	PKCι_R	TCCATGGGCATCACTGGTTC
rela	human	RelA_F	GTGGGGACTACGACCTGAATG
	human	RelA_R	AGATCTTGAGCTCGGCAGTG
mtor	human	mTOR_F	TCGCTGAAGTCACACAGACC
	human	mTOR_R	CTTTGGCATATGCTCGGCAC
bcl2	human	BCL2_F	AACATCGCCCTGTGGATGAC
	human	BCL2_R	TTCACTTGTGGCCCAGATAGG
bax	human	BAX_F	ACAGGGGCCCTTTTGCTTC
	human	BAX_R	CTTGGTGGACGCATCCTGAG
cytoc	human	Cytochorome c_F	AGCGGGAGTGTTCGTTGTG
	human	Cytochorome c_R	CCTCCCTTTTCAACGGTGTG
jun	human	Jun_F	ACGGCGGTAAAGACCAGAAG
	human	Jun_R	CCAAGTTCAACAACCGGTGC
GAPDH	human	GAPDH_F	GTCAACGGATTTGGTCGTAT
	human	GAPDH_R	TGGTGATGGGATTTCCATTG
RPL27	human	RPL27_F	CTGTCGTCAATAAGGATGTCT
	human	RPL27_R	CTTGTTCTTGCCTGTCTTGT

3.4 Discussion

TRAIL, a proinflammatory cytokine produced by the mammalian immune system, is known to induce apoptosis in cancer cells while leaving non-diseased cells largely unharmed (Johnstone *et al.* 2008; Kim *et al.* 2000). Hence, there has been intense interest in using TRAIL has a therapeutic target to treat cancers (Smyth *et al.* 2003; Wang *et al.* 2003). However, not all cancers respond to TRAIL (Ehrhardt *et al.* 2003; Khanbolooki *et al.* 2006).

Previously, we investigated the TRAIL resistant mechanism in HT1080 cells using a computational model (Piras *et al.* 2011). We predicted that the suppression of a novel pro-survival molecule would result in significant enhancement of apoptosis through *signaling flux redistribution* (Selvarajoo *et al.* 2008). PPI Database search indicated that the pro-survival molecule is a member of PKC. To experimentally validate this result, in this paper, we investigated the effects of two TRAIL-resistant cancer cells to PKC inhibition.

Firstly, using different doses of PKC inhibitor BIM-I together with various levels of TRAIL stimulation, we observed approximately 99% and 95% cell death occurred for HT1080 and HT29 cells, respectively (Figure 3.1). Notably, the effect on control TIG-1 and MRC-5 cells were less significant, at approximately 40% and 20% cell death, respectively.

Secondly, to confirm the mechanism for cell death is through apoptosis, we measured the activations of PARP and caspase-3 over 3 h in TRAIL-stimulated HT1080 cells untreated and treated with BIM-I, and compared with activations of p38 and JNK. We found that PARP, caspase-3 cleavages and p38 phosphorylation were significantly enhanced in BIM-I treated cells (Figure 3.2), while JNK activity was very low. These results are in consistency with the previous prediction of our computational model (Piras *et al.* 2011). We also investigated the expressions of major pro- and anti-apoptotic genes, and found them to be mostly repressed at their transcription levels, especially after 1 h for BIM-I treated cells (Figure 3.3).

Thirdly, to identify the crucial PKC family member for single specific target, we investigated the mRNA expressions of all 10 major isoforms in HT1080 cells. We selected the top 4 significantly expressed isoforms for developing siRNA KDs, and subsequent experiments demonstrated that PKCδ is a key target for enhancing cell death in TRAIL-resistant HT1080 cells (Figure 3.4).

It is worthy to mention other previous works that have studied PKC in different cancer types (Gatsinzi *et al.* 2012; Harper *et al.* 2003; Okhrimenko *et al.* 2005a; Okhrimenko *et al.* 2005b; Shankar *et al.* 2008). Although these works have demonstrated the importance of PKC, the investigations were performed in different cell lines or stimulations. In this work, however, we focused mainly on HT1080 and limitedly on HT29 cells. In addition, we bring to the attention the power of using

multidisciplinary research to systemically identify a key target that can be experimentally tested. Therefore, to our knowledge, this is the first time the usefulness of a computational model is shown to identify a consistent and key target for regulating TRAIL-resistance. In summary, our work provides further evidence for the utility of systemic approaches in providing effective treatment strategies to tackle complex diseases.

Chapter 4

Concluding remarks

4.1 Main findings

This thesis describes the understanding of the proinflammatory response in TNF signaling pathway and the TRAIL resistant mechanisms in cancer cells using a dynamical computational model based on the well-established perturbation response approach. Using computational models in TNF and TRAIL signaling pathway, we found key molecules to control the proinflammatory response and to enhance the cancer cell death. Following the model predictions, experiments were also conducted to verify the model prediction.

In chapter 2, to identify the key target to suppress the expression of the proinflammaory genes, such as *Il-6*, *ccl-7*, *mmp-3, mmp-13*, we developed a computational model. Among the candidate molecules, we found that *in silico* RIP1 KO highly regulates the expression of proinflammatory genes. To validate these results, we experimentally tested our predictions and finally, using RIP1 inhibitor Necrostatin-1, we verified all measured genes were significantly impaired.

In chapter 3, to identify the most effective target to enhance the cell death in TRAIL-resistant human fibrosarcoma (HT1080) cells, we also developed a computational model for TRAIL signaling pathway. Using this model, we simulated cell survival and apoptotic molecule activations, such as MAP kinase, NF-κB and caspase-3. Next, we performed several *in silico* KO and found that protein kinase C (PKC) is the crucial target. To validate our prediction, we performed experiments using

PKC inhibitor, Bisindlymaleimide I (BIM-I) on HT1080 and human colon adenocarcinoma (HT29) cells. As a result, we verified that the inclusion of BIM-I showed significant enhancement of apoptosis through the suppression of PKC family members with corresponding impairment of cancer cell viability (over 95% cell death for HT1080 and HT29.) On the other hand, the control unstimulated cancer and normal cells (TIG1 and MRC5) with BIM-I did not show any adverse results.

4.2 Future directions

Further analysis is required to understand the heterogeneous response in TRAIL signaling. In chapter 3, we showed that TRAIL (200ng/ml) and PKC inhibitor BIM-I (10μM) co-stimulation lead 99% cell death in TRAIL resistant HT1080 cells. This shows that, although the populations of the cancer cells are highly variable and heterogeneous (40% cell death in wildtype), TRAIL and BIM-I co-stimulation showed a highly deterministic response of cancer cells towards cell death. This raises a novel question about the cause of heterogeneous response in cancer cells. To reveal this issue, it is required to understand the biological noise that occurs at single cells level (Eldar *et al.* 2010, Losick *et al.* 2008, Raj *et al.* 2010).

The computational model for TRAIL signaling pathway is originally developed using the first order linear response approach to understand the response of each signaling molecule at population level (Piras *et al.* 2011). For further understating

of the single cell response, we have extended our original TRAIL signaling model using Gellespie algorithm, where each reaction is turned 'on' or 'off' randomly or stochastically in time, according to the absolute values of their average reaction rates (Gillespie 2007; Piras *et al.* 2012). We observed stochastic behavior of each molecule (IκB, JNK, p38 and canspase-8) in each of the 1000 cells under four conditions (wildtype, FADD KD, RIP KD, TRAF2 KD) with low, medium and high number of activated TRAIL receptors. The lower number of receptors showed noisier response and higher number showed the temporal profiles that converged towards the deterministic population response (Figure 4.1). Therefore single cell analysis can support the understanding of the heterogeneous response of cancer cells.

Nevertheless, although cancer cells behavior is heterogeneous, targeting PKC leads to 99% of the cell death in HT1080 cells. Therefore PKC can be a "noise generator" in cancer cells. Hence by hitting PKC, the biological noise is eliminated and the response of cancer cells could switch from heterogeneous state to deterministic state. However this is still a hypothesis, and to prove this, more theoretical study and experiments are required.

Although the issue of heterogeneous response is still remaining, we plan to investigate the other TRAIL resistant cancer cells, such as pancreatic cancer, melanoma, and neuroblastoma (Eggert *et al.* 2001; Fulda *et al.* 2001; Hinz *et al.* 2000) using our average perturbation response approach and the experimental verification. Doing so, we

hope to identify other candidates to enhance the cell death in resistance cell types. Cell type differences in signaling networks may also be revealed through this approach.

Throughout this thesis, understanding the intracellular system was shown to be essential to discover the target molecules to kill the cancerous cells or suppress the proinflammatory responses. Using the original top-down approach, we predicted the potential intracellular targets from the computational models and verified them experimentally. This work shows systems biology strategies pave the way for the drug development to regulate the immune-mediated diseases and contributes the advancement of systems immunology.

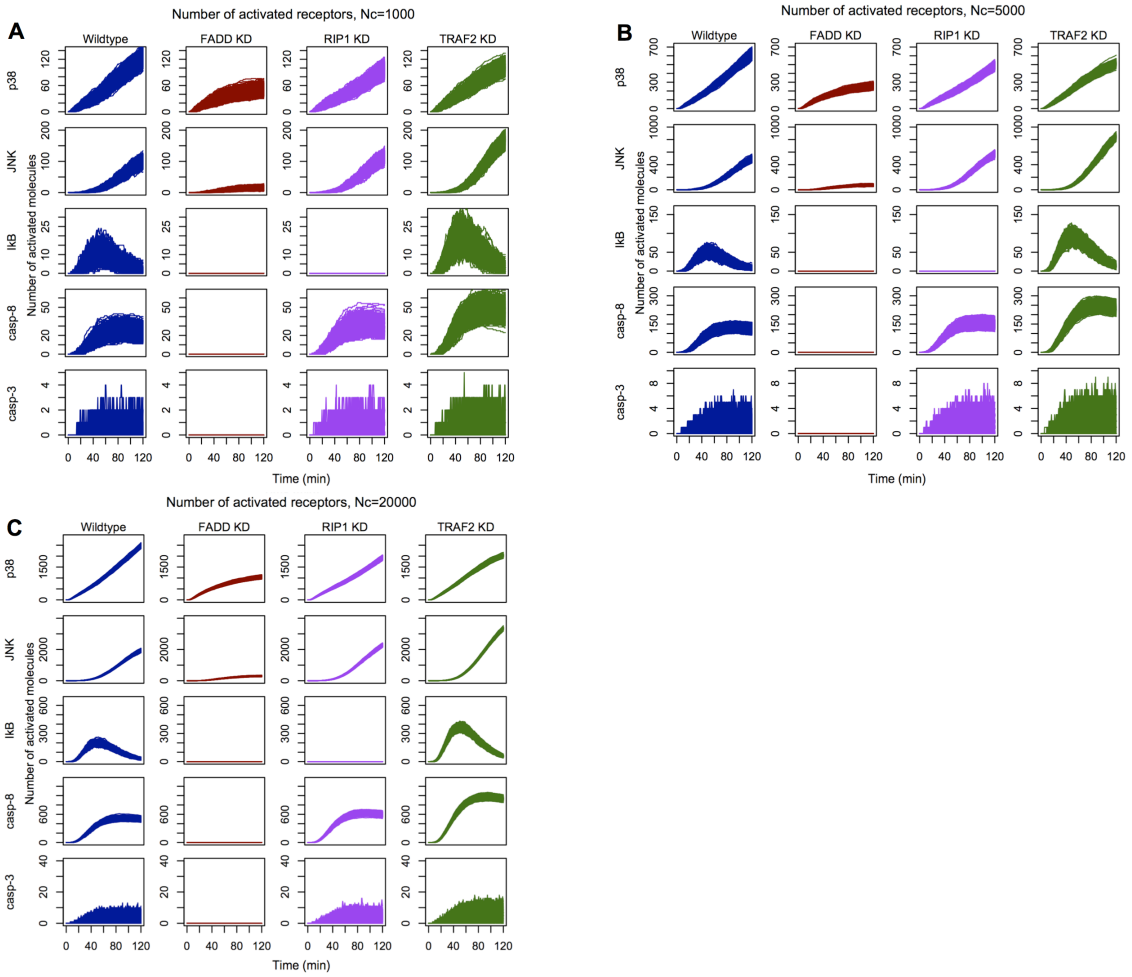

Figure 4.1 Stochastic simulation profiles of TRAIL signaling molecules. Stochastic response simulation profiles of p38, JNK, IκB, caspase-8 and -3 in wildtype (blue), FADD KD (brown), RIP KD (purple) and TRAF2 KD (green) for 1000 cells with **(A)** low, **(B)** medium and **(C)** high number of activated TRAIL receptors (adapted from Piras *et al.* 2012).

Acknowledgements

I would like to thank the people who made this research possible. First, I deeply thank my supervisor, Professor Kumar Selvarajoo who guided me through this work with a lot of insight and substantial discussions. Without him, I would have not spent time for such an exciting research. He will always inspire me for my life. I also would like to thank Dr. Vincent Piras and systems immunology group members for valuable discussions and support. They gave me new insights through daily discussions. I am grateful to previous systems immunology group members, Dr. Masa Tsuchiya, Daiki Yamada, Midori Hashimoto, Dr. Mohamed Helmy, Dr. Kalesh Sasidharan, Krisna Chaithanya, Naoki Fujikawa, Tomohiro Ooshige, Jean-Marie Schaeffer, Christelle Mazereau, Tomas Gomes Cardoso, Laura Khoudeir, Oriane Siméoni and Vincent Massieye. Dr. Sho Tabata and Dr. Mitsuhiro Kitagawa taught me the experiments from the basics and supported cell signaling projects.

I would like to thank the administrative staff in SFC and TTCK campus, Ayumi Mikami, Satomi Yokoi, Akiko Shiozawa and Yoko Tsuchiya. I definitely acknowledge Professor Masaru Tomita for all his support for the research projects.

I appreciate the valuable time spent with all my friends. I would like to say thank you to Shinya Murata, Satoru Ariga, Atsuko Shinhara, Hiroyuki Nakamura, Hiroaki Suzumura, Satoshi Tamaki, Kahori Ikeda-Takane, Kaoru Sugahara-Kikuta,

Kazuhide Sekiyama, Dr. Taiko Nishino, Dr. Cornelia Amariei and Tsubasa Watabe who I have enjoyed studying and working with. Without them, I would not have spent such a joyful life until now. And I would also like to thank to IAB alumni, Nobuto Saito, Saeka Murata-Tani, Dr. Kosuke Fujishima, Dr. Junichi Sugahara, Kaori Sekiyama, Hiromi Toyoshima, Dr. Haruna Kaneko-Imamura. I would like to express my gratitude for their hospitality.

Last but not at least, I especially thank my parents Kenichi, Ayako and my brother Yujiro for their continual support and encouragement throughout my life.

References

Abrams TJ, Lee LB, Murray LJ, Pryer NK & Cherrington JM (2003). SU11248 inhibits KIT and platelet-derived growth factor receptor beta in preclinical models of human small cell lung cancer. *Mol Cancer Ther* **2,** 471–478.

Akira S, Akira S, Uematsu S, Uematsu S, Takeuchi O & Takeuchi O (2006). Pathogen recognition and innate immunity. *Cell* **124,** 783–801.

Albert R & Wang RS (2009). Discrete dynamic modeling of cellular signaling networks. *Methods Enzymol* **467,** 281–306.

Aldridge BB, Burke JM, Lauffenburger DA & Sorger PK (2006). Physicochemical modelling of cell signalling pathways. *Nat Cell Biol* **8,** 1195–1203.

Aldridge BB, Saez-Rodriguez J, Muhlich JL, Sorger PK & Lauffenburger DA (2009). Fuzzy Logic Analysis of Kinase Pathway Crosstalk in TNF/EGF/Insulin-Induced Signaling. *PLoS Comput Biol* **5,** e100340.

Balkwill F (2006). TNF-alpha in promotion and progression of cancer. *Cancer Metastasis Rev* **25,** 409–416.

Balkwill F (2009). Tumour necrosis factor and cancer. *Nat Rev Cancer* **9,** 361–371.

Barabási AL & Oltvai ZN (2004). Network biology: understanding the cell's functional organization. *Nat Rev Genet* **5,** 101–113.

Beutler B (2004). Innate immunity: An overview. *Mol Immunol* **40,** 845–859.

Birtwistle MR, Hatakeyama M, Yumoto N, Ogunnaike BA, Hoek JB & Kholodenko BN (2007). Ligand-dependent responses of the ErbB signaling network: experimental and modeling analyses. *Mol Syst Biol* **3,** 144.

Blau L, Knirsh R, Ben-Dror I, Oren S, Kuphal S, Hau P, Proescholdt M, Bosserhoff AK & Vardimon L (2012). Aberrant expression of c-Jun in glioblastoma by internal ribosome entry site (IRES)-mediated translational activation. *Proc Natl Acad Sci* **109,** E2875–E2884.

Bradley JR (2008). TNF-mediated inflammatory disease. *J Pathol* **214,** 149–160.

Brändlin I, Eiseler T, Salowsky R & Johannes FJ (2002). Protein kinase C (mu) regulation of the JNK pathway is triggered via phosphoinositide-dependent kinase 1 and protein kinase C (epsilon). *J Biol Chem* **277,** 45451–45457.

Bruggeman FJ & Westerhoff HV. (2007). The nature of systems biology. *Trends Microbiol* **15,** 45–50.

Bruggeman FJ, Westerhoff HV, Hoek JB & Kholodenko BN (2002). Modular response analysis of cellular regulatory networks. *J Theor Biol* **218,** 507–520.

Burnette WN (1981). "Western blotting": electrophoretic transfer of proteins from sodium dodecyl sulfate--polyacrylamide gels to unmodified nitrocellulose and radiographic detection with antibody and radioiodinated protein A. *Anal Biochem* **112,** 195–203.

Burstein HJ & Schwartz RS (2008). Molecular origins of cancer. *N Engl J Med* **358,** 527.

Bushell M, Stoneley M, Kong YW, Hamilton TL, Spriggs KA, Dobbyn HC, Qin X, Sarnow P & Willis AE (2006). Polypyrimidine Tract Binding Protein Regulates IRES-Mediated Gene Expression during Apoptosis. *Mol Cell* **23,** 401–412.

Bushell M, Stoneley M, Sarnow P & Willis AE (2004). Translation inhibition during the induction of apoptosis: RNA or protein degradation? *Biochem Soc Trans* **32,** 606–610.

Carroll DL (1996). Chemical laser modeling with genetic algorithms. *AIAA J* **34,** 338–346.

Chaouiya C (2007). Petri net modelling of biological networks. *Brief Bioinform* **8,** 210–219.

Chaudhry SI, Hooper S, Nye E, Williamson P, Harrington K & Sahai E (2013). Autocrine IL-1β-TRAF6 signalling promotes squamous cell carcinoma invasion through paracrine TNFα signalling to carcinoma-associated fibroblasts. *Oncogene* **32,** 747–758.

Cho KH, Shin SY, Lee HW & Wolkenhauer O (2003). Investigations into the analysis and modeling of the TNF alpha-mediated NF-kappa B-signaling pathway. *Genome Res* **13,** 2413–2422.

Coussens LM & Werb Z (2002). Inflammation and cancer. *Nature* **420,** 860–867.

Daigeler A, Brenzel C, Bulut D, Geisler A, Hilgert C, Lehnhardt M, Steinau HU, Flier A, Steinstraesser L, Klein-Hitpass L, Mittelkötter U, Uhl W & Chromik AM (2008). TRAIL and Taurolidine induce apoptosis and decrease proliferation in human fibrosarcoma. *J Exp Clin Cancer Res* **27,** 82.

Daigeler A, Chromik AM, Haendschke K, Emmelmann S, Siepmann M, Hensel K, Schmitz G, Klein-Hitpass L, Steinau HU, Lehnhardt M & Hauser J (2010). Synergistic effects of sonoporation and taurolidin/TRAIL on apoptosis in human fibrosarcoma. *Ultrasound Med Biol* **36,** 1893–1906.

Davis PD, Hill CH, Keech E, Lawton G, Nixon JS, Sedgwick AD, Wadsworth J, Westmacott D & Wilkinson SE (1989). Potent selective inhibitors of protein kinase C. *FEBS Lett* **259,** 61–63.

Degterev A, Hitomi J, Germscheid M, Ch'en IL, Korkina O, Teng X, Abbott D, Cuny GD, Yuan C, Wagner G, Hedrick SM, Gerber SA, Lugovskoy A & Yuan J (2008). Identification of RIP1 kinase as a specific cellular target of necrostatins. *Nat Chem Biol* **4,** 313–321.

Degterev A, Huang Z, Boyce M, Li Y, Jagtap P, Mizushima N, Cuny GD, Mitchison TJ, Moskowitz MA & Yuan J (2005). Chemical inhibitor of nonapoptotic cell death with therapeutic potential for ischemic brain injury. *Nat Chem Biol* **1,** 112–119.

Del Prete MJ, Robles MS, Guáo A, Martínez-A C, Izquierdo M & Garcia-Sanz JA (2002). Degradation of cellular mRNA is a general early apoptosis-induced event. *FASEB J* **16,** 2003–2005.

DeRisi J, Penland L, Brown PO, Bittner ML, Meltzer PS, Ray M, Chen Y, Su YA & Trent JM (1996). Use of a cDNA microarray to analyse gene expression patterns in human cancer. *Nat Genet* **14,** 457–460.

Devin A, Cook A, Lin Y, Rodriguez Y, Kelliher M & Liu Z (2000). The distinct roles of TRAF2 and RIP in IKK activation by TNF-R1: TRAF2 recruits IKK to TNF-R1 while RIP mediates IKK activation. *Immunity* **12,** 419–429.

Dimberg LY, Anderson CK, Camidge R, Behbakht K, Thorburn A & Ford HL (2012). On the TRAIL to successful cancer therapy? Predicting and counteracting resistance against TRAIL-based therapeutics. *Oncogene* **32,** 1341–1350.

Druker BJ (2004). Imatinib as a paradigm of targeted therapies. *Adv Cancer Res* **91,** 1–30.

Eggert A, Grotzer MA, Zuzak TJ, Wiewrodt BR, Ho R, Ikegaki N & Brodeur GM (2001). Resistance to tumor necrosis factor-related apoptosis-inducing ligand (TRAIL)-induced apoptosis in neuroblastoma cells correlates with a loss of caspase-8 expression. *Cancer Res* **61,** 1314–1319.

Ehrhardt H, Fulda S, Schmid I, Hiscott J, Debatin KM & Jeremias I (2003). TRAIL induced survival and proliferation in cancer cells resistant towards TRAIL-induced apoptosis mediated by NF-kappaB. *Oncogene* **22,** 3842–3852.

Eldar A & Elowitz MB (2010). Functional roles for noise in genetic circuits. *Nature* **467,** 167–173.

Elmore S (2007). Apoptosis: a review of programmed cell death. *Toxicol Pathol* **35,** 495–516.

Ermolaeva MA, Michallet MC, Papadopoulou N, Utermöhlen O, Kranidioti K, Kollias G, Tschopp J & Pasparakis M (2008). Function of TRADD in tumor necrosis factor receptor 1 signaling and in TRIF-dependent inflammatory responses. *Nat Immunol* **9,** 1037–1046.

Fallahi-Sichani M, Flynn JL, Linderman JJ & Kirschner DE (2012). Differential risk of tuberculosis reactivation among anti-TNF therapies is due to drug binding kinetics and permeability. *J Immunol* **188,** 3169–3178.

Falschlehner C & Boutros M (2012). Innate immunity: regulation of caspases by IAP-dependent ubiquitylation. *EMBO J* **31,** 2750–2752.

Fisher RA (1930). The Genetical Theory of Natural Selection. *Genetics* **154,** 272.

Fulda S, Küfer MU, Meyer E, van Valen F, Dockhorn-Dworniczak B & Debatin KM (2001). Sensitization for death receptor- or drug-induced apoptosis by re-expression of caspase-8 through demethylation or gene transfer. *Oncogene* **20,** 5865–5877.

Funakoshi-Tago M, Kamada N, Shimizu T, Hashiguchi Y, Tago K, Sonoda Y & Kasahara T (2009). TRAF6 negatively regulates TNFalpha-induced NF-kappaB activation. *Cytokine* **45,** 72–79.

Gatsinzi T, Ivanova EV & Iverfeldt K (2012). TRAIL resistance in human neuroblastoma SK-N-AS cells is dependent on protein kinase C and involves inhibition of caspase-3 proteolytic processing. *J Neurooncol* **109,** 503–512.

Gillespie DT (2007). Stochastic simulation of chemical kinetics. *Annu Rev Phys Chem* **58,** 35–55.

Gobbi G, Di Marcantonio D, Micheloni C, Carubbi C, Galli D, Vaccarezza M, Bucci G, Vitale M & Mirandola P (2012). TRAIL up-regulation must be accompanied by a reciprocal PKCε down-regulation during differentiation of colonic epithelial cell: Implications for colorectal cancer cell differentiation. *J Cell Physiol* **227,** 630–638.

Grivennikov S & Karin M (2008). Autocrine IL-6 Signaling: A Key Event in Tumorigenesis? *Cancer Cell* **13,** 7–9.

Grivennikov SI, Greten FR & Karin M (2010). Immunity, inflammation, and cancer. *Cell* **140,** 883–899.

Guido NJ, Wang X, Adalsteinsson D, McMillen D, Hasty J, Cantor CR, Elston TC & Collins JJ (2006). A bottom-up approach to gene regulation. *Nature* **439,** 856–860.

Hao C, Beguinot F, Condorelli G, Trencia A, Van Meir EG, Yong VW, Parney IF, Roa WH & Petruk KC (2001). Induction and intracellular regulation of tumor necrosis factor-related apoptosis-inducing ligand (TRAIL) mediated apoptosis in human malignant glioma cells. *Cancer Res* **61,** 1162–1170.

Hao S & Baltimore D (2009). The stability of mRNA influences the temporal order of the induction of genes encoding inflammatory molecules. *Nat Immunol* **10,** 281–288.

Hao S & Baltimore D (2013). RNA splicing regulates the temporal order of TNF-induced gene expression. *Proc Natl Acad Sci U S A* **110,** 11934–11939.

Harper N, Hughes MA, Farrow SN, Cohen GM & MacFarlane M (2003). Protein kinase C modulates tumor necrosis factor-related apoptosis-inducing ligand-induced apoptosis by targeting the apical events of death receptor signaling. *J Biol Chem* **278,** 44338–44347.

Hayakawa Y & Smyth MJ (2006). Innate Immune Recognition and Suppression of Tumors. *Adv Cancer Res* **95,** 293–322.

Hayashi K, Piras V, Tabata S, Tomita M & Selvarajoo K (2013). A systems biology approach to suppress TNF-induced proinflammatory gene expressions. *Cell Commun Signal* **11,** 84.

Heidorn SJ, Milagre C, Whittaker S, Nourry A, Niculescu-Duvas I, Dhomen N, Hussain J, Reis-Filho JS, Springer CJ, Pritchard C & Marais R (2010). Kinase-Dead BRAF and Oncogenic RAS Cooperate to Drive Tumor Progression through CRAF. *Cell* **140,** 209–221.

Helmy M, Gohda J, Inoue JI, Tomita M, Tsuchiya M & Selvarajoo K (2009). Predicting novel features of toll-like receptor 3 signaling in macrophages. *PLoS One* **4,** e4661.

Hinz S, Trauzold A, Boenicke L, Sandberg C, Beckmann S, Bayer E, Walczak H, Kalthoff H & Ungefroren H (2000). Bcl-XL protects pancreatic adenocarcinoma cells against CD95- and TRAIL-receptor-mediated apoptosis. *Oncogene* **19,** 5477–5486.

Hodgkin AL & Huxley AF (1952). A quantitative description of membrane current and its applications to conduction and excitation in nerve. *J Physiol* **117,** 500–544.

Hoffmann A, Levchenko A, Scott ML & Baltimore D (2002). The IkappaB-NF-kappaB signaling module: temporal control and selective gene activation. *Science* **298,** 1241–1245.

Hood L, Heath JR, Phelps ME & Lin B (2004). Systems biology and new technologies enable predictive and preventative medicine. *Science* **306,** 640–643.

Hoops S, Gauges R, Lee C, Pahle J, Simus N, Singhal M, Xu L, Mendes P & Kummer U (2006). COPASI - A COmplex PAthway SImulator. *Bioinformatics* **22,** 3067–3074.

vban Horssen R, Ten Hagen TLM & Eggermont AMM (2006). TNF-alpha in cancer treatment: molecular insights, antitumor effects, and clinical utility. *Oncologist* **11,** 397–408.

Ihn H (2008). Autocrine TGF-beta signaling in the pathogenesis of systemic sclerosis. *J Dermatol Sci* **49,** 103–113.

Janeway CA & Medzhitov R (2002). Innate immune recognition. *Annu Rev Immunol* **20,** 197–216.

Jo M, Kim TH, Seol DW, Esplen JE, Dorko K, Billiar TR & Strom SC (2000). Apoptosis induced in normal human hepatocytes by tumor necrosis factor-related apoptosis-inducing ligand. *Nat Med* **6,** 564–567.

Johnstone RW, Frew AJ & Smyth MJ (2008). The TRAIL apoptotic pathway in cancer onset, progression and therapy. *Nat Rev Cancer* **8,** 782–798.

Kaneva MK, Kerrigan MJP, Grieco P, Curley GP, Locke IC & Getting SJ (2012). Chondroprotective and anti-inflammatory role of melanocortin peptides in TNF-α activated human C-20/A4 chondrocytes. *Br J Pharmacol* **167,** 67–79.

Karlebach G & Shamir R (2008). Modelling and analysis of gene regulatory networks. *Nat Rev Mol Cell Biol* **9,** 770–780.

Keane MM, Ettenberg SA, Nau MM, Russell EK & Lipkowitz S (1999). Chemotherapy augments TRAIL-induced apoptosis in breast cell lines. *Cancer Res* **59,** 734–741.

Kermack WO & McKendrick AG (1933). Contributions to the Mathematical Theory of Epidemics. III. Further Studies of the Problem of Endemicity. *Proc R Soc A Math Phys Eng Sci* **141,** 94–122.

Khanbolooki S, Nawrocki ST, Arumugam T, Andtbacka R, Pino MS, Kurzrock R, Logsdon CD, Abbruzzese JL & McConkey DJ (2006). Nuclear factor-kappaB maintains TRAIL resistance in human pancreatic cancer cells. *Mol Cancer Ther* **5,** 2251–2260.

Kholodenko BN (2000). Negative feedback and ultrasensitivity can bring about oscillations in the mitogen-activated protein kinase cascades. *Eur J Biochem* **267,** 1583–1588.

Kholodenko BN, Kiyatkin A, Bruggeman FJ, Sontag E, Westerhoff HV & Hoek JB (2002). Untangling the wires: a strategy to trace functional interactions in signaling and gene networks. *Proc Natl Acad Sci U S A* **99,** 12841–12846.

Kim K, Fisher MJ, Xu SQ & el-Deiry WS (2000). Molecular determinants of response to TRAIL in killing of normal and cancer cells. *Clin Cancer Res* **6,** 335–346.

Kitano H (2002). Systems biology: a brief overview. *Science* **295,** 1662–1664.

Lamothe B, Lai Y, Xie M, Schneider MD & Darnay BG (2013). TAK1 is essential for osteoclast differentiation and is an important modulator of cell death by apoptosis and necroptosis. *Mol Cell Biol* **33,** 582–595.

Lanier LL (2005). NK cell recognition. *Annu Rev Immunol* **23,** 225–274.

Liacini A, Sylvester J, Li WQ, Huang W, Dehnade F, Ahmad M & Zafarullah M (2003). Induction of matrix metalloproteinase-13 gene expression by TNF-α is mediated by MAP kinases, AP-1, and NF-κB transcription factors in articular chondrocytes. *Exp Cell Res* **288,** 208–217.

Liacini A, Sylvester J, Li WQ & Zafarullah M (2002). Inhibition of interleukin-1-stimulated MAP kinases, activating protein-1 (AP-1) and nuclear factor kappa B (NF-κB) transcription factors down-regulates matrix metalloproteinase gene expression in articular chondrocytes. *Matrix Biol* **21,** 251–262.

Ljunggren HG & Malmberg KJ (2007). Prospects for the use of NK cells in immunotherapy of human cancer. *Nat Rev Immunol* **7,** 329–339.

Locksley RM, Killeen N & Lenardo MJ (2001). The TNF and TNF receptor superfamilies: Integrating mammalian biology. *Cell* **104,** 487–501.

Losick R & Desplan C (2008). Stochasticity and cell fate. *Science* **320,** 65–68.

Mantovani A, Sozzani S, Locati M, Allavena P & Sica A (2002). Macrophage polarization: tumor-associated macrophages as a paradigm for polarized M2 mononuclear phagocytes. *Trends Immunol* **23,** 549–555.

Monton MRN & Soga T (2007). Metabolome analysis by capillary electrophoresis-mass spectrometry. *J Chromatogr A* **1168,** 237–246.

Morán F, Vlad MO, Bustos M, Trivino JC & Ross J (2007). Species connectivities and reaction mechanisms from neutral response experiments. *J Phys Chem A* **111,** 1844–1851.

Murray JD (2012). Vignettes from the field of mathematical biology: the application of mathematics to biology and medicine. *Interface Focus* **2,** 397–406.

O'Brien SG et al. (2003). Imatinib compared with interferon and low-dose cytarabine for newly diagnosed chronic-phase chronic myeloid leukemia. *N Engl J Med* **348,** 994–1004.

Okhrimenko H, Lu W, Xiang C, Hamburger N, Kazimirsky G & Brodie C (2005*a*). Protein kinase C-epsilon regulates the apoptosis and survival of glioma cells. *Cancer Res* **65,** 7301–7309.

Okhrimenko H, Lu W, Xiang C, Ju D, Blumberg PM, Gomel R, Kazimirsky G & Brodie C (2005*b*). Roles of tyrosine phosphorylation and cleavage of protein kinase Cdelta in its protective effect against tumor necrosis factor-related apoptosis inducing ligand-induced apoptosis. *J Biol Chem* **280,** 23643–23652.

O'Malley WE, Achinstein B & Shear MJ (1962). Action of bacterial polysaccharide on tumours: II: Damage of sarcoma 37 by serum of mice treated with serratia marcescens polysaccharide, and induced tolerance. *J Natl Cancer Inst* **29,** 1169–1175.

Orth JD, Thiele I & Palsson BØ (2010). What is flux balance analysis? *Nat Biotechnol* **28,** 245–248.

Piras V, Hayashi K, Tomita M & Selvarajoo K (2011). Enhancing apoptosis in TRAIL-resistant cancer cells using fundamental response rules. *Sci Rep* **1,** 144.

Piras V, Hayashi K, Tomita M & Selvarajoo K (2012). Investigation of stochasticity in TRAIL signaling cancer model, *Proceedings of IEEE/ICME Complex Medical Engineering* 609–614.

Piras V, Tomita M & Selvarajoo K. (2014). Transcriptome-wide variability in single embryonic development cells. *Sci Rep* **4,** 7137.

Pitti RM, Marsters SA, Ruppert S, Donahue CJ, Moore A & Ashkenazi A (1996). Induction of apoptosis by Apo-2 ligand, a new member of the tumor necrosis factor cytokine family. *J Biol Chem* **271,** 12687–12690.

Putnam AJ, Schulz VV, Freiter EM, Bill HM & Miranti CK (2009). Src, PKCalpha, and PKCdelta are required for alphavbeta3 integrin-mediated metastatic melanoma invasion. *Cell Commun Signal* **7,** 10.

Raj A, Rifkin SA, Andersen E & van Oudenaarden A (2010). Variability in gene expression underlies incomplete penetrance. *Nature* **463,** 913–918.

Roman-Blas JA & Jimenez SA (2006). NF-κB as a potential therapeutic target in osteoarthritis and rheumatoid arthritis. *Osteoarthr Cartil* **14,** 839–848.

Ross J (2008). Determination of complex reaction mechanisms. Analysis of chemical, biological and genetic networks. *J Phys Chem* **112,** 2134–2143.

Santos SDM, Verveer PJ & Bastiaens PIH (2007). Growth factor-induced MAPK network topology shapes Erk response determining PC-12 cell fate. *Nat Cell Biol* **9,** 324–330.

Sellam J & Berenbaum F (2010). The role of synovitis in pathophysiology and clinical symptoms of osteoarthritis. *Nat Rev Rheumatol* **6,** 625–635.

Selvarajoo K (2006). Discovering differential activation machinery of the Toll-like receptor 4 signaling pathways in MyD88 knockouts. *FEBS Lett* **580,** 1457–1464.

Selvarajoo K (2011). Macroscopic law of conservation revealed in the population dynamics of Toll-like receptor signaling. *Cell Commun Signal* **9,** 9.

Selvarajoo K (2012). Understanding multimodal biological decisions from single cell and population dynamics. *Wiley Interdiscip Rev Syst Biol Med* **4,** 385–399.

Selvarajoo K (2013a). Interpreting the dynamics and patterns of living systems. *Bioscience* **63,** 721–722.

Selvarajoo K (2013b). Uncertainty and certainty in cellular dynamics. *Front Genet* **4,** 68.

Selvarajoo K (2014). Parameter-less approaches for interpreting dynamic cellular response. *J Biol Eng* **8,** 23.

Selvarajoo K & Giuliani A (2012). Finding self-organization from the dynamic gene expressions of innate immune responses. *Front Physiol* **3,** 192.

Selvarajoo K, Takada Y, Gohda J, Helmy M, Akira S, Tomita M, Tsuchiya M, Inoue JI & Matsuo K (2008). Signaling flux redistribution at toll-like receptor pathway junctions. *PLoS One* **3,** e3430.

Selvarajoo K & Tomita M (2013). Physical laws shape biology. *Science* **339,** 646.

Selvarajoo K, Tomita M & Tsuchiya M (2009). Can complex cellular processes be governed by simple linear rules? *J Bioinform Comput Biol* **7,** 243–268.

Selvarajoo K & Tsuchiya M (2007). Systematic Determination of Biological Network Topology: Nonintegral Connectivity Method (NICM). In *Introduction to Systems Biology*, ed. Choi S, pp. 449–471. The Humana Press, New Jersey.

Shankar E, Sivaprasad U & Basu A (2008). Protein kinase C epsilon confers resistance of MCF-7 cells to TRAIL by Akt-dependent activation of Hdm2 and downregulation of p53. *Oncogene* **27,** 3957–3966.

Shi RX, Ong CN & Shen HM (2005). Protein kinase C inhibition and x-linked inhibitor of apoptosis protein degradation contribute to the sensitization effect of luteolin on tumor necrosis factor-related apoptosis-inducing ligand-induced apoptosis in cancer cells. *Cancer Res* **65,** 7815–7823.

Slamon DJ, Leyland-Jones B, Shak S, Fuchs H, Paton V, Bajamonde A, Fleming T, Eiermann W, Wolter J, Pegram M, Baselga J & Norton L (2001). Use of chemotherapy plus a monoclonal antibody against HER2 for metastatic breast cancer that overexpresses HER2. *N Engl J Med* **344,** 783–792.

Smyth MJ, Takeda K, Hayakawa Y, Peschon JJ, van den Brink MRM & Yagita H (2003). Nature's TRAIL--on a path to cancer immunotherapy. *Immunity* **18,** 1–6.

Solomon EP, Berg LR & Martin DW (2011). *Biology*. 9th edn. Thomson Brooks/Cole: Pacific Grove.

Spits H & Di Santo JP (2011). The expanding family of innate lymphoid cells: regulators and effectors of immunity and tissue remodeling. *Nat Immunol* **12,** 21–27.

Spriggs KA, Bushell M, Mitchell SA & Willis AE (2005). Internal ribosome entry segment-mediated translation during apoptosis: the role of IRES-trans-acting factors. *Cell Death Differ* **12,** 585–591.

Stuckey DW & Shah K (2013). TRAIL on trial: preclinical advances in cancer therapy. *Trends Mol Med* **19,** 685–694.

Su F, Viros A, Milagre C, Bollag G & Zhang C (2012). RAS Mutations in Cutaneous Squamous-Cell Carcinomas in Patients Treated with BRAF Inhibitors. *N Engl J Med* **366,** 207–215.

Swann JB, Vesely MD, Silva A, Sharkey J, Akira S, Schreiber RD & Smyth MJ (2008). Demonstration of inflammation-induced cancer and cancer immunoediting during primary tumorigenesis. *Proc Natl Acad Sci U S A* **105,** 652–656.

Tada K, Okazaki T, Sakon S, Kobarai T, Kurosawa K, Yamaoka S, Hashimoto H, Mak TW, Yagita H, Okumura K, Yeh WC & Nakano H (2001). Critical roles of TRAF2 and TRAF5 in tumor necrosis factor-induced NF-kappa B activation and protection from cell death. *J Biol Chem* **276,** 36530–36534.

Tan P & Selvarajoo K (2003). Modelling of biochemical pathways. US Patent *No. 20,030,113,761*.

Tang M, Wei X, Guo Y, Breslin P, Zhang S, Zhang S, Wei W, Xia Z, Diaz M, Akira S & Zhang J (2008). TAK1 is required for the survival of hematopoietic cells and hepatocytes in mice. *J Exp Med* **205,** 1611–1619.

Tasseff R, Nayak S, Salim S, Kaushik P, Rizvi N & Varner JD (2010). Analysis of the molecular networks in androgen dependent and independent prostate cancer revealed fragile and robust subsystems. *PLoS One* **5,** e8864.

Theobald U, Mailinger W, Baltes M, Rizzi M & Reuss M (1997). In vivo analysis of metabolic dynamics in Saccharomyces cerevisiae : I. Experimental observations. *Biotechnol Bioeng* **55,** 305–316.

Thomas MP & Lieberman J (2013). Live or let die: Posttranscriptional gene regulation in cell stress and cell death. *Immunol Rev* **253,** 237–252.

Tian B, Nowak DE & Brasier AR (2005). A TNF-induced gene expression program under oscillatory NF-kappaB control. *BMC Genomics* **6,** 137.

Toullec D, Pianetti P, Coste H, Bellevergue P, Grand-Perret T, Ajakane M, Baudet V, Boissin P, Boursier E & Loriolle F (1991). The bisindolylmaleimide GF 109203X is a potent and selective inhibitor of protein kinase C. *J Biol Chem* **266,** 15771–15781.

Trauzold A, Siegmund D, Schniewind B, Sipos B, Egberts J, Zorenkov D, Emme D, Röder C, Kalthoff H & Wajant H (2006). TRAIL promotes metastasis of human pancreatic ductal adenocarcinoma. *Oncogene* **25,** 7434–7439.

Trauzold A, Wermann H, Arlt A, Schütze S, Schäfer H, Oestern S, Röder C, Ungefroren H, Lampe E, Heinrich M, Walczak H & Kalthoff H (2001). CD95 and TRAIL receptor-mediated activation of protein kinase C and NF-kappaB contributes to apoptosis resistance in ductal pancreatic adenocarcinoma cells. *Oncogene* **20,** 4258–4269.

Turing AM (1952). The Chemical Basis of Morphogenesis. *Society* **237,** 37–72.

Vance W, Arkin A & Ross J (2002). Determination of causal connectivities of species in reaction networks. *Proc Natl Acad Sci U S A* **99,** 5816–5821.

Vandesompele J, De Preter K, Pattyn F, Poppe B, Van Roy N, De Paepe A & Speleman F (2002). Accurate normalization of real-time quantitative RT-PCR data by geometric averaging of multiple internal control genes. *Genome Biol* **3,** RESEARCH0034.

Varfolomeev E, Maecker H, Sharp D, Lawrence D, Renz M, Vucic D & Ashkenazi A (2005). Molecular determinants of kinase pathway activation by Apo2 ligand/tumor necrosis factor-related apoptosis-inducing ligand. *J Biol Chem* **280,** 40599–40608.

Vivier E, Raulet DH, Moretta A, Caligiuri MA, Zitvogel L, Lanier LL, Yokoyama WM & Ugolini S (2011). Innate or Adaptive Immunity? The Example of Natural Killer Cells. *Science* **331,** 44–49.

Wang RS, Saadatpour A & Albert R (2012). Boolean modeling in systems biology: an overview of methodology and applications. *Phys Biol* **9,** 055001.

Wang S & El-Deiry WS (2003). TRAIL and apoptosis induction by TNF-family death receptors. *Oncogene* **22,** 8628–8633.

Wang Z, Gerstein M & Snyder M (2009). RNA-Seq: a revolutionary tool for transcriptomics. *Nat Rev Genet* **10,** 57–63.

Wang ZQ, Stingl L, Morrison C, Jantsch M, Los M, Schulze-Osthoff K & Wagner EF (1997). PARP is important for genomic stability but dispensable in apoptosis. *Genes Dev* **11,** 2347–2358.

Welman A, Griffiths JR, Whetton AD & Dive C (2007). Protein kinase C delta is phosphorylated on five novel Ser/Thr sites following inducible overexpression in human colorectal cancer cells. *Protein Sci* **16,** 2711–2715.

Werner SL, Barken D & Hoffmann A (2005). Stimulus specificity of gene expression programs determined by temporal control of IKK activity. *Science* **309,** 1857–1861.

Werner SL, Kearns JD, Zadorozhnaya V, Lynch C, O'Dea E, Boldin MP, Ma A, Baltimore D & Hoffmann A (2008). Encoding NF-κB temporal control in response to TNF: Distinct roles for the negative regulators IκBα and A20. *Genes Dev* **22,** 2093–2101.

Wertz IE & Dixit VM (2010). Regulation of death receptor signaling by the ubiquitin system. *Cell Death Differ* **17,** 14–24.

Wiens A, Venson R, Correr CJ, Otuki MF & Pontarolo R (2010). Meta-analysis of the efficacy and safety of adalimumab, etanercept, and infliximab for the treatment of rheumatoid arthritis. *Pharmacotherapy* **30,** 339–353.

Wiley SR, Schooley K, Smolak PJ, Din WS, Huang CP, Nicholl JK, Sutherland GR, Smith TD, Rauch C & Smith CA (1995). Identification and characterization of a new member of the TNF family that induces apoptosis. *Immunity* **3,** 673–682.

Wilkinson SE, Parker PJ & Nixon JS (1993). Isoenzyme specificity of bisindolylmaleimides, selective inhibitors of protein kinase C. *Biochem J* **294,** 335–337.

Wu J & Lanier LL (2003). Natural Killer Cells and Cancer. *Adv Cancer Res* **90,** 127–156.

Yaish P, Gazit A, Gilon C & Levitzki A (1988). Blocking of EGF-dependent cell proliferation by EGF receptor kinase inhibitors. *Science* **242,** 933–935.

Yanase N, Hayashida M, Kanetaka-Naka Y, Hoshika A & Mizuguchi J (2012). PKC-δ mediates interferon-α-induced apoptosis through c-Jun NH2-terminal kinase activation. *BMC Cell Biol* **13,** 7.

Yarilina A, Park-Min KH, Antoniv T, Hu X & Ivashkiv LB (2008). TNF activates an IRF1-dependent autocrine loop leading to sustained expression of chemokines and STAT1-dependent type I interferon-response genes. *Nat Immunol* **9,** 378–387.

Yeo ZX, Wong ST, Arjunan SNV, Piras V, Tomita M, Selvarajoo K, Giuliani A & Tsuchiya M (2007). Sequential logic model deciphers dynamic transcriptional control of gene expressions. *PLoS One* **2,** e776.

Zhang L & Fang B (2005). Mechanisms of resistance to TRAIL-induced apoptosis in cancer. *Cancer Gene Ther* **12,** 228–237.

Zhang XD, Nguyen T, Thomas WD, Sanders JE & Hersey P (2000). Mechanisms of resistance of normal cells to TRAIL induced apoptosis vary between different cell types. *FEBS Lett* **482,** 193–199.

Zhu H, Bilgin M, Bangham R, Hall D, Casamayor A, Bertone P, Lan N, Jansen R, Bidlingmaier S, Houfek T, Mitchell T, Miller P, Dean RA, Gerstein M & Snyder M (2001). Global analysis of protein activities using proteome chips. *Science* **293,** 2101–2105.

Zi Z (2011). Sensitivity analysis approaches applied to systems biology models. *IET Syst Biol* **5,** 336–346.

Appendix A

Description of the computational model in TRAIL signaling pathway

In chapter 3, the experiments are conducted based on our original TRAIL computational model published in 2011 (Piras *et al.* 2011). Here, the details about TRAIL computational model are shown below. In this computational model, we utilized the perturbation response approach using the law of conservation (see Materials and methods in chapter 2).

A.1 TRAIL signaling pathway and experimental activation profiles of signaling molecules

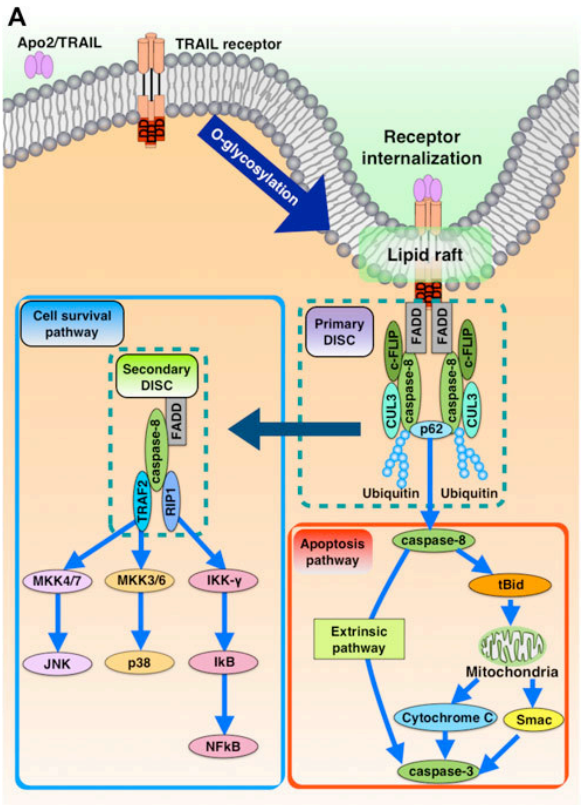

(A) Schematic topology of TRAIL signaling pathway.

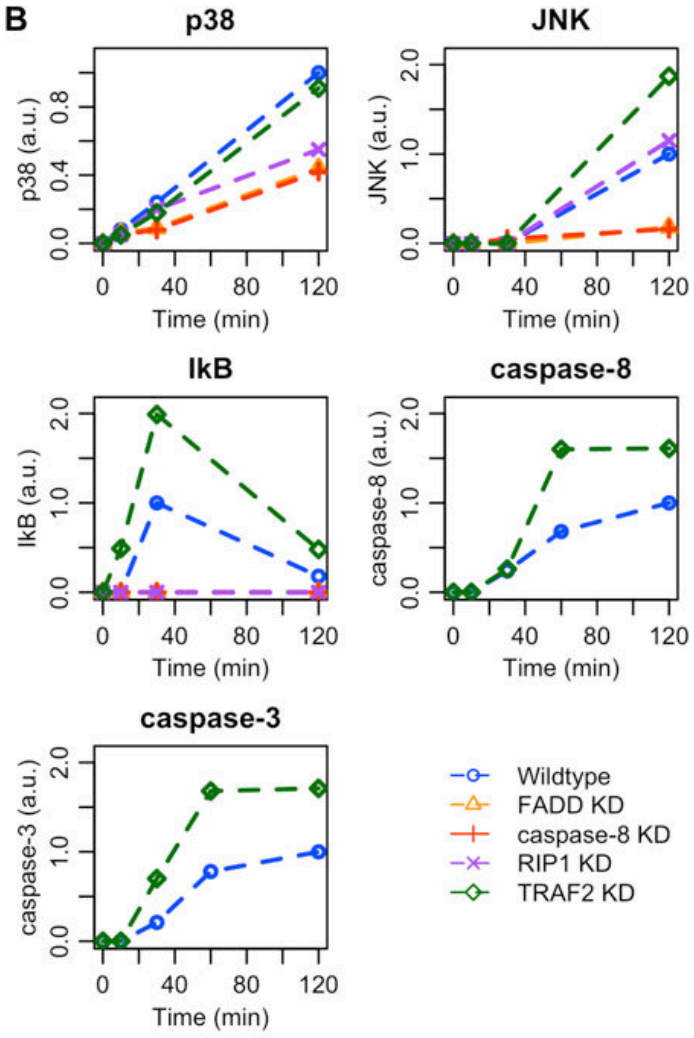

(B) Experimental activation profiles of p38, IκB, JNK, caspase-8 and -3 in wildtype, RIP1 KD*, FADD KD*, caspase-8 KD*, and TRAF2 KD in arbitrary units (a.u.) at t = 0, 10, 30, 60** and 120 min after TRAIL stimulation of HT1080 cells. The original source was obtained from Varfolomeev *et al.* (2005) and was processed through imageJ. *data is unavailable for caspase-8 and -3, ** available only for caspase-8 and -3. Note: interpolated dotted lines between experimental data points are inserted as a guide, they might not represent the actual temporal dynamics.

A.2 Simulation of initial TRAIL signaling model

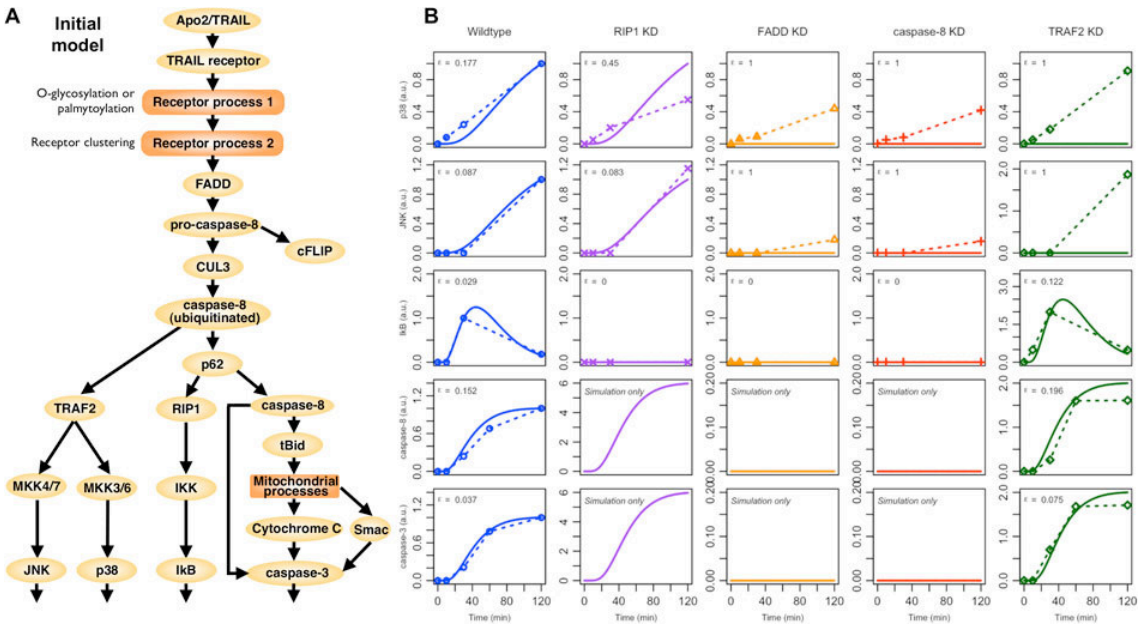

(A) Static topology of the TRAIL signaling pathway used in developing our computational model. Note that we lump the similar effects of DR4/5 as TRAILR1/2, and ignore the response of DcR1/R2/OPG. Also, note that we include molecular conditions such as receptor clustering as additional first-order terms. (B) Comparison of simulations (solid lines) with experimental data (dotted lines) in wildtype, RIP1 KD, FADD KD, caspase-8 KD* and TRAF2 KD in arbitrary units (a.u.). *caspase-8 KD also refers to pro-caspase-8 KD.

A.3 Revealing novel features of TRAIL signaling using modeling strategy and response rules

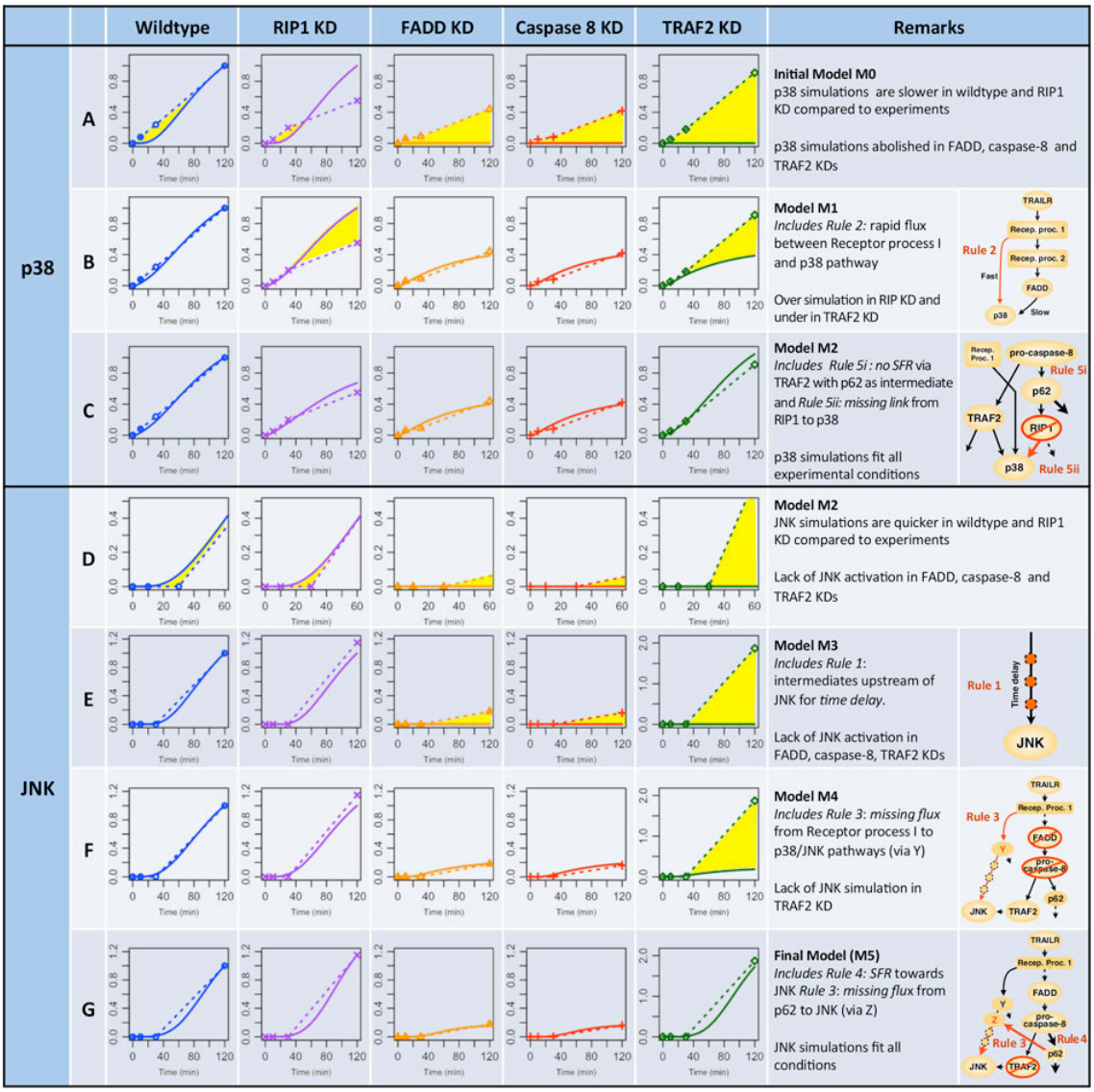

Model simulations compared with experiments. For p38, (A) M0, the initial model, (B) M1 with the addition of a rapid bypass, and (C) M2 with the addition of a missing link between RIP1 and p38 pathway. For JNK (D) M2, (E) M3 with intermediates to introduce delay in activation, (F) M4 with a missing link for the activation of JNK in FADD and caspase-8 KDs, and (G) M5 a missing link between p62 and JNK pathway to show enhancement through *SFR* in TRAF2 KD.

A.4 Simulations of the proposed TRAIL signaling topology

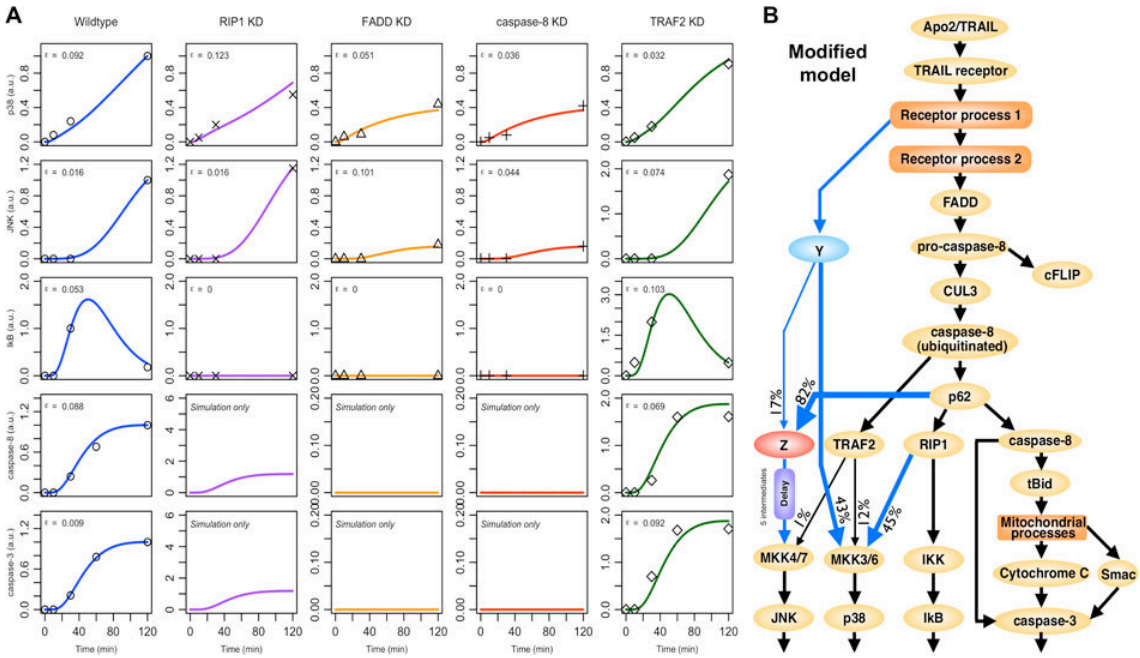

(A) Comparison of M5 simulations (solid lines) with experimental data (black points) in wildtype, RIP1 KD, FADD KD, caspase-8 KD and TRAF2 KD. (B) Static topology of the proposed model for TRAIL signaling pathway. Modifications are indicated by blue arrows. Here, Z indicates PKC.

A.5 The finalized TRAIL model reactions and parameters

	Reaction/process			*k* (1/s)	Remarks
1	Apo2/TRAIL	→	TRAIL receptor	8.13E-3	Binding of TRAIL ligand to receptor
2	TRAIL receptor	→	Receptor process 1	8.17E-3	O-glycosylation, internalization of receptors, formation of lipid rafts, etc.
3	Receptor process 1	→	Receptor process 2	7.89E-3	
4	Receptor process 2	→	Y	1.04E-3	Activation of novel molecule Y
5	Y	→	MKK3/6	4.31E-1	Rapid activation of MKK3/6 via Y
6	Receptor process 2	→	FADD	1.08E-3	FADD binds to TRAIL receptors
7	FADD	→	pro-caspase-8	1.06E-3	pro-caspase-8 binds to FADD
8	pro-caspase-8	→	CUL3	1,99E-3	Activation of CUL3
9	pro-caspase-8	→	c-FLIP	1.00E-3*	Activation of cFLIP *(*arbitrary value)*
10	CUL3	→	Ubiquitination of caspase-8	1.00E-2	Ubiquitination of caspase-8
11	Ubiquitination of caspase-8	→	p62	9.92E-1	Activation of p62/sequestosome
12	Ubiquitination of caspase-8	→	TRAF2	8.67E-2	Activation of TRAF2 by pro-caspase-8
13	p62	→	Z	3.09E-1	Activation of novel molecule Z by p62
14	p62	→	RIP1	6.77E-2	Activation of RIP1 by p62
15	p62	→	caspase-8 (active form)	2.72E-2	Activation of caspase-8 (cleaved)
16	caspase-8 (active form)	→	tBid	1.13E-5	Activation of tBid by caspase-8
17	caspase-8 (active form)	→	caspase-3	1.48E-6	Activation of caspase-3 (extrinsic pathway)
18	tBid	→	mitochondria	5.09E-2	Apoptotic intrinsic pathway via tBid
19	mitochondria	→	Cytochrome C	2.64E-1	Activation of Cytochrome C
20	mitochondria	→	Smac	2.79E-1	Activation of Smac
21	Cytochrome C	→	caspase-3	2.81E-1	Activation of caspase-3 via apoptosome
22	Smac	→	caspase-3	1.68E-1	Smac-dependent activation of caspase-3
23	caspase-3	→	Apoptosis process	8.85E-3	caspase-3 depletion term
24	RIP1	→	IKK	4.00E-4	Activation of IKK by RIP1
25	RIP1	→	MKK3/6	5.04E-1	Activation of MKK3/6 by RIP1 (novel)
26	IKK	→	IκB	3.45E-1	Activation of IκB by IKK
27	IκB	→	NF-κB	8.99E-4	Activation of NF-κB by IκB
28	NF-κB	→	Survival process	1.00E-1*	NF-κB depletion term *(*arbitrary value)*
29	TRAF2	→	MKK3/6	7.24E-5	Activation of MKK3/6 by TRAF2
30	TRAF2	→	MKK4/7	2.63E-6	Activation of JNK pathway by TRAF2
31	MKK3/6	→	p38	2.37E-4	Activation of p38 by MKK3/6
32	p38	→	Survival process	1.31E-5	p38 depletion term
33	Y	→	Z	3.07E-1	Intermediates for delayed JNK activation
34	Z	→	X1	8.76E-4	
35	X1	→	X2	3.18E-3	
36	X2	→	X3	7.48E-3	
37	X3	→	MKK4/7	2.21E-3	Activation of JNK through bypass
38	MKK4/7	→	JNK	1.81E-4	Activation of JNK by MKK4/7
39	JNK	→	Survival process	2.36E-4	JNK depletion term

Note that to simulate each KD condition, we imposed null parameter value(s) for all reaction(s) involving the KD molecule.

A.6 Identifying key target for sensitizing TRAIL resistance

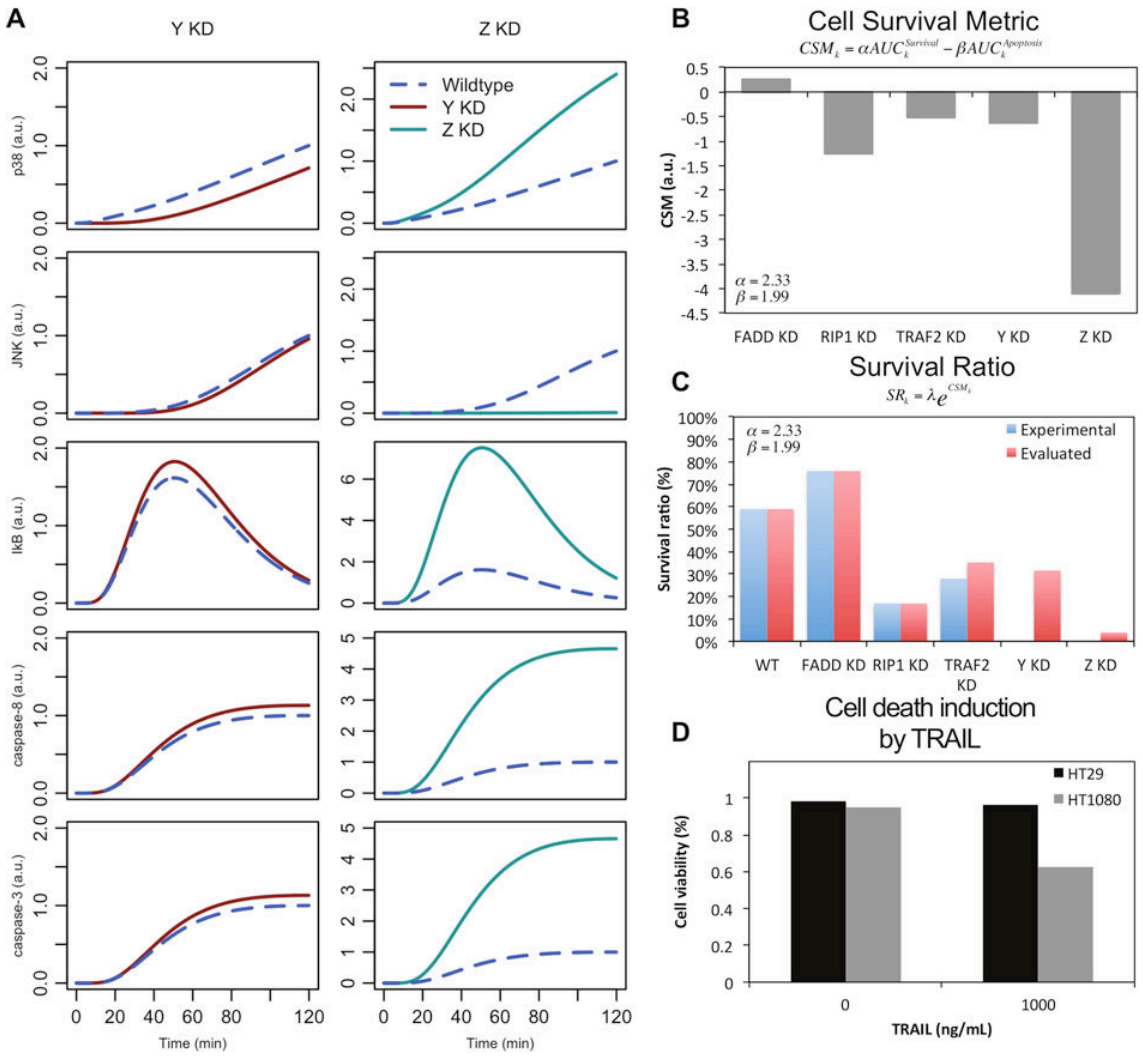

(A) Simulation profiles of p38, JNK, IκB, caspase-8 and -3 in ***Y*** and ***Z*** (=PKC) KDs. (B) *Cell survival metric* (*CSM*) for all KDs. (C) Survival ratio, *SR*, (experimental versus evaluated, from $t = 0$ to 120 min) in all conditions. Evaluated data is obtained using experimental data of RIP1 and FADD KDs. (D) Wildtype HT1080 and HT29 (control) cells shows 60% and 95% survival, respectively, for 1000 ng/mL of TRAIL stimulation.

Appendix B

List of Abbreviations

AP	activating protein
ARE	AU rich element; miRNA, micro RNA
BIM-I	bisindolylmaleimide I
BSA	bovine serum albumin
cIAP	cellular inhibitor of apoptosis proteins
DD	death domain
DKO	double knock out
DMSO	dimethyl sulfoxide
ECL	enhanced chemiluminescence
ELISA	enzyme linked immunosorbent assays
ERK	extracellular signal-regulated kinase
FADD	fas-associated death domain protein
HOIL-1	heme-oxidized iron regulatory protein 2 ubiquitin ligase-1
HOIP	HOIL-1-interacting protein;
IL	interleukin
IRES	internal ribosome entry site
IRF	interferon regulatory factor
IκB	inhibitors of NF-κB
JNK	c-Jun N-terminal kinases
KO	knock out
LUBAC	linear ubiquitin chain assembly complex
MAP	mitogen-activated protein

mRNA	messenger RNA
MEF	murine embryonic fibroblast
MMP	matrix metalloproteinase
MTT	methyl thiazolyl tetrazorium
NF-κB	nuclear factor-κB
Nec-1	necrostatin-1
PKC	protein kinase C
PVDF	polyvinylidene difluoride
RIP1	receptor-interacting protein 1
SDS-PAGE	sodium dodecyl sulfate-polyacrylamide gel electrophoresis
SFR	signaling flux redistribution
SHARPIN	SH3 and multiple ankyrin repeat domains protein-associated RH domain interacting protein
TAK1	transforming growth factor β (TGFβ)-activated kinase 1
TBST	tris-buffered saline with tween 20
TNF	tumor necrosis factor
TNFR	TNF receptor
TNFRSF	TNFR superfamily
TRADD	tumor necrosis factor receptor 1 associated death domain protein
TRAIL	TNF-related apoptosis-inducing ligand
qRT-PCR	quantitative real-time polymerase chain reactions